

UNIVERSITÀ DEGLI STUDI DI NAPOLI FEDERICO II



DEPARTMENT OF CHEMICAL, MATERIALS AND PRODUCTION ENGINEERING (DICMAPI)

PhD in “INDUSTRIAL PRODUCT AND PROCESS ENGINEERING”

XXIX cycle

“HARNESSING BIOPHYSICAL SIGNALS FOR IN VITRO TISSUE GUIDANCE”

Supervisor

Prof. Maurizio Ventre

Coordinator

Prof. Giuseppe Mensitieri

PhD Student

Valerio Coppola

2014/2017

Table of contents

Chapter 1

• 1.1 Introduction	1
• 1.2 Understanding the role of materials signals on cell behaviour	3
<i>1.2.1. Molecular structures and dynamics of cell adhesion</i>	4
• 1.3 Design and fabrication of materials to control cell adhesion	8
<i>1.3.1. General concepts</i>	8
<i>1.3.2. Technologies for materials patterning: from the micro- down to the nano-scale</i>	10
<i>1.3.2.1 Top-down technologies</i>	10
<i>1.3.2.2 Bottom-up technologies</i>	14
• 1.4 The effect of micro- and nano-patterns on cell behaviour	17
• 1.5 Material signals as stem cell regulators	19
• 1.6 Insights on the molecular mechanisms regulating the material-cytoskeleton crosstalk (Nuclear mechanotransduction)	21
• 1.7 Material signals as tissue regulators	23
• 1.8 Scope of the thesis	27
• 1.9 Bibliography	29

Chapter 2

• 2.1 Introduction	37
• 2.2 Materials and methods	40
2.2.1 <i>Preparation of micropatterned substrates</i>	40
2.2.2 <i>Cell culture</i>	41
2.2.3 <i>Tissue staining and image acquisition</i>	41
2.2.4 <i>Cell-collagen structure characterization</i>	42
2.2.5 <i>Mechanical testing</i>	43
• 2.3 Results	45
• 2.4 Discussion	62
• 2.5 Bibliography	67

Chapter 3

• 3.1 Introduction	70
• 3.2 Materials and methods	74
3.2.1 <i>Preparation of micropatterned substrates</i>	74
3.2.2 <i>CDMs production</i>	74
3.2.3 <i>Decellularization</i>	74
3.2.4 <i>dCDM ultrastructural characterization (SEM)</i>	75
3.2.5 <i>Mechanics characterization of dCDMs</i>	75
3.2.6 <i>Stem cells culture</i>	76
3.2.7 <i>Cell staining</i>	77
3.2.8 <i>Image analysis</i>	77
3.2.9 <i>Statistics</i>	78
• 3.3 Results	79
• 3.4 Discussion	90
• 3.5 Bibliography	95

Chapter 4

• 4.1 Introduction	98
• 4.2 Materials and methods	100
<i>4.2.1 Preparation of nanopatterned substrates and tissue devices</i>	100
<i>4.2.2 Cell culture</i>	100
<i>4.2.3 Tissue staining and image acquisition</i>	101
<i>4.2.4 Edge effect characterization</i>	101
<i>4.2.5 TDs characterization (SEM)</i>	102
• 4.3 Results	103
• 4.4 Discussion	120
• 4.5 Bibliography	124

Chapter 5

• 5.1 Conclusions	126
--------------------------	-----

Chapter 1

1.1 Introduction

Morphogenesis and homeostasis of tissues are the results of intricate and delicate interplays occurring between cells and the surrounding chemical/physical microenvironment. Even small perturbations of such interactions may cause malformations or dysfunctions (1). For a long time, the extracellular matrix (ECM) has been regarded as a passive supporting frame in which cells were considered to be the main actors. Today, the ECM is undoubtedly recognized as an active structure, source of the signals that promote, guide and sustain cellular functions. Signals displayed by the ECM can be in the form of biochemical signals (fixed proteins or diffusible factors) mechanical stimuli, (hard/elastic, soft/compliant or gel-like tissues), topographic signals (fibrils, fibres, pores, meshes, protrusions). The effects of soluble factors on cell behaviour have been extensively investigated in the past decades and the related studies constitute the foundation of modern experimental cellular and molecular biology. Conversely, the effects of the fixed ECM signals -for instance adhesion sites, topography and mechanical properties- on cell functions are much less known. This raises relevant issues, especially in an *in vitro* context. In fact, the

inherent chemical/physical characteristics of the material substrate for cell cultures cannot be disregarded a priori. For example, cell conditioning with biochemical stimuli might be affected by material properties, which can be relevant when drawing out definitive conclusions on the treatment (2). In particular, properties such as material stiffness, roughness, ligand density and availability, surface charge, hydrophobicity, invariably come in contact with cells and affect their response. In fact, there is growing evidence that this type of signals can be as effective as soluble signals in regulating cell fate and functions (3). Within this context, cell adhesion acquires a central role, since adhesion is a prerequisite for the perception of surface topography, material stiffness and ligand positioning. Additionally, adhesion formation and dynamics dictate the assembly of the actomyosin cytoskeleton, whose contractile forces strongly affect multiple cell functions, such as spreading, migration, proliferation and differentiation (4). Therefore, all the material signals affecting adhesion processes invariably alter the mechanical identity of the cell. The transduction of mechanical signals, i.e. mechanotransduction, either exogenous or generated by the contractile activity of the cytoskeleton, is a new research field that is steadily gaining importance as it holds the promise to provide novel elements to interpret complex biological processes, such as morphogenesis, tissue repair and tumor progression (5). Mechanotransduction relies on the physical interaction occurring at the interface of ECM and cells or, from a biomaterial science perspective, material-cytoskeleton crosstalk. Unravelling such a complex material-cytoskeleton crosstalk would provide novel criteria for designing biomaterial surfaces able to impart specific instructions to cells through adhesive signals at the interface.

1.2 Understanding the role of materials signals on cell behaviour

Cells contacting surfaces perceive different chemical/physical features of the material simultaneously. These may include roughness, hydrophobicity, ligand density and distribution, stiffness and charge. Literature reports demonstrated that cell adhesion, spreading, migration, proliferation and differentiation are very sensitive to the biochemical/biophysical characteristics of material surfaces (reviewed in (3, 6)). However, the molecular mechanisms underpinning the transduction of the material signals into intracellular biochemical events eventually dictating cell response are scarcely understood and only few biological responses have been recently clarified (7–9). Therefore, developing artificial systems that display perfectly controlled arrays of signals acquires a bivalent purpose: first, engineered platforms might enable to gain a better insight into the mechanisms regulating cell biology and cell-signal interaction; second, it will allow conceiving novel biomaterials able to control and instruct cells to fulfil specific tasks both *in vivo* and *in vitro* settings. To these aims, the control of signals should be orthogonal, i.e. modulation of different signal types independently, and should be performed on different length scales. Recent advancements in materials science and technology, have made available a broad spectrum of tools and strategies to engineer novel functional biomaterials that can reproduce set of stimuli that cells, more specifically SCs, experience *in vivo*, thus controlling their fate *in vitro*. Synthetic materials are sufficiently versatile to be functionalized with various arrays of biochemical and biophysical signals thus their properties can be in principle tailored in order to study cell response to specific signal combinations in a consistent and systematic manner.

Furthermore, *in vitro* experiments are usually carried out by using cell populations. These are highly heterogeneous, which makes difficult to assess cell response to selected signals as these can be differently perceived by the cells. Additionally, paracrine effects and cell-cell interactions may overlap to the signal thus complicating the scenario even further. Micro- and nano-fabrication technologies can provide an effective way-out to this issue by

providing well-defined chemical-physical environment to isolated cells thus allowing to study cell response to exogenous stimulation in a systematic and effective manner.

1.2.1. Molecular structures and dynamics of cell adhesion

Prior to introducing the strategies and technologies that enable to control cell fate and functions through material features, is it useful to briefly describe the mechanisms governing cell adhesion to materials, which is a central element for the recognition and response to surface characteristics.

Various types of receptors located on the cell membrane have been identified and characterized during the last decades. These include integrins, glycosaminoglycans and glycosylphosphatidylinositol-linked receptors, syndecans, non-integrin collagen and laminin receptors (10). Among these, the transmembrane, heterodimeric integrin receptors have been widely investigated and are recognized as key elements in providing stable adhesion and in initiating biochemical events that eventually affect cell behaviour (11). Adhesion complexes and focal adhesions (FAs) result from the binding of integrins to specific ligands displayed by the ECM or by the material substrate. Adhesion formation and dynamics has been widely studied and characterized (12, 13). From a materials engineering perspective, important design parameters are: *i.* characteristic dimensions of adhesion assembly; *ii.* stimuli that most effectively affect the adhesion process. Then, the desired signal needs to be embossed onto the material surface at the specific length scale to affect cell response via adhesion. To provide information and elements useful for material surface engineering we start by deconstructing the adhesion process down to the intimate interaction of molecules with materials.

Central players in signal recognition and cell adhesion are the integrins. Prior to binding to ligands, integrin dimers need to undergo to a conformational change (i.e. activation), which improves affinity towards the ligands and enables the interaction with reinforcing and signalling molecules from the cytoplasmic side. Adhesion to a substrate does not depend on the formation of receptor-ligand complexes only, but requires the maturation and growth of these initial clusters into large and stable multiprotein structures. The temporal evolution and

functions of such structures are tightly connected to the dynamics of the cytoskeleton. These processes and the mutual relationships have been widely characterized in 2D setups. During the early phases of adhesion formation few integrin dimers cluster together to form the so called nascent adhesions, predominantly in the cell lamellipodium i.e. a flat membrane process constituting the cell's leading edge. In this region, extensive actin polymerization is observed that forms a branched network of fibrils (14). The growing actin filaments clash on the cell membrane and are displaced backwards generating a retrograde flow. Activated integrins can engage the actin flow through cytoplasmic reinforcing proteins such as talin, vinculin and α -actinin. Interestingly, these adhesion proteins show a slower retrograde motion with respect to actin, indicating that a slippage between actin and integrin occurs. The existence of such a slippage enables the transmission of forces from the cell to the extracellular environment (15). As the process continues and the membrane is furtherly stretched, the relative position of nascent adhesions respect to the lamellipodium changes and these adhesions may either disassemble or mature into larger focal complexes, which in turn complexes can further mature and grow creating multiprotein assemblies 0.5–2 μm wide and up to 10 μm long FAs. Such a transition depends on the stability of the assemblies, the availability of ligands and the tension exerted on the adhesion. Actin is often assembled in the form of thick bundles in the central and rear regions of the cell. Myosin II contractility is a potent promoter of FA maturation. In fact, contractility cause vinculin, which mediates force transmission, to become activated and more affine to other proteins (16). Similarly, when talin is stretched by actin it exposes cryptic sites that allow additional binding sites for vinculin (17). Other proteins, such as paxillin, also exhibit a similar behaviour (18). This generates a catalytic process that reinforces the adhesion owing to the recruitment of cytoplasmic proteins. Unlike the nucleation of nascent adhesion in the lamellipodium, focal complex and FA maturation is dependent on actin-generated tension through myosin II (19).

Besides fulfilling an important structural role as anchoring points, FAs are also important signalling centres. Several components of, or in intimate connection with, the FAs are important signalling proteins as kinases (focal adhesion kinase - FAK, Src) and GTPases

(Rho, Rac). Mechanical forces exerted by the actomyosin machinery are transmitted to these proteins and this may alter their activity (20).

The transduction of mechanical stresses into biochemical signals, a process known as mechanotransduction, is emerging as an important element in the design of material systems that finely control cell functions. In fact, material features can be tuned in order to affect FA dynamics (formation and maturation). The signalling proteins in the FAs are activated by cytoskeletal tension and their activity sustains contractility. This generates a positive feedback loop that is halted stopped by either disrupting FAs or by inhibiting contractility (21). Mechanotransduction may also act on a different level. In fact, the actin cytoskeleton is directly connected to the nuclear envelope. Therefore, actin generated forces can deform the nucleus, thus causing a structural modification of DNA sequences and, possibly, altering gene expression (22). These concepts are valid both in case of exogenous mechanical stresses (fluid flows or stretching of the cell membrane) and of endogenously generated forces, through the actomyosin cytoskeleton.

The mechanical coupling between the cytoskeleton and the external surface in contact with the cell enables the perception of biochemical (ligand density and patterning) and biophysical (topography and mechanical characteristics) signals of the extracellular environment. In other words, the biochemical and biophysical information or signals possessed by the extracellular environment all pass through a common gate represented by the FAs. Similarly, the forces generated by cells to probe and interact with the surroundings are mediated by the FAs. Several models have been developed in an attempt to relate FAs, cytoskeletal stresses and structures with nuclear deformation. Among these, the tensegrity model proved to capture interesting aspects concerning cell shape and mechanics, along with mechanotransduction (23). It basically relies on the concept that the cell shape and intracellular force transfer are dictated by cytoskeletal pre-stress generated by actomyosin contractility that is balanced by force resisting structures like microtubules that support compression and ECM-linked FAs. According to this model structural stability depends on tensional integrity, which requires a direct connection among tensile and compressive elements. Beside stability, tensegrity structures rapidly reorient upon force application or

deformation (23). Owing to the physical coupling of FAs, cytoskeleton and nuclear membrane, mechanical forces propagating through the cytoplasm can eventually promote rearrangements of chromatin in the nucleus. Thus, mechanical forces at FAs might exert a long-range mechano-chemical conversion in the nucleus (24). Furthermore, the model predicts that the pre-stressed cytoskeleton causes the mechanical signal to travel to the nucleus in a much faster manner (hundreds of ms) than signal propagation induced by soluble factors (few seconds) (24). The presence of a pre-stressed cytoskeleton also exerts an important regulatory role on the activity of stress-sensitive ion channels, i.e. transmembrane complexes that gate ion flow across the membrane, which is necessary to fulfil specific biological functions (25). Therefore, force transmission on plasma membrane through FAs-cytoskeleton linkages is important for activating stress sensitive ion-channels. The actin cytoskeleton can be anchored to the cell membrane through proteins of the ezrin–radixin–moesin (ERM) family. Contractile forces may pre-stress the membrane surrounding ion channels and such a pre-stress can modulate the response of the channels to forces propagating through the cytoskeleton (26).

Therefore, FAs are at the helm of a complex crosstalk occurring between the cytoskeleton and the supporting material, in which the characteristics of either of these entities affect the other. Through mechanotransduction pathways, controlling FA formation and dynamics with material signals may ultimately trigger specific signalling and transcription events.

1.3 Design and fabrication of materials to control cell adhesion

1.3.1. General concepts

Correct and stable attachment to specific ECM sites is necessary for several cellular processes such as migration, proliferation and survival of anchored-dependent cells (27). Failures occurring during cell attachment or adhesion to incorrect sites might lead to programmed cell death (28). In case of cell cultures on or within man-made constructs, cells do not interact with the constituting material directly, but to the protein or peptide layer that cover its surfaces (29). Such a layer might spontaneously adsorb from the serum-enriched media, containing well-known cell adhesive proteins such as fibronectin, vitronectin and laminin. In fact, the culturing environment, as well as the native biological one, is a heterogeneous system with various proteins, glycoproteins and lipids. The supporting material for cell culture displays surfaces with preferential affinity to certain proteins while may repel others. Additionally, the adsorbed protein layer is far from being homogeneous in composition since cells secrete, remodel or even degrade components of the matrix. Therefore, exerting a precise control on the chemical/physical properties of the surface to enable the adsorption of specific proteins from such a complex system is an important aspect in scaffold or substrate engineering. Alternatively, bioactive moieties can be deliberately introduced into the culturing system, via chemical methods (30, 31). However, issues related to the uncontrolled adsorption of serum molecules or to the biosynthesis of new proteins by cells might still be present. The chemical-physical properties of both the materials and of the proteins define the way in which the cell adhesive layer is configured, which ultimately promotes or suppress cell adhesion (32). For instance, biomaterials usually used as scaffolding materials or as cell culturing supports, such as poly-L-lactide (PLLA), poly(lactic-co-glycolic acid) (PLGA), polycaprolactone (PCL) are highly hydrophobic in their unmodified state, which causes proteins to be adsorbed in a denatured and rigid state. In this configuration, ligands are less accessible to receptors (33). Conversely, highly hydrophilic materials bind the adsorbed proteins with weak forces that could not withstand cell-generated forces ultimately leading to cell detachment (33). Therefore, optimal

conditions for cell adhesion are usually found in intermediate hydrophilic properties of the material surface. Numerous studies reported an enhanced cytoskeletal organisation on hydrophilic substrates (34, 35). For instance, Webb et al. showed increased spreading, well developed cytoskeleton and FA formation of fibroblasts on hydrophilic glass substrates, whereas cells displayed a spindle like shape with minimal actin assembly and FAs on hydrophobic surfaces (36).

Surface nano-roughness was shown to play an important role in protein adsorption. Several reports found protein conformational changes when adsorbed onto nano-rough substrates as compared with flat surfaces, which might affect cell adhesion process (37, 38). In fact, Dolatshahi-Pirouz et al. found an increased number of FAs and filopodia on FN coated nano rough tantalum substrates with average feature size of 5 nm with respect to flat surfaces, which correlated with an increased adsorption of FN along with a better presentation of adhesive ligands (39).

Altogether, these data suggest that the chemical-physical properties of the cell substrate, or alternatively, its surface, need to be carefully engineered in order to regulate FA formation. This notwithstanding, the concepts expressed so far are of general validity, but are not sufficient to conceive strategies to exert a fine control on FA size, positioning, orientation and on the cytoskeleton assembly consequently. As seen in the previous section, FAs not only provide a mechanical link with the extracellular environment, but they are also important biochemical signalling hubs whose signalling activities change as they mature (40). For instance, integrin/ligand binding determines whether cytoplasmic mechanotransducers can undergo conformational changes thus triggering a signalling cascade. Additionally, ligand positioning and patterning may dictate the magnitude and direction of forces, which directly impact cytoskeleton stress, along with cell and nuclear shape consequently. Basically, this is the heart and soul of mechanosensing and mechanotransduction, for which cells perceive the mechanical properties of the extracellular environment and transduce this information in intracellular biochemical events.

Therefore, material surfaces need to be engineered in order to interact with great precision with integrin clusters, i.e. at the nanometric level. Additionally, exerting a control

on FA size, position and orientation determines the structure of the cytoskeleton and, hence, the mechanical identity of the cells. To achieve this, an effective and stable mismatch in adhesion sites (i.e. well defined locations on which integrin can bind and cluster juxtaposed to non-adhesive zones) must be created. Therefore, patterning biochemical/biophysical signals with a nanometric resolution is key central.

1.3.2. Technologies for materials patterning: from the micro- down to the nano-scale

Among the myriad of technologies developed so far, we refer to those that emboss patterns of biochemical and biophysical signals affecting FA formation, positioning, size and stability in a controlled manner. Other processes and technologies may also generate patterned surfaces that exert a certain degree of control on cell adhesion, but these surfaces possess a level of randomness in the distribution of features and the long-range order of such features is limited. Therefore, with such technologies, it is not possible to precisely modulate FA morphology in a pre-determined manner.

Generally, micro- and nano-fabrication technologies are divided in top-down and bottom-up approaches. Top-down approaches rely on the deposition or removal of materials by using a predefined 'guiding pattern'. In bottom-up approaches, the physical-chemical properties of individual building blocks determine their mutual interactions, self-assembly or organization that result in the formation of nano- or micro-scale structures. In what follows we review some of the most relevant technologies that have been successfully employed in the engineering of material surfaces to control cell adhesion processes.

1.3.2.1 Top-down technologies

Photolithographic technologies, originally developed for the semiconductor industry, are among the most used to fabricate micron- and submicron-patterned material surfaces. Photolithography consists in the exposure of a substrate, typically Silicon, coated with light-sensitive photoresist with a patterned UV light. Light patterning is most conveniently performed by applying a specifically designed reflective mask. In case of 'positive' photoresists, only those parts exposed to the radiation are soluble in organic solvents.

Conversely, in 'negative' photoresists the solvent dissolves the non-exposed parts, thus creating an inverse pattern. This process requires specialized equipment and high capital costs. However, the technology is nowadays very well consolidated and raw materials are affordable: therefore, the fabrication of patterned surfaces can be outsourced. Further developments of this technology enable the fabrication of patterns with mask-less procedures by means of optical interference techniques (41) or stereo-lithography (42). Patterns thus generated need to be transferred to suitable materials for cell cultures in the form of biochemical, topographic or mechanical patterns. Various techniques have been developed so far to achieve high fidelity pattern transfer. Replica molding (REM) relies upon the curing or hardening of a polymeric material previously poured on a patterned mold. Thermally curable polydimethylsiloxane (PDMS) is one of the most used material for REM owing to its excellent stability, biocompatibility and transparency. After curing PDMS is "peeled-off" the mold (or master) and it displays the inverse topographic pattern of the mold. Other materials employed in REM for fabricating cellular substrates are PCL and polyurethanes (43, 44). Substrates thus produced can be used straightaway or as molds to produce other samples. Alternatively, patterned polymers, elastomers in particular, are employed as stamps to deposit bioactive proteins in an ordered fashion in a process known as microcontact printing (μ CP). In more details, the elastomeric stamps are 'inked' with the material, usually a protein solution that will constitute the pattern. The transfer of the 'ink' onto the substrate requires that the process is energetically favourable than remaining anchors on the stamp. The surface chemistries of both the stamp and substrate are crucial parameters eventually determining transfer efficiency. Owing to the stamp compliance, high aspect ratio stamps, feature height much larger than the width, cannot be readily used the structures as the features may collapse on each other during the peeling off the template or during the inking process due to capillary action or they collapse on the target surface (45, 46). Another problem might arise in case of small feature heights and wide grooves, in which case grooves can come in conformal contact with the target surface when the stamp is compressed. However, this issue can be easily handled by reinforcing the stamp with a rigid back-cover. The soft nature of the stamp might be exploited to generate features with size different from those of the stamp: this can

be compressed or stretched inducing a substantial deformation of the raised and recessed features (47). Nanocontact printing is an evolution of μ CP and enables to emboss patterns with 100 nm resolution by means of rigid stamps 'inked' with high molecular weight solutions that have reduced diffusion (48).

Methods like those previously described, in which elastomeric substrates are used as final support or as intermediate template, fall within a broader category of processes known as soft-lithography (49). Conventional soft-lithography uses light sources, usually UV light, to impress the photoresist. Therefore, the spatial resolution of the topographic features that can be created is limited by the diffraction of light. More specifically, features of $\sim 1 \mu\text{m}$ can be achieved easily, whereas submicron features require the use of special equipment. Narrower features can be fabricated by means of specifically developed technologies such as electron beam lithography (EBL) and focused ion beam lithography (FIB). These techniques allow the fabrication of structures down to ten nanometers. The working principle of these techniques is not dissimilar to conventional photolithography: rather than light, a beam of electrons (in EBL) or a beam of heavier ions (in FIB) passes through a mask to expose a sensitive resist. Specifically, designed *apparati* enable a mask-less, direct wiring on the resist, by moving the collimated beam with electromagnetic lenses. The features thus generated in the resist can be transferred to the underlying substrate via reactive ion etching (see below). Additionally, with FIB, the heavy ions constituting the beam allow atoms to be displaced from or deposited onto the material surface, in which case it is possible to achieve subtractive or additive lithography on the final substrate directly, without further development.

Nanoimprint lithography (NIL) utilizes masters with nano-scale features and enables embossing nanopatterns, as lower as tens of nm on synthetic substrates (50). Two types NIL can be performed depending on the type of the material to be patterned. In particular, thermal-NIL is a process similar to hot-embossing in which a layer of thermoplastic material is heated above its glass transition temperature. The stiff nanopatterned template is pressed against the thermoplastic layer, which conforms the pattern of the template. In light-based-NIL an optical transparent mold is in contact with a light sensitive polymer

precursor. The latter crosslinks upon light exposure thus generating an inverse replica of the mold (51).

Another direct-writing method to pattern surfaces with high spatial resolution is the Dip-pen nanolithography (DPN). It derives from scanning probe microscope-based lithography, but unlike this, which aims at manipulating surfaces, DPN actually delivers tiny quantities of matter. More specifically, the tip of the scanning probe microscope is coated with the molecules of interest, usually in a solution termed 'ink', which is subsequently placed on a surface. By controlling the movement of the tip, molecular patterns are written on the substrate. In its original form DPN was used to deposit alkanethiol molecules on gold with a spatial resolution down to 30 nm (52). Careful optimization of the processing conditions allowed depositing biomolecules of various types, among which proteins and peptides (53, 54). More recently, Moldovan et al. integrated microfluidic channels into the cantilever to create systems able to ensure a constant supply of ink to the substrate. This was a major advancement in the field, as it allows to keep molecules correctly solvated, which is crucial to retain the biological activity of biomolecules (55). Direct writing techniques are intrinsically slow and patterning large areas might be cumbersome. In case of DPN, tip parallelization may solve this issue, if at the expenses of versatility (56).

While the above-mentioned methods allow to emboss even complex structures with nano-scale precision on a wide variety of synthetic or inorganic materials, they suffer of high relatively high costs, low processing times, which make the patterning of large areas, or at least sufficiently large for cell culture applications, non-practical.

Electrospinning is a technology that allows the fabrication of large nano-fibrous mats, with fibres having diameters in the order of 100 nm, in few minutes and in a low-cost manner. These benefits goes at the expenses of the accuracy in controlling fibre positioning and orientation. The process can be applied to a broad variety of polymers solubilized in adequate solvents. For example, PCL (57, 58), PLLA (59), PLGA (60), hydroxybutyl chitosan (61) and hydroxyapatite/chitosan (62) were successfully employed for the production of porous scaffold with nanoscale fibres. Generally, a high voltage (kV) is applied to metallic needle through which a polymeric solution slowly flows. The pendant drop at the needle tip

becomes charged; if the electrostatic repulsion in the charged components of the droplet surpasses the surface tension, then the droplet stretches and liquid jet departs and is eventually collected on a grounded metallic plate. During the displacement from the droplet to the collector, the liquid jet is furtherly stretched due to electrostatic forces and the solvent quickly evaporates owing to the high surface to volume ration of the fibre. In such a configuration, the electrospinning technology ma only produce mats of randomly aligned fibres. If the metallic collector is substituted by a rotating mandrel, then the fibres can be wound around it, thus producing an aligned fabric (63).

Surface roughening methods are inexpensive, emboss nanometric patterns on large areas and very quickly. Despite these advantages, features are in general randomly distributed on material surfaces and it is difficult to control their characteristic size. Chemical etching relies on reactions between etchants and materials and on the intrinsic heterogeneities of the surfaces at the nanoscale, which cause the etching reaction to occur randomly and at different rates, eventually producing nano-pitted surfaces in which recesses have various depths and pitches. Reactive Ion Etching (RIE) usually involves SF₆ and C₄F₈ gases directed against silicon-based glass via radio-frequency electric field. Gas ions interact with the glass surface knocking-off material atoms or damaging the structure. The presence of impurities such as Al, K and Na result in cluster formation of less volatile species (such as AlF₃, KF, NaF, etc.) on the glass surface. These clusters form randomly features that shield glass surface from further bombardment and reaction with reactive ions, whereas extensive etching occurs in the intercluster regions. Differently from chemical etching, in RIE the process can be controlled by controlling gas pressure, voltage and frequency. Furthermore, owing to the ‘directional’ bombardment, topographic features are usually more anisotropic with respect to the isotropic pits observed with chemical etching. Furthermore, RIE has been integrated with photolithography to generate patterned nano-rough islands on flat glass surfaces (64).

1.3.2.2 Bottom-up technologies

These technologies usually rely on the interaction occurring among building blocks, which can be molecules, nanoparticles, polymers or polymer domains, in specific processing

conditions. The interactions result in the spontaneous self-assembly of the building blocks giving rise to micron- or nano-scale structures. For instance, block copolymer self-assembly and polymer de-mixing, allow fabricating synthetic materials displaying nano-scale islands separated by recesses. Surface nano-structuring with copolymer self-assembly is driven by the tendency of copolymer films (that usually coat a supporting substrate) to separate under specific thermodynamic conditions. Since polymer blocks are covalently linked, phase separation occurs intermolecularly and on length scales comparable with those of the blocks (65). This generates microphases that can be arranged in arrays of pits, ridges and worm-like structures with characteristic dimensions in the order of $\sim 10\text{--}100$ nm. Phases can be selectively removed with chemical/physical treatments, leaving the remaining on the supporting substrate thus generating the nanostructured surface. Similarly, separation of polymer-polymer blends can result in the formations of microphases whose morphological characteristics are governed by thermodynamic dependent parameters (for instance the composition of the blend) and kinetic parameters (temperature of the process) (66). Generally, these structures favour the formation of FAs atop the protruding islands or ridges, limiting their maturation. Despite the fact that these techniques do not allow to exert a fine control on the spatial assembly of the topographic features, which usually present in the form of 'worm-like' or 'dot-like' patterns (67), they are characterized by a high yielding, low costs and fast processing times.

A technique that proved to be particularly suitable for the fabrication of nanoengineered substrates for cell cultures is block copolymer micelle nanolithography (68). The technique relies on the spontaneous formation of microphase-separated micelles of amphiphilic block copolymers. During formation, micelles can entrap metallic nanoparticles in their core. Monolayers of evenly spaced micelles are formed on a material surface by dip-coating. Removing the polymeric micelles by means of plasma treatment leaves quasi-hexagonal patterns of metallic particles. By modulating the processing conditions, arrays of particles having spacing within the 10 -100 nm range can be formed (69). Beside the above mentioned advantages, patterns of complex shapes are difficult to fabricate with this technique.

We conclude this section recalling that adhesion processes occur on different length scales: from few nano-meters of integrin clusters up to 10 μm of mature FAs. An all-round technology able to create patterns to control adhesion processes on multiple-length scales, within reasonable timeframes and costs, has not been developed so far. Therefore, to exert a tight control on adhesion dynamics, multiple techniques should be integrated.

1.4 The effect of micro- and nano-patterns on cell behaviour

Proteins or fragments containing cell adhesion motifs can be conjugated to material surfaces via covalent binding or by physical interactions. Chemical conjugation might alter the structure of the proteins decreasing their bioactivity (70, 71). Cell adhesion is a spatially discontinuous process occurring in the ventral side of cells. Uniform coating of material surfaces cannot address the important question about how individual ligands should be clustered and/or spaced in order to initiate the formation of adhesion complexes or promote their maturation. Micro- and nano-fabrication technologies provided essential instruments to engineer substrates on which cell adhesive regions could be controlled and modulated in terms of size, positioning and spacing with micron- or submicron-scale precision.

The activity of the cytoskeleton has been implicated in the formation of cell processes and in the definition of cell shape. Therefore, it is expected that controlling adhesion processes impacts actin dynamics, eventually affecting cell morphology and behaviour.

In order to be effective in controlling FA localization and shape, micro- or nano-patterning techniques require to achieve a sharp adhesion mismatch on the surface. Pattern embossed with μ CP or other biofunctionalization techniques that rely on adhesive spots surrounded by a protein repellent background were indeed useful to confine FAs and to study cell behaviour in specifically controlled adhesion settings. However, this sort of technique requires specific chemicals, proteins or peptide for the functionalization and multiple steps to achieve the desired pattern. Micron- or nano-scale structured surface in the form of hills and recesses, i.e. topographic patterns, can be as effective as the biochemical patterns in controlling the formation of FAs and confine their growth. Micron scale topographic patterns are typically manufactured from master fabricated via lithographic techniques. Nanometric masters can be produced by means of direct writing methods (EBL or FIB) conjugated with imprinting techniques. Moreover, topographic patterns can be used straightaway by performing a simple coating with protein and usually do not require additional biochemical functionalization. Proteins adsorbed on the topographic pattern make some zones readily available to the cell membrane to enable FAs formation. These zones are separated by others that are impervious recesses in which cell protrusion cannot penetrate and form stable FAs. Topographic patterns with submicron scale arrays of pits, post or gratings were designed in order to constrain FA formation and growth to the feature top, i.e. on the pillar top, in the interpit area or on the grating ridges. In fact, very deep and narrow material recesses may not be penetrated by filopodia or lamellipodia. In such a condition, the

cell is suspended on the top of the pattern and FA formation is limited to specific pattern regions thus allowing to gain a remarkable control over adhesion processes.

Studies of cells cultivated on nanopits patterns demonstrated that size and pitch of the nanopits are key parameter in governing cell adhesion (72, 73). More recently, Tsimbouri et al. reported that MSCs cultivated on Polycarbonate substrates displaying arrays of nanopits developed smaller FAs and a less contractile phenotype with respect to MSCs on slightly disordered, but not random, patterns which locally displayed larger patches for FA assembly and therefore promoted a more contractile phenotype (74).

While pillar and pits arrays have the ability to confine both FA width and length, micro- and nano-gratings constituted by parallel and alternating ridges and grooves allow FAs to grow in a specific direction. Consequently, actin fibres also are aligned parallel to the pattern direction and this causes the whole cell body to assume an elongated morphology and migrate along the pattern direction, a phenomenon usually referred to as 'contact guidance'. Depending on feature geometry and surface characteristics, FAs can form on the ridge top or on the groove bottom or whether the pattern features effectively confine FA growth, thus affecting cell behaviour. For instance, Kim et al. demonstrate that NIH3T3 fibroblasts cultivated on a substrate with graded topography (ridge width 1 μm and height 400 nm and lateral spacing continuously varying from 1 to 9 μm) displayed enhanced alignment on the narrower topography, whereas cell speed was optimal at the intermediate ridge spacing (75).

However, it has to be pointed out that cell-pattern coalignment may depend also on cell type and culturing conditions. In fact, biochemical supplements may interact with the topographic features, thus altering the way the signal is perceived by cells, as demonstrated by Teixeira et al.. The authors reported that epithelial cells on narrow ridges could be parallel to the pattern direction if cultivated in normal culturing conditions, whereas they were predominantly orthogonal if medium which contained biochemical supplements such as insulin-like growth factor and epidermal growth factor, was used (76).

1.5 Material signals as stem cell regulators

Evidences that materials surfaces engineered to affect cell adhesion and spreading profoundly affected stem cell fate and functions traces back to two decades ago. Cell shape (cell area and other geometrical characteristics), may play an important role in lineage specification. In fact, adhesive islands of complex shapes, proved to exert a profound effect on cytoskeletal structures, polarity and contractility, all of which can impact stem cell fate (77). McBeath et al. correlated the spreading process to MSC differentiation (78). Authors demonstrated that small adhesive islands induced hMSC adipogenesis, whereas larger ones promoted osteogenesis in presence of mixed differentiation media.

Along this line, Kilian et al. showed that the shape of the adhesive islands also played an important role in driving hMSC differentiation. They found that high aspect ratio rectangles or shapes with sharp corners, on which cells exhibited larger FAs, promoted a contractile phenotype and osteogenesis. Conversely, islands with blunt edges promoted adipogenesis. Additionally, Yao et al. demonstrated that shape changes were sufficient to specify MSC commitment even in the absence of biochemical stimulation (79). These results suggested that cells are able integrate microenvironmental cues, to regulate differential response to growth factors.

Directed stem cell differentiation certainly is a crucial aspect of cell- and tissue engineering-based therapies. Less intuitively, though, prolonged stem cell maintenance possesses important practical implications. Conventional culturing conditions of stem cells usually result in spontaneous, uncontrolled differentiation thus generating heterogeneous populations of stem cells, which are of little use both *in vitro* and in clinical settings. Recently, Zhang and Kilian investigated the role of cell shape confinement in the retention of stemness markers (80). They found that hMSCs cultivated on small adhesive islands expressed higher levels of the multipotency markers compared to cells cultured on non-patterned surfaces.

Nanostructured materials displaying topographic nanopatterns may be used in order to display the signal in a persistent manner and can be engineered in order to control FA

features at the nanometric level and, thus, stem cell fate. Dalby et al. fabricated different nano-pits patterns on PMMA (81). The substrates thus engineered provided cells with different interpit areas to form FAs. The authors investigated whether the spatial assembly of patterns affected hMSC differentiation without induction media. Perfectly arranged patterns resulted in a decrease in osteoprogenitor cell density compared with planar surfaces, whereas the disordered nano-pits arrays significantly promoted osteogenesis (82). Follow up studies performed by the same group demonstrated that hMSCs cultivated on PCL possessing perfectly symmetrical nano-pit arrays retained stem-cell phenotype and maintained stem-cell growth over eight weeks (83). These data show the extraordinary sensitivity of stem cells in integrating nanoscale adhesion cues (few nanometers), which results in dramatic differences in fate decision. Furthermore, the data suggest that topographic patterns that allow FA assembly, thus stabilizing intracellular tension, promote osteogenesis. Conversely, patterns that induce the formation of sufficiently large FAs to allow proliferation, but below a certain size threshold that triggers the activation of differentiation pathways, are requested to maintain multipotency.

1.6 Insights on the molecular mechanisms regulating the material-cytoskeleton crosstalk (Nuclear mechanotransduction)

The examples reported above clearly demonstrated that adhesion- and cytoskeleton-mediated signalling regulated signalling pathways ultimately affecting cell fate and functions. However, cell generated forces via the actomyosin cytoskeleton may directly influence gene expression by altering the shape and structure of the nucleus. A direct consequence of the alteration of cell morphology is the build-up of cytoskeletal stresses that can remodel the spatial organization of chromosomes and may increase the accessibility of molecules that affect gene expression to chromatin (84, 85). Furthermore, the mechanical properties of the nucleus are not fixed, but change in response to specific states. For example, SC nuclei are highly deformable and contain a dynamic chromatin (86–88). Conversely, differentiated cells possess stiffer nuclei and a more stationary chromatin structure (89). Therefore, not only the actin-generated force, but also the mechanical response of the nucleus are important mediators of mechanotransduction pathways. The complex interplays between cytoskeletal stresses, nuclear mechanics and gene expression have not been thoroughly elucidated. Yet, recent studies have demonstrated that adhesive signals, in the form of material stiffness or adhesive islands, influence nuclear morphology through cytoskeletal structures (90, 91). To gain a better insight into the effects of cell shape and cytoskeletal organization on chromatin structure and gene expression, Li et al. cultivated hMSCs on micro-grooved PDMS that controlled cell morphology and nuclear shape. The authors reported that shape changes affected histone deacetylase (HDAC) activity and histone acetylation (92), that are directly involved in chromatin compaction. Since HDAC has been suggested to act as an inhibitor of cell reprogramming, Downing et al. used micro-grooved PDMS substrates to improve iPSCs generation (93). The authors found that biophysical signals induced marked changes in histone acetylation and methylation patterns that are dependent on cell and nuclear morphology and actomyosin contraction. These epigenetic changes significantly increased reprogramming efficiency and the presentation of material signals affecting cell adhesion might replace soluble epigenetic modifiers. Nuclear

mechanics and cytoskeletal structures affected the dynamics of subnuclear heterochromatin, which could in turn variously affect genomic processes and thus cell behaviour.

Altogether, these data demonstrate that material signals affecting the adhesion process trigger integrin, cytoskeleton or nuclear mechanotransduction pathway that exert a potent effect at the transcriptional level. Systematic studies aimed at assessing whether a pathway dominates over the others have not been performed yet. However, owing to the intimate connections between FAs, cytoskeletal assemblies and nuclear morphology, we believe that mechanotransduction acts as an intricate network allowing multiple aspects to work in concert.

1.7 Material signals as tissue regulators

The data reported so far undoubtedly demonstrate the relevance of material signals and more specifically signal patterning, in affecting and possibly regulating cell fate. This aspect may find practical applications in the fabrication of culturing devices to expand undifferentiated populations of stem cells, or guide homogeneous differentiations for cell-based therapies. Alternatively, patterned signals could be embossed on the surface of prostheses able to improve their integration within the host and their performances *in vivo*. However, the vast majority of the research on this topic relies on the investigation of isolated cells, whereas the effects of material features on dense cell populations in which cell-cell contacts cannot be neglected has been largely overlooked. Additionally, cells subjected to long-term cultures invariably remodel their microenvironment by producing or degrading extracellular components. Therefore, cell-ECM-material signals form a tripartite module in which each element affect the others and their dynamic interplay define the structure and functions of the whole tissue. Yet, the role of material signal on tissuegenesis or tissue remodelling is unknown.

For therapeutic products, it is necessary a tight reproducibility on the generation of structural and functional controlled engineered tissue. For instance, Kim et al. developed a nanotopographically controlled *in vitro* model of myocardium that mimics both the structural and the functional properties of native myocardial (94). The engineered tissue fate was highly sensitive to variation of the nanoscale topographic features of the substratum. The high degree of sensitivity of the cell and tissue structure to the nanoscale substrate topography can represent a powerful mechanism for engineering the desired functionality of model tissues.

Iannone et al. have recently demonstrated that nanopatterned surfaces guide the self-organization process of hMSCs *in vitro* by first governing FA assembly and then the magnitude and orientation of cell generated forces. These aspects eventually proved to be key triggers of an *in vitro* tissuegenesis (95). In more details, hMSCs were cultivated on nanograted PDMS substrates with parallel ridges of 700 nm evenly spaced by 700 nm grooves, 250 nm deep. Cells elongated and aligned parallel to the pattern direction within

few hours after seeding (Figure 1A). After 1 week of culture, cells self-organized in 3D-multilayered structures invariably oriented orthogonal to the pattern (Figure 1B). Promoting and stabilizing collagen biosynthesis and assembly with ascorbic acid resulted in the spontaneous generation of cylindrical 100 μm thick and few mm long structures that were reminiscent of embryo tendons (Figure 1C, D).

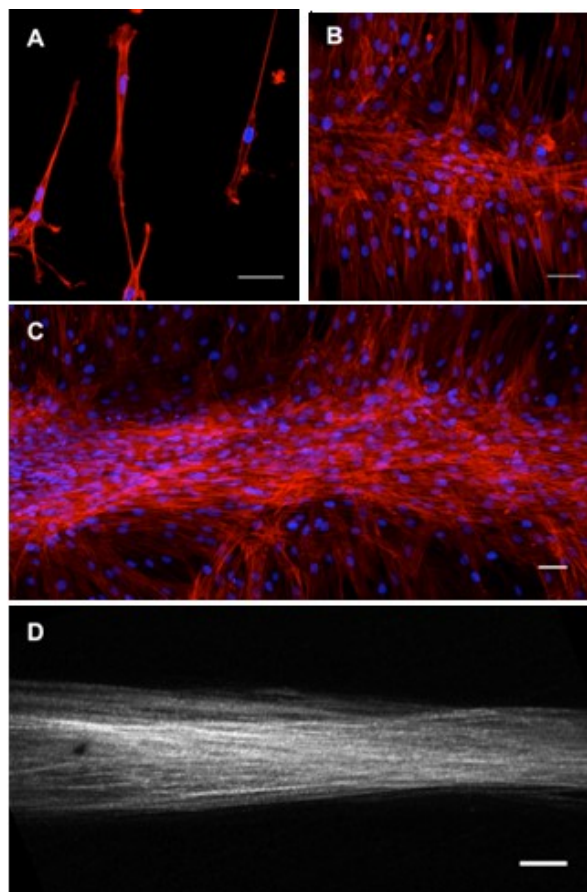


Fig. 1. Role of surface nanopatterning in the *in vitro* tissueogenesis. Confocal images of (A) hMSCs cultivated on nanograted PDMS for 24 h; (B) after 7 days of culture; (C) after additional 7 days of culture in presence of ascorbic acid. (D) Multiphoton imaging reveals a bright second harmonic generated signals produced by densely packed collagen fibrils. Pattern direction is parallel to the vertical axis. Actin is stained with TRITC phalloidin (red); cell nuclei are stained with DAPI (blue). Bar = 50 μm . Reprinted with permission from Ventre and Netti, 2016. Copyright 2016 American Chemical Society

Tenogenesis was confirmed by gene expression analysis with rt-PCR in which the upregulation of tendon-specific and -associated markers was evident. Further investigations performed in time-lapse video microscopy, aimed at deconstructing the dynamic of tenogenesis, revealed that first cells coaligned to the nanopattern and then self-organized by exerting a centripetal coordinated contraction, eventually resulting in the in the generation of a multi-layered structure. Strikingly, an intermediate level of adhesion was required to enable cell self-organization, as improving (with fibronectin functionalization) or reducing (by reducing ridge width) cell adhesion led to the generation of cell multilayers or spheroids respectively. Therefore, not only the direction of the nanopattern, but also the initial adhesion conditions plays a fundamental role in the process of *in vitro* tenogenesis. These findings suggest that surface nanopatterning can effectively control MSC behaviour from adhesion and elongation up to collective cell differentiation and tissuegenesis. This opens up new strategies to design material surfaces able to guide tissuegenesis events *in vitro*; in principle, by modulating pattern features and adhesivity, it is possible to control cell self-organization, differentiation, tissue microarchitecture, and functions.

Furthermore, the production of synthetic materials characterized by a nanotopography that influence cell arrangement, mimicking the natural ECM, have been employed to different tissue engineering studies (96–98). However, it is very difficult to precisely recapitulate the complex morphology and composition of a native ECM by using synthetic materials (99).

To this intent, natural tissues derived from animal or from *in vitro* cultured cells were proposed as starting point to fabricate nano-fibrous materials (100). Cell derived ECM avoids problems such as pathogen transfer and host immune response, in comparison with support derived from animal tissues (101).

A tight control in the organization of cell derived ECM can be generated, in principle by using a cell sheet engineering approach combined with microfabrication technology (102).

Subsequent to ECM synthesis and organization, cellular components of the cell sheet can be removed by decellularization, leaving an intact ECM sheet for an off-the-shelf cell culture scaffold. This kind of approach have been applied in the fabrication of tissue-engineered

blood vessels with seeded smooth muscle cells and endothelial cells, which showed superior mechanical properties (103).

1.8 Scope of the thesis

The main aim of the thesis is to get a better insight on how cell-material interactions can affect the microarchitecture of complex tissues generated *in vitro*. Material signals, has been shown to strongly influence cell behaviour in many processes, such as migration, orientation, differentiation and, thus, supra-cellular organization. Topographic signals used in a combinatorial approach with the inherent mechanical and chemical properties of the material surface or serum proteins might be used to regenerate and/or reproduce functional tissues.

However, it is very difficult to recapitulate the complexity of a native environment in a 3D context using current technologies. It is also necessary to point out that cells in nature are subjected to continuous modifications of the local environment and are constantly changing their behaviour accordingly, so that it is unlikely that “static” signals can outline such a complex state.

Then, we proposed a scaffold less approach to the direct production of an engineered functional tissue, using the endogenous matrix produced in a controlled manner as a signal reservoir that affect dynamically cell behaviour. We modulated the mechanisms involved in the organization of cells in complex tissues, by controlling the initial conditions of cell adhesion through material signals. The intimate understanding of the phenomena involved in such a process can, in principle, allow to use the right trigger to obtain a tissue which structure and function is established *ab initio*. Topography in concert with material mechanics and physical-chemical characteristics of the surface, were proposed as stable and consistent triggers to regulate complex architectures of tissues.

In this work, we exploited nanotechnologies for the production of tissues with specific function in Chapter 2. Here, patterned PDMS substrates are used as cell culture supports to promote organized tissue assemblies. In more details, our research group has previously demonstrated the powerful ordering effect on cells and cell population of topography. Therefore, we hypothesized that topographic signal could indirectly regulate tissue structure via cell ordering. Thus, we evaluated the effect of different kind of topographic pattern on the assembly of the architecture in the whole tissue thickness. In Chapter 3 we exploited the

complex arrays of signals displayed by endogenously synthesized and assembled matrices as systems to control stem cell behaviour. In particular, we focused our attention on stemness retention as a function of the spatial organization of cell derived matrices.

Finally, we brought further level of complexity in the initial condition of culture in order to exert an additional control over tissue assembly in Chapter 4. We examined in depth the dynamics of the multilayering process, and we found that the sharp edges of the culturing substrate profoundly affected this process. Boundaries act as meso-scale constraints that can trigger cell-mediated remodeling of the tissue. This, combined with surface nanopatterning, provides a useful tool to control the three-dimensional architecture of ECM-rich tissues.

1.9 Bibliography

1. C. M. Nelson, M. J. Bissell, Of extracellular matrix, scaffolds, and signaling: tissue architecture regulates development, homeostasis, and cancer. *Annu. Rev. Cell Dev. Biol.* **22**, 287–309 (2006).
2. J. S. Park *et al.*, The effect of matrix stiffness on the differentiation of mesenchymal stem cells in response to TGF- β . *Biomaterials*. **32**, 3921–3930 (2011).
3. M. Ventre, F. Causa, P. A. Netti, Determinants of cell-material crosstalk at the interface: towards engineering of cell instructive materials. *Journal of The Royal Society Interface*. **9**, 2017–2032 (2012).
4. M. J. Dalby, N. Gadegaard, R. O. C. Oreffo, Harnessing nanotopography and integrin–matrix interactions to influence stem cell fate. *Nature Materials*. **13**, 558–569 (2014).
5. K. A. Jansen *et al.*, A guide to mechanobiology: Where biology and physics meet. *Biochim. Biophys. Acta*. **1853**, 3043–3052 (2015).
6. M. Ventre, P. A. Netti, Engineering Cell Instructive Materials To Control Cell Fate and Functions through Material Cues and Surface Patterning. *ACS Applied Materials & Interfaces* (2016), doi:10.1021/acsami.5b08658.
7. S. Dupont *et al.*, Role of YAP/TAZ in mechanotransduction. *Nature*. **474**, 179–183 (2011).
8. K. Hamamura *et al.*, RhoA-Mediated Signaling in Mechanotransduction of Osteoblasts. *Connective Tissue Research*. **53**, 398–406 (2012).
9. N. Jain, K. V. Iyer, A. Kumar, G. V. Shivashankar, Cell geometric constraints induce modular gene-expression patterns via redistribution of HDAC3 regulated by actomyosin contractility. *Proceedings of the National Academy of Sciences*. **110**, 11349–11354 (2013).
10. S. Di Cio, J. E. Gautrot, Cell sensing of physical properties at the nanoscale: Mechanisms and control of cell adhesion and phenotype. *Acta Biomaterialia*. **30**, 26–48 (2016).
11. J. D. Humphries, N. R. Paul, M. J. Humphries, M. R. Morgan, Emerging properties of adhesion complexes: what are they and what do they do? *Trends in Cell Biology*. **25**, 388–397 (2015).
12. B. Geiger, K. M. Yamada, Molecular Architecture and Function of Matrix Adhesions. *Cold Spring Harbor Perspectives in Biology*. **3**, a005033–a005033 (2011).

13. J. T. Parsons, A. R. Horwitz, M. A. Schwartz, Cell adhesion: integrating cytoskeletal dynamics and cellular tension. *Nature Reviews Molecular Cell Biology*. **11**, 633–643 (2010).
14. S. Nicholson-Dykstra, H. N. Higgs, E. S. Harris, Actin Dynamics: Growth from Dendritic Branches. *Current Biology*. **15**, R346–R357 (2005).
15. L. B. Case, C. M. Waterman, Integration of actin dynamics and cell adhesion by a three-dimensional, mechanosensitive molecular clutch. *Nature Cell Biology* (2015), doi:10.1038/ncb3191.
16. D. W. Dumbauld *et al.*, How vinculin regulates force transmission. *Proceedings of the National Academy of Sciences*. **110**, 9788–9793 (2013).
17. A. del Rio *et al.*, Stretching Single Talin Rod Molecules Activates Vinculin Binding. *Science*. **323**, 638–641 (2009).
18. R. Janoštiak, A. C. Pataki, J. Brábek, D. Rösel, Mechanosensors in integrin signaling: The emerging role of p130Cas. *European Journal of Cell Biology*. **93**, 445–454 (2014).
19. C. K. Choi *et al.*, Actin and α -actinin orchestrate the assembly and maturation of nascent adhesions in a myosin II motor-independent manner. *Nature Cell Biology*. **10**, 1039–1050 (2008).
20. Y. Sawada *et al.*, Force Sensing by Mechanical Extension of the Src Family Kinase Substrate p130Cas. *Cell*. **127**, 1015–1026 (2006).
21. K. Bhadriraju *et al.*, Activation of ROCK by RhoA is regulated by cell adhesion, shape, and cytoskeletal tension. *Experimental Cell Research*. **313**, 3616–3623 (2007).
22. S. Gupta, N. Marcel, A. Sarin, G. V. Shivashankar, Role of Actin Dependent Nuclear Deformation in Regulating Early Gene Expression. *PLoS ONE*. **7**, e53031 (2012).
23. D. E. Ingber, N. Wang, D. Stamenović, Tensegrity, cellular biophysics, and the mechanics of living systems. *Reports on Progress in Physics*. **77**, 46603 (2014).
24. N. Wang, J. D. Tytell, D. E. Ingber, Mechanotransduction at a distance: mechanically coupling the extracellular matrix with the nucleus. *Nature Reviews Molecular Cell Biology*. **10**, 75–82 (2009).
25. B. Martinac, Mechanosensitive ion channels: molecules of mechanotransduction. *Journal of Cell Science*. **117**, 2449–2460 (2004).
26. S. Sukharev, F. Sachs, Molecular force transduction by ion channels - diversity and unifying principles. *Journal of Cell Science*. **125**, 3075–3083 (2012).

27. P. Paoli, E. Giannoni, P. Chiarugi, Anoikis molecular pathways and its role in cancer progression. *Biochimica et Biophysica Acta (BBA) - Molecular Cell Research*. **1833**, 3481–3498 (2013).
28. A. P. Gilmore, Anoikis. *Cell Death and Differentiation*. **12**, 1473–1477 (2005).
29. K. Anselme, L. Ploux, A. Ponche, Cell/Material Interfaces: Influence of Surface Chemistry and Surface Topography on Cell Adhesion. *Journal of Adhesion Science and Technology*. **24**, 831–852 (2010).
30. Z. Ma, Z. Mao, C. Gao, Surface modification and property analysis of biomedical polymers used for tissue engineering. *Colloids and Surfaces B: Biointerfaces*. **60**, 137–157 (2007).
31. R. Hassert, A. G. Beck-Sickinger, Tuning peptide affinity for biofunctionalized surfaces. *European Journal of Pharmaceutics and Biopharmaceutics*. **85**, 69–77 (2013).
32. D. Katti, R. Vasita, K. Shanmugam, Improved Biomaterials for Tissue Engineering Applications: Surface Modification of Polymers. *Current Topics in Medicinal Chemistry*. **8**, 341–353 (2008).
33. L. Bacakova, E. Filova, M. Parizek, T. Ruml, V. Svorcik, Modulation of cell adhesion, proliferation and differentiation on materials designed for body implants. *Biotechnology Advances*. **29**, 739–767 (2011).
34. J. M. Schakenraad, H. J. Busscher, C. R. H. Wildevuur, J. Arends, The influence of substratum surface free energy on growth and spreading of human fibroblasts in the presence and absence of serum proteins. *Journal of Biomedical Materials Research*. **20**, 773–784 (1986).
35. D. J. Iuliano, S. S. Saavedra, G. A. Truskey, Effect of the conformation and orientation of adsorbed fibronectin on endothelial cell spreading and the strength of adhesion. *Journal of Biomedical Materials Research*. **27**, 1103–1113 (1993).
36. K. Webb, V. Hlady, P. A. Tresco, Relative importance of surface wettability and charged functional groups on NIH 3T3 fibroblast attachment, spreading, and cytoskeletal organization. *J. Biomed. Mater. Res.* **41**, 422–430 (1998).
37. M. S. Lord *et al.*, The effect of silica nanoparticulate coatings on serum protein adsorption and cellular response. *Biomaterials*. **27**, 4856–4862 (2006).
38. M. B. Hovgaard, K. Rechendorff, J. Chevallier, M. Foss, F. Besenbacher, Fibronectin Adsorption on Tantalum: The Influence of Nanoroughness. *The Journal of Physical Chemistry B*. **112**, 8241–8249 (2008).

39. A. Dolatshahi-Pirouz *et al.*, Fibronectin Adsorption, Cell Adhesion, and Proliferation on Nanostructured Tantalum Surfaces. *ACS Nano*. **4**, 2874–2882 (2010).
40. M. Vicente-Manzanares, A. R. Horwitz, Adhesion dynamics at a glance. *Journal of Cell Science*. **124**, 3923–3927 (2011).
41. Y. Hu, Z. Wang, Z. Weng, M. Yu, D. Wang, Bio-inspired hierarchical patterning of silicon by laser interference lithography. *Applied Optics*. **55**, 3226 (2016).
42. K.-S. Lee, R. H. Kim, D.-Y. Yang, S. H. Park, Advances in 3D nano/microfabrication using two-photon initiated polymerization. *Progress in Polymer Science*. **33**, 631–681 (2008).
43. J. O. Gallagher, K. F. McGhee, C. D. W. Wilkinson, M. O. Riehle, Interaction of animal cells with ordered nanotopography. *IEEE Transactions on Nanobioscience*. **1**, 24–28 (2002).
44. J. Christopher Love, D. Wolfe, G. Whitesides, in *Dekker Encyclopedia of Nanoscience and Nanotechnology, Second Edition - Six Volume Set (Print Version)*, J. Schwarz, C. Contescu, Eds. (CRC Press, 2004; <http://www.crcnetbase.com/doi/abs/10.1201/9781439834398.ch174>).
45. C. Y. Hui, A. Jagota, Y. Y. Lin, E. J. Kramer, Constraints on Microcontact Printing Imposed by Stamp Deformation. *Langmuir*. **18**, 1394–1407 (2002).
46. E. Delamarche, H. Schmid, B. Michel, H. Biebuyck, Stability of molded polydimethylsiloxane microstructures. *Advanced Materials*. **9**, 741–746 (1997).
47. Y. Xia, G. M. Whitesides, Extending Microcontact Printing as a Microlithographic Technique. *Langmuir*. **13**, 2059–2067 (1997).
48. H.-W. Li, B. V. O. Muir, G. Fichet, W. T. S. Huck, Nanocontact Printing: A Route to Sub-50-nm-Scale Chemical and Biological Patterning. *Langmuir*. **19**, 1963–1965 (2003).
49. Y. Xia, G. M. Whitesides, Soft Lithography. *Angewandte Chemie International Edition*. **37**, 550–575 (1998).
50. M. D. Austin *et al.*, Fabrication of 5 nm linewidth and 14 nm pitch features by nanoimprint lithography. *Applied Physics Letters*. **84**, 5299 (2004).
51. H. Schiff, Nanoimprint lithography: An old story in modern times? A review. *Journal of Vacuum Science & Technology B: Microelectronics and Nanometer Structures*. **26**, 458 (2008).
52. R. D. Piner, “Dip-Pen” Nanolithography. *Science*. **283**, 661–663 (1999).

53. K.-B. Lee, S.-J. Park, C. A. Mirkin, J. C. Smith, M. Mrksich, Protein Nanoarrays Generated By Dip-Pen Nanolithography. *Science*. **295**, 1702–1705 (2002).
54. H. Jiang, S. I. Stupp, Dip-Pen Patterning and Surface Assembly of Peptide Amphiphiles. *Langmuir*. **21**, 5242–5246 (2005).
55. N. Moldovan, K.-H. Kim, H. D. Espinosa, Design and Fabrication of a Novel Microfluidic Nanoprobe. *Journal of Microelectromechanical Systems*. **15**, 204–213 (2006).
56. S. Lenhart, P. Sun, Y. Wang, H. Fuchs, C. A. Mirkin, Massively Parallel Dip-Pen Nanolithography of Heterogeneous Supported Phospholipid Multilayer Patterns. *Small*. **3**, 71–75 (2007).
57. S. H. Lim, X. Y. Liu, H. Song, K. J. Yarema, H.-Q. Mao, The effect of nanofiber-guided cell alignment on the preferential differentiation of neural stem cells. *Biomaterials*. **31**, 9031–9039 (2010).
58. J. Xie *et al.*, The differentiation of embryonic stem cells seeded on electrospun nanofibers into neural lineages. *Biomaterials*. **30**, 354–362 (2009).
59. L. He *et al.*, Synergistic effects of electrospun PLLA fiber dimension and pattern on neonatal mouse cerebellum C17.2 stem cells. *Acta Biomaterialia*. **6**, 2960–2969 (2010).
60. M. Massumi *et al.*, The Effect of Topography on Differentiation Fates of Matrigel-Coated Mouse Embryonic Stem Cells Cultured on PLGA Nanofibrous Scaffolds. *Tissue Engineering Part A*. **18**, 609–620 (2012).
61. J. M. Dang, K. W. Leong, Myogenic Induction of Aligned Mesenchymal Stem Cell Sheets by Culture on Thermally Responsive Electrospun Nanofibers. *Advanced Materials*. **19**, 2775–2779 (2007).
62. H. Peng *et al.*, Electrospun biomimetic scaffold of hydroxyapatite/chitosan supports enhanced osteogenic differentiation of mMSCs. *Nanotechnology*. **23**, 485102 (2012).
63. B. M. Baker, R. L. Mauck, The effect of nanofiber alignment on the maturation of engineered meniscus constructs. *Biomaterials*. **28**, 1967–1977 (2007).
64. W. Chen *et al.*, Nanotopography Influences Adhesion, Spreading, and Self-Renewal of Human Embryonic Stem Cells. *ACS Nano*. **6**, 4094–4103 (2012).
65. S. Krishnamoorthy, C. Hinderling, H. Heinzelmann, Nanoscale patterning with block copolymers. *Materials Today*. **9**, 40–47 (2006).

66. J. Y. Lim *et al.*, Osteoblast Adhesion on Poly(L-lactic Acid)/Polystyrene Demixed Thin Film Blends: Effect of Nanotopography, Surface Chemistry, and Wettability. *Biomacromolecules*. **6**, 3319–3327 (2005).
67. H. L. Khor *et al.*, Response of Cells on Surface-Induced Nanopatterns: Fibroblasts and Mesenchymal Progenitor Cells. *Biomacromolecules*. **8**, 1530–1540 (2007).
68. R. Glass, M. M. Iler, J. P. Spatz, Block copolymer micelle nanolithography. *Nanotechnology*. **14**, 1153–1160 (2003).
69. T. Lohmüller *et al.*, *Biointerphases*, in press, doi:10.1116/1.3536839.
70. K. S. Masters, K. S. Anseth, in *Advances in Chemical Engineering* (Elsevier, 2004; <http://linkinghub.elsevier.com/retrieve/pii/S0065237703290025>), vol. 29, pp. 7–46.
71. R. P. Sebra, S. K. Reddy, K. S. Masters, C. N. Bowman, K. S. Anseth, Controlled polymerization chemistry to graft architectures that influence cell-material interactions. *Acta Biomaterialia*. **3**, 151–161 (2007).
72. M. J. P. Biggs, R. G. Richards, N. Gadegaard, C. D. W. Wilkinson, M. J. Dalby, Regulation of implant surface cell adhesion: characterization and quantification of S-phase primary osteoblast adhesions on biomimetic nanoscale substrates. *Journal of Orthopaedic Research*. **25**, 273–282 (2007).
73. M. J. Dalby *et al.*, Nanotopographical stimulation of mechanotransduction and changes in interphase centromere positioning. *Journal of Cellular Biochemistry*. **100**, 326–338 (2007).
74. P. M. Tsimbouri *et al.*, Using Nanotopography and Metabolomics to Identify Biochemical Effectors of Multipotency. *ACS Nano*. **6**, 10239–10249 (2012).
75. D.-H. Kim *et al.*, Mechanosensitivity of fibroblast cell shape and movement to anisotropic substratum topography gradients. *Biomaterials*. **30**, 5433–5444 (2009).
76. A. I. Teixeira *et al.*, The effect of environmental factors on the response of human corneal epithelial cells to nanoscale substrate topography. *Biomaterials*. **27**, 3945–3954 (2006).
77. J. James, E. D. Goluch, H. Hu, C. Liu, M. Mrksich, Subcellular curvature at the perimeter of micropatterned cells influences lamellipodial distribution and cell polarity. *Cell Motility and the Cytoskeleton*. **65**, 841–852 (2008).
78. R. McBeath, D. M. Pirone, C. M. Nelson, K. Bhadriraju, C. S. Chen, Cell Shape, Cytoskeletal Tension, and RhoA Regulate Stem Cell Lineage Commitment. *Developmental Cell*. **6**, 483–495 (2004).

79. X. Yao, R. Peng, J. Ding, Effects of aspect ratios of stem cells on lineage commitments with and without induction media. *Biomaterials*. **34**, 930–939 (2013).
80. D. Zhang, K. A. Kilian, The effect of mesenchymal stem cell shape on the maintenance of multipotency. *Biomaterials*. **34**, 3962–3969 (2013).
81. M. J. Dalby *et al.*, The control of human mesenchymal cell differentiation using nanoscale symmetry and disorder. *Nature Materials*. **6**, 997–1003 (2007).
82. F. Kantawong *et al.*, Whole proteome analysis of osteoprogenitor differentiation induced by disordered nanotopography and mediated by ERK signalling. *Biomaterials*. **30**, 4723–4731 (2009).
83. R. J. McMurray *et al.*, Nanoscale surfaces for the long-term maintenance of mesenchymal stem cell phenotype and multipotency. *Nature Materials*. **10**, 637–644 (2011).
84. K. V. Iyer, S. Pulford, A. Mogilner, G. V. Shivashankar, Mechanical Activation of Cells Induces Chromatin Remodeling Preceding MKL Nuclear Transport. *Biophysical Journal*. **103**, 1416–1428 (2012).
85. Y.-C. Poh *et al.*, Dynamic force-induced direct dissociation of protein complexes in a nuclear body in living cells. *Nature Communications*. **3**, 866 (2012).
86. J. D. Pajerowski, K. N. Dahl, F. L. Zhong, P. J. Sannak, D. E. Discher, Physical plasticity of the nucleus in stem cell differentiation. *Proceedings of the National Academy of Sciences*. **104**, 15619–15624 (2007).
87. S. Talwar, A. Kumar, M. Rao, G. I. Menon, G. V. Shivashankar, Correlated Spatio-Temporal Fluctuations in Chromatin Compaction States Characterize Stem Cells. *Biophysical Journal*. **104**, 553–564 (2013).
88. E. Meshorer *et al.*, Hyperdynamic Plasticity of Chromatin Proteins in Pluripotent Embryonic Stem Cells. *Developmental Cell*. **10**, 105–116 (2006).
89. D. Bhattacharya, S. Talwar, A. Mazumder, G. V. Shivashankar, Spatio-Temporal Plasticity in Chromatin Organization in Mouse Cell Differentiation and during *Drosophila* Embryogenesis. *Biophysical Journal*. **96**, 3832–3839 (2009).
90. Q. Li, A. Kumar, E. Makhija, G. V. Shivashankar, The regulation of dynamic mechanical coupling between actin cytoskeleton and nucleus by matrix geometry. *Biomaterials*. **35**, 961–969 (2014).
91. J. Swift *et al.*, Nuclear Lamin-A Scales with Tissue Stiffness and Enhances Matrix-Directed Differentiation. *Science*. **341**, 1240104–1240104 (2013).

92. Y. Li *et al.*, Biophysical Regulation of Histone Acetylation in Mesenchymal Stem Cells. *Biophysical Journal*. **100**, 1902–1909 (2011).
93. T. L. Downing *et al.*, Biophysical regulation of epigenetic state and cell reprogramming. *Nature Materials*. **12**, 1154–1162 (2013).
94. D.-H. Kim *et al.*, Nanoscale cues regulate the structure and function of macroscopic cardiac tissue constructs. *Proc. Natl. Acad. Sci. U.S.A.* **107**, 565–570 (2010).
95. M. Iannone *et al.*, Nanoengineered Surfaces for Focal Adhesion Guidance Trigger Mesenchymal Stem Cell Self-Organization and Tenogenesis. *Nano Letters*. **15**, 1517–1525 (2015).
96. S. Koutsopoulos, S. Zhang, Long-term three-dimensional neural tissue cultures in functionalized self-assembling peptide hydrogels, Matrigel and Collagen I. *Acta Biomaterialia*. **9**, 5162–5169 (2013).
97. A. Subramanian, U. M. Krishnan, S. Sethuraman, Fabrication, Characterization and In Vitro Evaluation of Aligned PLGA–PCL Nanofibers for Neural Regeneration. *Annals of Biomedical Engineering*. **40**, 2098–2110 (2012).
98. Y.-D. Lin *et al.*, *Science Translational Medicine*, in press, doi:10.1126/scitranslmed.3003841.
99. S. Badylak, D. Freytes, T. Gilbert, Extracellular matrix as a biological scaffold material: Structure and function. *Acta Biomaterialia*. **5**, 1–13 (2009).
100. J. E. Reing *et al.*, Degradation products of extracellular matrix affect cell migration and proliferation. *Tissue Eng Part A*. **15**, 605–614 (2009).
101. H. Lu, T. Hoshiba, N. Kawazoe, G. Chen, Autologous extracellular matrix scaffolds for tissue engineering. *Biomaterials*. **32**, 2489–2499 (2011).
102. N. Matsuda, T. Shimizu, M. Yamato, T. Okano, Tissue Engineering Based on Cell Sheet Technology. *Advanced Materials*. **19**, 3089–3099 (2007).
103. N. L’Heureux, S. Pâquet, R. Labbé, L. Germain, F. A. Auger, A completely biological tissue-engineered human blood vessel. *FASEB J*. **12**, 47–56 (1998).

Chapter 2

2.1 Introduction

Tissues usually have to accomplish multiple and complex scopes *in vivo*, which are of biological, biochemical, mechanical and structural nature. To achieve this level of functionality, tissues are characterized by the presence of adaptive and responsive entities, like cells, proteins, sugars, lipids, that are precisely assembled in the space, thus constituting an organized architecture. For instance, arrays of fibres orderly arranged in space and embedded in a gel-like matrix, endow biological tissues with mechanical properties that perfectly withstand physiological loads. Even a modest alteration of the native structure might have a detrimental effect on the stability of tissues thus impairing their functionality (1, 2). Within the classical Tissue Engineering scheme, strategies aiming at regenerating tissues must lead to a microarchitecture that replicates the spatial features observed *in vivo* (3, 4). Signals in the form of biochemical moieties, topographic patterns or mechanical properties need to be clearly presented to cells to control the processes of biosynthesis and protein spatial assembly (5–7). In order to be effective, these signals must act on a cellular (micron scale) and sub-cellular/receptor (nano scale) level. However, encoding micro- or nano-metric patterns of signals in three-dimensional (3D) bulky scaffolds is not straightforward. First, micro- and nano-fabrication technologies are able to imprint patterns of signals with the adequate spatial resolution and on large areas, but they are most suitable in two-dimensional contexts (8). Second, the fabrication of 3D patterns can be performed with consolidated technologies (e.g. 3D printing, bio-plotting), but the

spatial resolution that can be achieved is well above that required for a proper guidance on a protein/cellular level (9). More sophisticated technologies, as multiphoton lithography, can produce 3D structures with submicrometric resolution (10). However, the implementation of these techniques requires the use of very expensive equipment and time-consuming processes. Furthermore, the choice of biocompatible materials that can be used with these technology is limited.

Scaffold-free approaches represent an alternative path to the above-mentioned techniques as they envisage the cultivation of cells in specific conditions, that enable the processes of cell self-organization and matrix biosynthesis, ultimately generating viable tissues *in vitro* (11). Among the various culturing conditions, planar assemblies of cells and matrices have been widely investigated (12). However, the cell-matrix membranes thus produced are of scarce clinical interest as they are very compliant and cannot withstand physiological loads. Thicker tissues can be produced by stacking a certain number of membranes one on the top of the other and by allowing the structure to consolidate, owing to the spontaneous cellular sheet self-organization (13, 14). Indeed, preliminary examples of *in vivo* implantation of multi-layered membranes have been reported. For instance, smooth muscle and endothelial progenitor cells bilayers were used to treat a rat ischemic myocardium. The structurally mature patch improved myocardial functions and initiated robust angiogenesis (15). In a different application, Lin et al. demonstrated that a three-layer adipose stem cell derived matrix enhanced the healing of a full thickness skin wound model (16). Owing to the promising performances of cell/tissue sheet in both *in vitro* and *in vivo* applications, efforts were made to control cell positioning and the spatial assembly of the secreted extracellular matrix (ECM). Along this line, surface patterning with biochemical or topographical signals proved to be effective in controlling cell adhesion processes and biosynthetic events (17). Typically, linear gratings are encoded on material surface in order to orient cells and matrix in a common direction (18, 19). The resulting sheet displays aligned ECM fibres and an anisotropic mechanical behaviour consequently (20). This notwithstanding, in order to have a tight control on the 3D arrangement of the proteinaceous micro constituents it is necessary that the ordering effect of the patterned signal is transmitted throughout the thickness. However, while some authors demonstrated that the surface patterning induces a cell/matrix alignment and such an alignment is maintained within the membrane, other report different trends (20–22).

Given the importance of tissue microarchitecture in affecting and possibly dictating tissue functions, we designed an experimental campaign to investigate the role of the

guiding effect provided by material patterning on cell organization and matrix structure. To this aim we cultivated MC3T3-E1 cells on linear pattern exhibiting long-range order or on non-linear pattern with short-range order. We characterized the *in vitro* tissueogenesis and the spatial assembly of the tissue sheets constituents by means of confocal and multiphoton microscopy. Finally, we characterized the mechanical properties of the *in vitro* generated tissues sheets in uniaxial traction tests and we related the response to the micro structural features of the tissues.

2.2 Materials and methods

2.2.1 Preparation of micropatterned substrates

Patterned substrates were obtained by replica molding of polydimethylsiloxane (PDMS, Sylgard 184, Dow Corning) on two different masters. We refer to linear substrates as those obtained from a polycarbonate master consisting of 1.5 cm^2 nanograted (700 nm ridges with $1.4 \text{ }\mu\text{m}$ pitch and 250 nm depth) (Fig. 1A). Non-linear substrates, instead, were obtained on SU-8 patterned master, produced with 2D laser printer (Heisenberg). The pattern consisted of an area of 1.5 cm^2 displaying channels with a groove and ridge width of $2 \text{ }\mu\text{m}$ and depth of $1 \text{ }\mu\text{m}$ arranged in a trapezoidal wave shape (Fig. 1B). Wave period is $495 \text{ }\mu\text{m}$ and the linear ramps are $255 \text{ }\mu\text{m}$. The two consecutive ramps are connected by a $20 \text{ }\mu\text{m}$ straight channel. Flat PDMS substrates were used as control and were produced by using a polystyrene dish as mold.

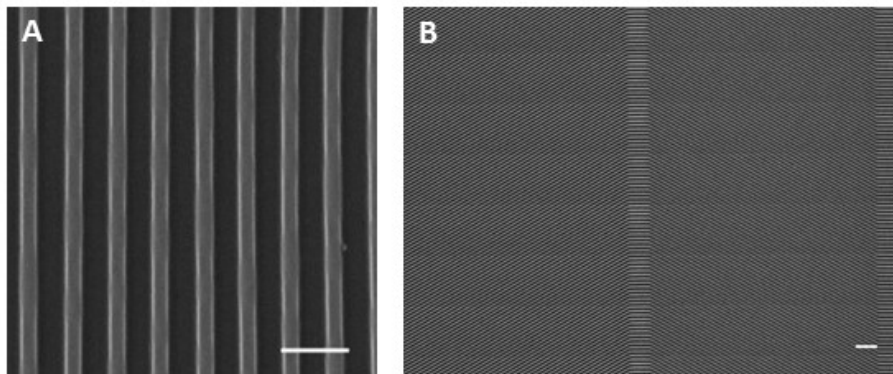


Fig. 1. Scanning Electron Micrograph of either linear (A) or non-linear patterned (B) substrate. Bars are $2 \text{ }\mu\text{m}$ and $20 \text{ }\mu\text{m}$ respectively.

PDMS was prepared by mixing elastomer base and curing agent at 10:1 weight ratio. The solution was degassed, poured onto the master and then cured at 60°C for 2 h. Cured PDMS substrates were treated with oxygen plasma in order to improve cell adhesion. Briefly, the treatment was performed with a Plasma Femto (Diener) equipped with 13.56 MHz 100 W power generator for the plasma excitation. Plasma exposure was 1 min and then substrates were sterilized by UV exposure for 30 min. Samples were then incubated with serum-supplemented culture medium overnight prior to cell culturing experiments.

2.2.2. Cell culture

MC3T3-E1 preosteoblasts (ATCC) were cultured in alpha MEM with deoxyribonucleosides, ribonucleosides and 2 mM L-glutamine, supplemented with 10% fetal bovine serum, penicillin (100 units ml⁻¹), streptomycin (100 mg ml⁻¹) (Gibco). The cells were incubated at 37 °C in a humidified atmosphere of 95% air and 5% CO₂. The culture medium was changed every two days. After 3 days of culture, cells were detached with trypsin/EDTA (0.25% w/v trypsin/0.02 mM EDTA) (Gibco) and seeded on linear, non-linear and flat substrates.

Collagen rich tissue sheets were produced by seeding cells at the density of 2·10⁴ cells cm⁻² (sub-confluent) on the linear pattern, non-linear pattern and flat substrates, and cultivating the cells for 2 weeks in presence of 25 µg/mL of ascorbic acid.

The experiments concerning the inhibition of cell contractility were performed by using culture media supplemented either with ML7 (myosin light chain kinase inhibitor, Sigma), previously solubilized in dimethyl sulfoxide, at the final concentration of 20µM, or with Blebbistatin (Sigma) in a DMSO (Sigma) solution at a final concentration of 50µM. ML7 or Blebbistatin supplemented media were used after 1 week of culture in standard condition. Afterwards, inhibitors were supplemented to media that were changed 3 times per week.

2.2.3 Tissue staining and image acquisition

After 2 weeks cells were fixed with 4% paraformaldehyde for 20 min and then permeabilized with 0.1% Triton X-100 (Sigma) in phosphate-buffered saline (PBS). Samples were blocked in PBS/bovine serum albumin 1% solution (Sigma) for 30 min, to avoid non-specific binding. Actin staining was performed by incubating samples with TRITC-phalloidin (Sigma) in PBS for 30 min at room temperature. Then, for nuclear staining, samples were incubated with a 1:10000 solution of SYTOX Green (Invitrogen, 10 mg/mL in dimethyl sulfoxide) in PBS for 5 min at room temperature. Samples were thoroughly rinsed in PBS and mounted on glass slides.

Fluorescent images of actin bundles and nuclear DNAs were collected with a Leica TCS SP 5 (Leica Microsystems). Samples were excited with 543 nm (actin) and 488 nm (nuclei) laser lines, and the emissions were collected in the 560–650 nm and 500–530 nm ranges, respectively. Collagen fibres were visualized through second harmonic generation

(SHG) microscopy, i.e. samples were excited with a femtosecond laser (Coherent) at 840 nm and the emission was collected in the 415-425 nm interval.

2.2.4 Cell-collagen structure characterization

In order to gain a better insight into cell and collagen arrangement within the tissue sheet, z-stacks of tile-scans of the whole sample were collected, thus obtaining large digital volumes of the tissues sheets. Tile-scans were obtained by a digital stitching of 6 images organized in a 3x2 grid. Image analysis of the stacked confocal micrographs was performed by running OrientationJ plug-in in Fiji software (23). The plug-in measures the distribution of actin filaments or collagen fibres direction. To assess whether variations in the distribution of orientations occurred through the tissue thickness, the algorithm was applied to the basal and apical plane. In more details, tile-scans of the basal or apical plane were divided into 6 non-overlapping regions (region of interest) and the algorithm was applied to each region. We specified the following parameters for the algorithm: Gaussian window dimension $\sigma=1.5$ pixel; Min. coherency = 20%; Min. energy=2%. Min. coherency and energy represent the anisotropy and the orientation degree respectively. Briefly, coherency is in a 0 – 100% range, in which the highest value indicates highly oriented structures and the lowest one the isotropic areas. Energy is a value correlated to the intensity of each pixel of the entire image, higher values correspond to pixels in an oriented structure (24).

The nuclear aspect ratio of cells in the basal or apical plane of tissues grown on patterned or flat substrates, was evaluated with the command “analyse particles” in Fiji. Briefly, digital images acquired with a 63x objective lens and containing the nucleus signal were binarized. Then the “analyse particle” command was run and the “shape descriptor” data were stored. Significant differences between basal or apical cells within each group (linear, flat or non-linear) were determined with t-test written in Matlab (The Mathworks). Significant differences among groups, i.e. either basal or apical cells on linear, flat or non-linear groups, were assessed with a one-way ANOVA test followed by a Tukey’s post-hoc test written in Matlab. *p* values less than 0.05 were considered significant.

To visualize the apical collagen ultrastructure with SEM, a decellularization protocol was performed. Briefly, tissues were glued on the edges to the PDMS substrates with Twinsil glue (Picodent) in order to prevent tissue tearing during handling. Then a 2 ml TrypLE express 1X (Gibco) solution was added to each sample for 20 min, to allow cell detachment yet preserving matrix structure. Afterwards, samples were rinsed twice with

dH₂O for 20 min on a tilting plate at 30 rpm. In order to purge out cellular remnants, samples were covered with a 0.69% Trizma base (Sigma), 0.26% EDTA (Sigma) and 1% Triton X-100 (Sigma) solution. After 1h, samples were rinsed thoroughly with dH₂O and then left on a tilting plate at 30 rpm overnight. Decellularized tissue sheets were dehydrated through an ascending series of water/ethanol solutions (10% steps, 10 min each) ending in 100% ethanol. Ethanol soaked samples were dried in a critical point dryer (EM CPD300, Leica). Subsequently, samples were coated with a 10 nm gold layer with a 208hr sputter coater (Cressington). Scanning electron microscopy (SEM) imaging was performed by means of an Ultra Plus Scanning Electron Microscope (Zeiss, Germany) with a 10 kV tension.

To quantify the amount of collagen produced on the non-linear and flat substrates, we used the Sircol Assay (Biocolor) on samples cultured for 2 weeks. Briefly, samples were digested by pepsin (0.1 mg/ml in 0.5M acetic acid) overnight incubation at 4 °C. Afterwards, the collagen solution was isolated and concentrated. This reacted with the dye to form the complex. 1 ml of alkali reagent was added and mixed to dissolve bound dye and samples were assayed at 540 nm on a Victor³ spectrophotometer (Perkin Elmer). Collagen standards were used as controls

2.2.5 Mechanical testing

For mechanical testing, samples were produced by sheets overlaying. More specifically, cells were cultivated on the patterned or flat PDMS substrates and in presence of a polycarbonate frame (PC, Millipore) with a dog-bone shaped hole in the centre (Fig. 2A). After two weeks of culture, sheets were mechanically peeled off by pulling the PC frame and two sheets were stacked one on the top of the other (Fig. 2B).

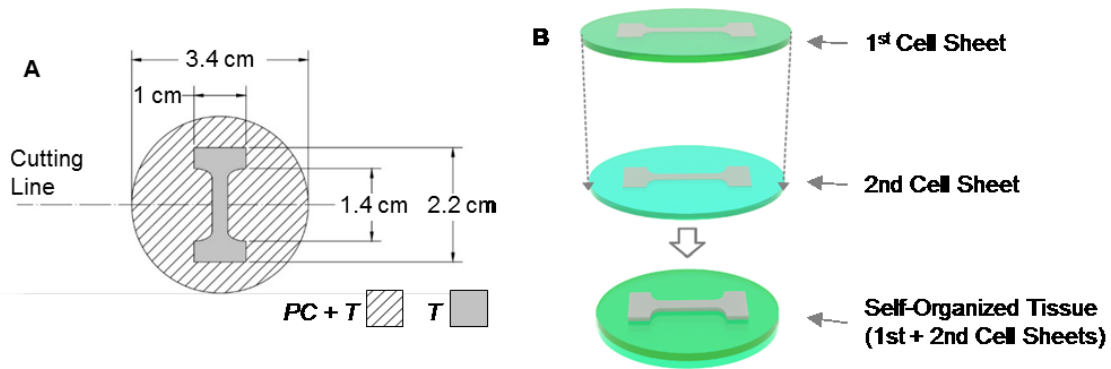


Fig. 2. A) Tissue grown on a polycarbonate (PC) frame. A dog-bone shaped hole is carved in the midpart of the PC frame thus allowing the tissue (grey) to be in close contact with the underlying pattern. This tissue is intertwined with the one growing on the PC frame (PC+T, diagonal hatch), thus forming a continuum. Prior to traction testing, the composite structure was mounted between the clamps of the traction machine and the frame was cut along the “cutting line”. B) Schematic representation of the tissue overlapping process by which the self-organized tissue is obtained (bottom).

To allow the self-assembly of the tissue sheets, the multilayers were supplemented with 200 μ l of cell culture medium and placed in the incubator for 30 min. Afterwards, 2 ml of medium were added to the dishes, which remained in culture for additional 1 week in the same conditions.

The tissues produced in the dog-bone shaped frames were gently removed from the dish. Afterwards, the samples were mounted between the clamps of a 2752 dynamometer (Instron). Before starting the uniaxial test, frame edges were cut in transversal direction, thus exposing only the cell and matrix assembly to the uniaxial stress. Cross-bar displacement speed was set at 5 mm/min and data acquisition rate was set at 100 ms.

The parameters strain at break, tensile strength, initial slope (i.e. slope of the stress-strain curve in the 0-0.05 interval), linear slope (i.e. slope of the linear part of the stress-strain curve) were extracted from the stress-strain charts. Significant differences between groups were assessed with a one-way ANOVA test written in Matlab (The Matworks) followed by a Tukey’s post-hoc test. p values less than 0.05 were considered significant.

2.3 Results

In order to assess how the 3D organization of cells and the de novo synthesized matrix is affected by the guiding effect of material signals, we cultivated MC3T3-E1 preosteoblasts on either anisotropic (linear) or isotropic (flat) PDMS substrates. PDMS has received much attention as a popular material for developing substrate platforms in mechanobiological applications, owing to its numerous advantages over other polymeric materials. More specifically, PDMS is characterized by tunable elastomeric properties, low cost, gas permeability, optical transparency, low auto fluorescence, nano-scale precision, and high fidelity of feature production when cast on micro- and nano-fabricated masters (25). However, the use of PDMS for cell culture often poses several challenges over long-term studies. The intrinsic high surface hydrophobicity of PDMS has been identified by many studies to be the primary factor that causes poor cell adhesion. Surface treatment with oxygen plasma has been proposed as a convenient strategy to improve the PDMS surface hydrophilicity (26). This treatment allows the PDMS surface to adsorb proteins (27) that may enhance cell adhesion, facilitating long-term cell studies (28). If kept in a wet environment, surface hydrophilicity is conserved for a long period (26).

We used MC3T3-E1 preosteoblasts as they are a stable cell line that is able to synthesize abundant collagen when supplemented with ascorbic acid (18). An issue may arise on whether MC3T3 can undergo to an osteoblastic differentiation during long term culture. However, Quarles et al. demonstrated that MC3T3-E1 cell undergo to osteoblast differentiation only in presence of both ascorbate and β -glycerol phosphate. In the absence β -glycerol phosphate, MC3T3-E1 cells express low levels of alkaline phosphatase in long term cultures and fail to express a fully differentiated osteoblast phenotype as evidenced by the inability to form and mineralize extracellular matrix. Therefore, β -glycerol phosphate is absolutely required for mineralization in ascorbate-treated cultures (29). MC3T3-E1 cells, in their preosteoblastic state, form thick (around 30 μ m) sheets *in vitro* predominantly constituted by ECM, as opposed to conventional cell-sheets almost entirely constituted by cells. Thus, we will refer to the cell-matrix assemblies generated *in vitro* as tissue sheets rather than cell sheets. To understand how MC3T3-E1 perceived the topographic signal in an environment in which both cell-cell contact and cell-matrix interactions are non-negligible, as well as how such a signal could be transferred through the tissue sheet

thickness, we investigated tissue sheets microarchitecture after one week (short term) and two weeks (long term) of culture.

In short term cultures, cells perceived the topographic signal and formed a layer of closely packed cells, coaligned to the pattern direction (Fig. 3A). Collagen fibres also displayed a similar coalignment to the pattern (Fig. 3B). On flat surfaces, cell and collagen did not display the same level of packing having randomly oriented cells with a polygonal shape (Fig. 3C, D).

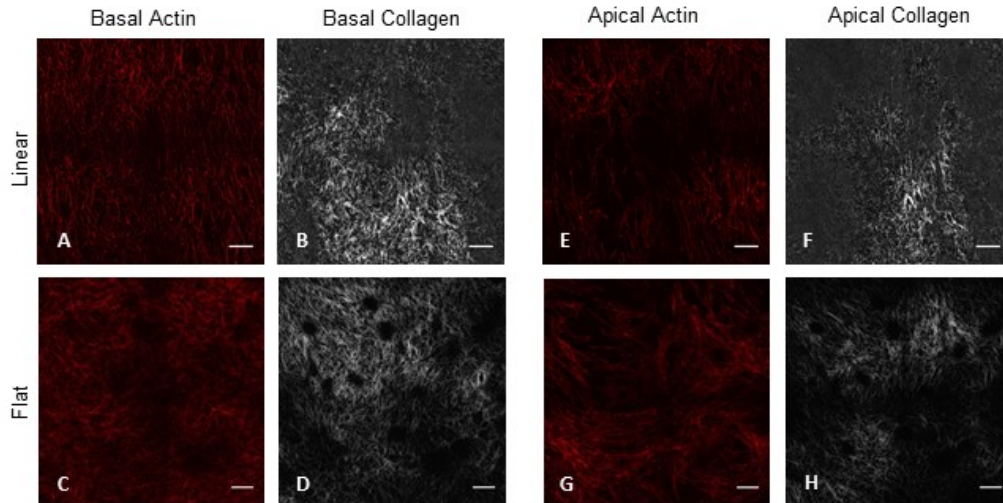


Fig. 3. Tissue sheets grown on linear patterned or flat substrates after 1 week of culture. Confocal images of actin bundles stained with phalloidin (A, C, E, G) and collagen acquired with SHG (B, D, F, H). Bars 100 μm .

In both cases, we observed a tendency of the cells to get arranged in the form of bilayers, with basal cells in contact with the PDMS and a top apical layer separated by a thin ECM core. However, the bilayers were not homogeneously populated, especially in the apical region (Fig. 3E-H). Culturing cells for an additional week allowed the cells to form a more homogeneous apical plane that was separated by the basal plane by a thick collagen-rich stratum containing few and sparse cells. We observed markedly different cell and ECM organizations according to underlying surface topography (Fig. 4).

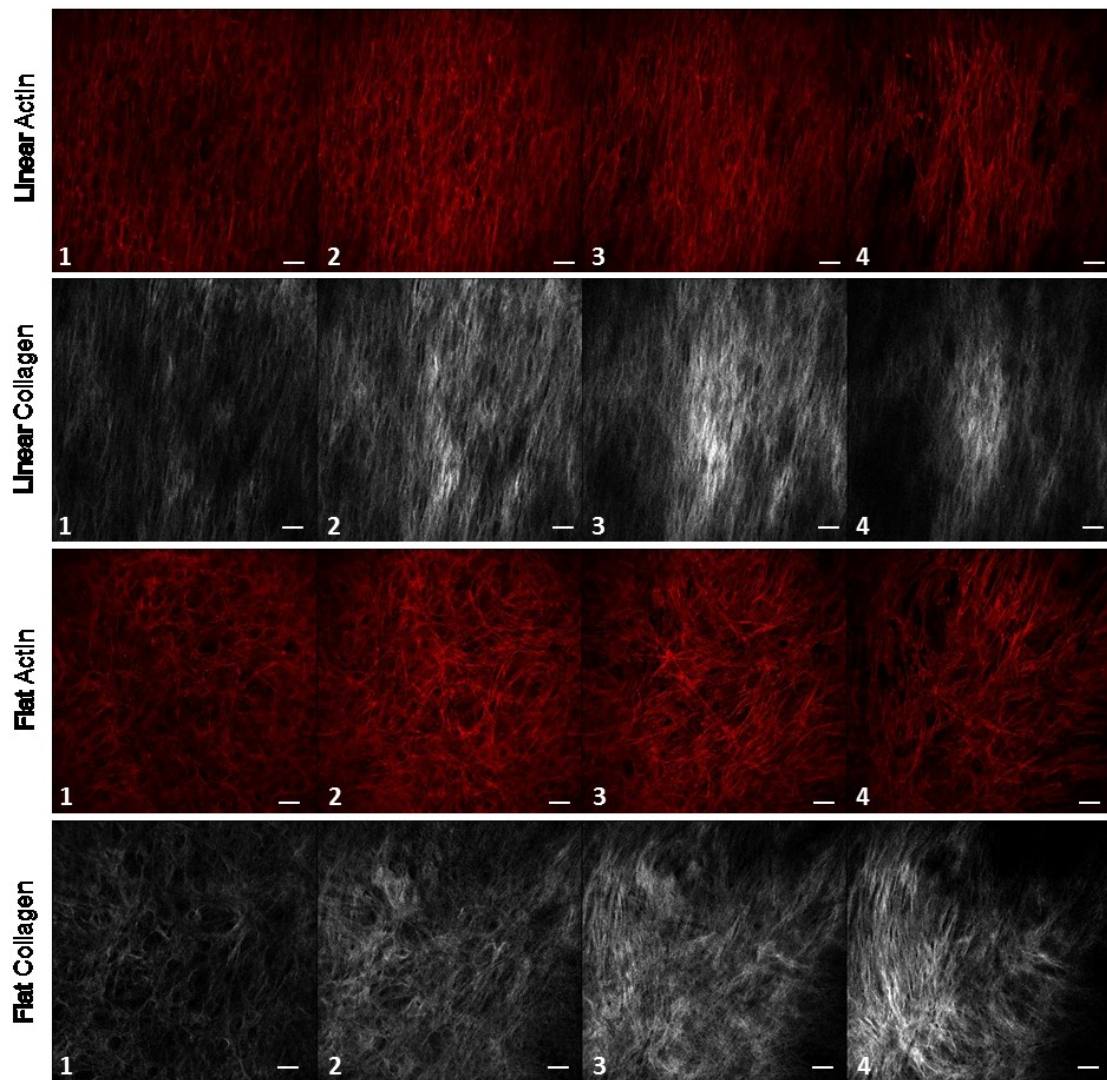


Fig. 4. Montage of tissue sheet z-stacks. Tissues are approximately $20\ \mu\text{m}$ thick. Montages are obtained with slices spaced of approximately $7\ \mu\text{m}$. The first slice is the basal plane (1); the last slice is the apical plane (4). Z-stacks are obtained from confocal images of actin bundles stained with phalloidin and collagen acquired with SHG. Bars $50\ \mu\text{m}$.

More specifically, confocal images of cells cultivated on linear patterns, revealed that cells on the basal plane displayed a spindle-like morphology with the major axis coaligned with the pattern direction (Fig. 5A). Similarly, collagen fibres adjacent to the basal plane were coaligned with cells and the pattern direction (Fig. 5B). Image analysis of actin bundles (phalloidin) and collagen fibres (SHG) performed with OrientationJ confirmed our observation, i.e. distributions displayed peaks very close to the direction of the pattern (Fig. 5C). In particular, the distribution of collagen fibres was sharper with respect to that

of actin bundles. A very similar pattern of orientations was observed in the apical plane with both cells and collagen fibres coaligned with the basal plane (Fig. 5D and E). In this case, however, the distribution of orientations of actin and collagen was very similar, with almost overlapping, sharp peaks (Fig. 5F).

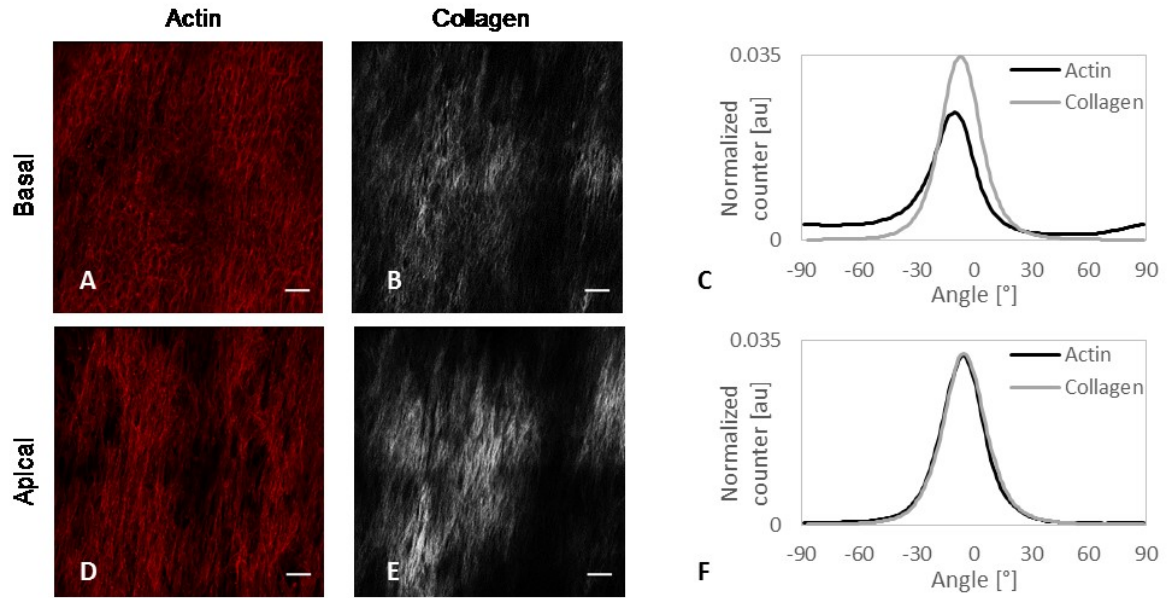


Fig. 5. Tissue sheets grown on linear patterns. Confocal images of actin bundles stained with phalloidin (A, D) and collagen acquired with SHG (B, E). Pattern direction is the vertical axis. Bars 100 μm . Distribution of orientations, determined with the OrientationJ plugin, of the actin (black) and collagen (grey) signals of the basal (C) and the apical (F) plane. Pattern direction is centred at 0° .

The strong similarity of the distributions of orientations of the basal collagen and apical actin may suggest that the de novo synthesized collagen acts as a guidance for the apical plane and that the ordering effect exerted by the topographic signal could propagate throughout the tissue thickness. To verify this, we analysed cell and collagen orientation of tissue sheets grown on flat substrates. In this case, cells residing on the basal plane showed a spread morphology with no specific orientations (Fig. 6A). Surprisingly, the orientation of collagen fibrils did not follow that of the cells (Fig. 6B), an occurrence that was confirmed by the analysis of orientations (Fig. 6C). The arrangement of cells and collagen in the apical plane followed a different trend. First, we did not observe a unique direction of orientation. Second, cells formed patches of coaligned cells (Fig. 6D) and the corresponding collagen fibres retained a similar orientation as that of the cells (Fig. 6E). In this case, the distribution of orientations of both actin and collagen showed several peaks (Fig. 6F).

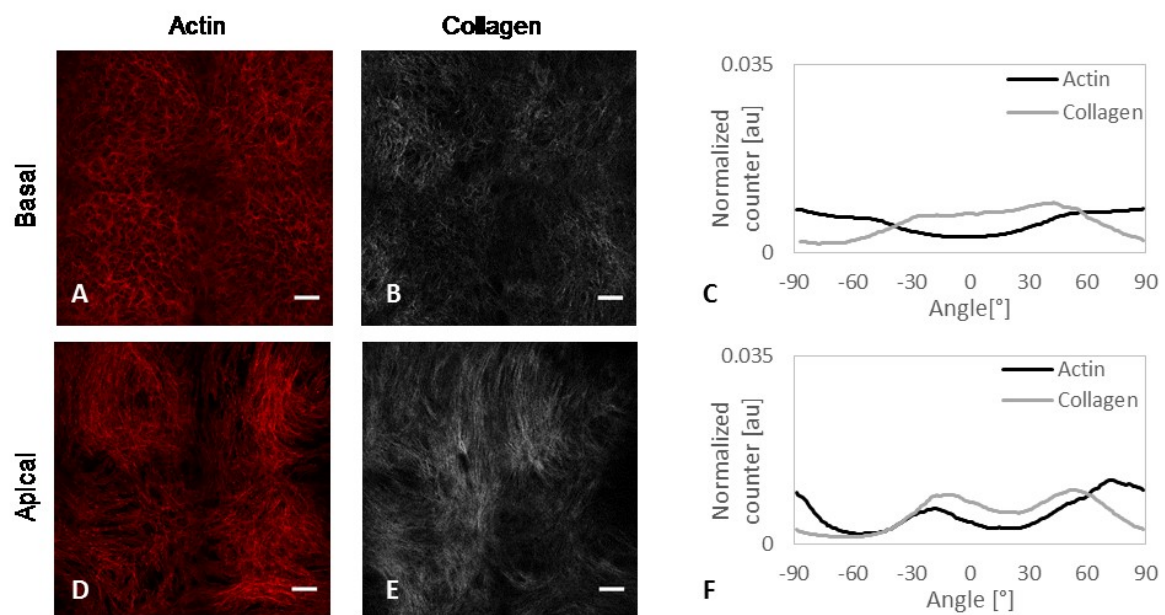


Fig. 6. Tissue sheets grown on flat surfaces. Confocal images of actin bundles stained with phalloidin (A, D) and collagen acquired with SHG (B, E). Bars 100 μm . Distribution of orientations, determined with the OrientationJ plugin, of the actin (black) and collagen (grey) signals of the basal (C) and the apical (F) plane.

Previous reports demonstrated that topographic patterns could exert an ordering effect on secreted proteins, such as collagen and fibronectin, where cells cultivated on flat surfaces produced randomly arranged fibres (18, 30). In our case, the distribution of the orientation of basal collagen fibres did not correlate with the orientation of basal cells, but it was similar to the distributions of both cells and collagen in the apical plane. This suggests that some sort of interactions occurred between the two planes, ultimately dictating the shape of the tissue sheet. In particular, we hypothesize that the contractile forces generated by the cells in the apical plane can remodel the underlying collagen owing to its compliant nature. Conversely, cells on the basal plane are firmly anchored to the stiff patterned substrate and exert a limited remodelling action on the basal collagen layer.

In order to better understand the mechanisms of matrix assembly, along with the role of cell-mediated remodelling in the process, we carried out cell cultures on wave-like, non-linear patterns whose shape and dimensions are depicted in Fig. 1.

We used such a pattern design as it introduces a discontinuity in the long-range order of linear patterns, resulting in a short-range order (495 μm) identified by two major direction of alignment. We then investigated whether the short-range order was maintained through the tissue thickness or it was affected by remodelling effects. In the first week of culture, cells in contact with the substrate formed a monolayer in which cell body was elongated and followed the wave-like contour of the pattern (Fig. 7A). Cells in the apical plane were present, but in a patch-like fashion thus forming a heterogeneously populated layer. This stated, we limited the image analysis on the basal actin and collagen in order to verify whether the non-linear pattern could still exert its ordering effect on a short-range. The distribution of actin orientations confirmed the qualitative observation, according to which actin fibres are oriented along two dominant directions, namely the pattern directions (Fig. 7C). Collagen in close proximity to the basal cell layer also displayed a wave-like configuration, however image analysis showed the presence of two broad peaks approximately corresponding to the actin peaks (Fig. 7B, C).

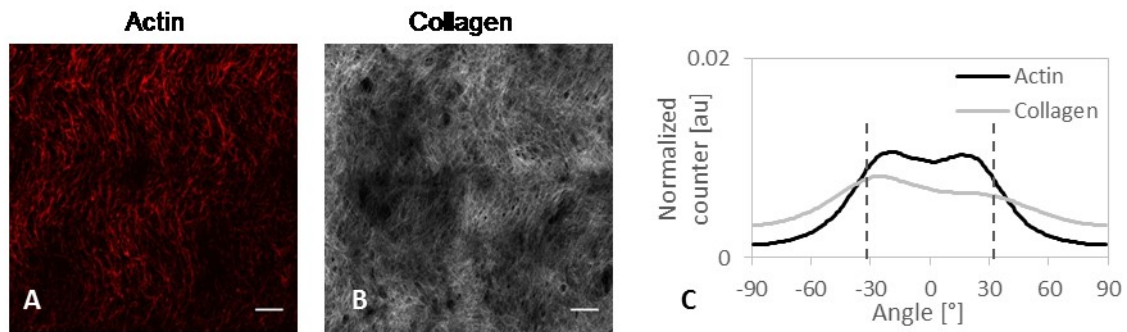


Fig. 7. Tissue sheets grown on non-linear surfaces after 1 week of culture. Confocal images of actin bundles stained with phalloidin (A) and collagen acquired with SHG (B). Distribution of orientations, determined with the OrientationJ plugin, of the actin (black) and collagen (grey) signals in the tissue sheet (C). Bars 100 μm . Dashed lines in C represent the pattern directions.

This suggests that collagen fibres are initially structured in an analogous manner as the neighbouring cells. Long-term cultures revealed a different scenario: cells on the basal plane were still closely packed, retracing the pattern features (Fig. 8A). Image analyses of SHG images (Fig. 8B) revealed that collagen was predominantly oriented along a single direction, which was intermediate to the two directions of the pattern (Fig. 8C). In the apical plane, we observed a similarity of the distribution of orientation of apical actin and collagen with the basal collagen (Fig. 8D-F).

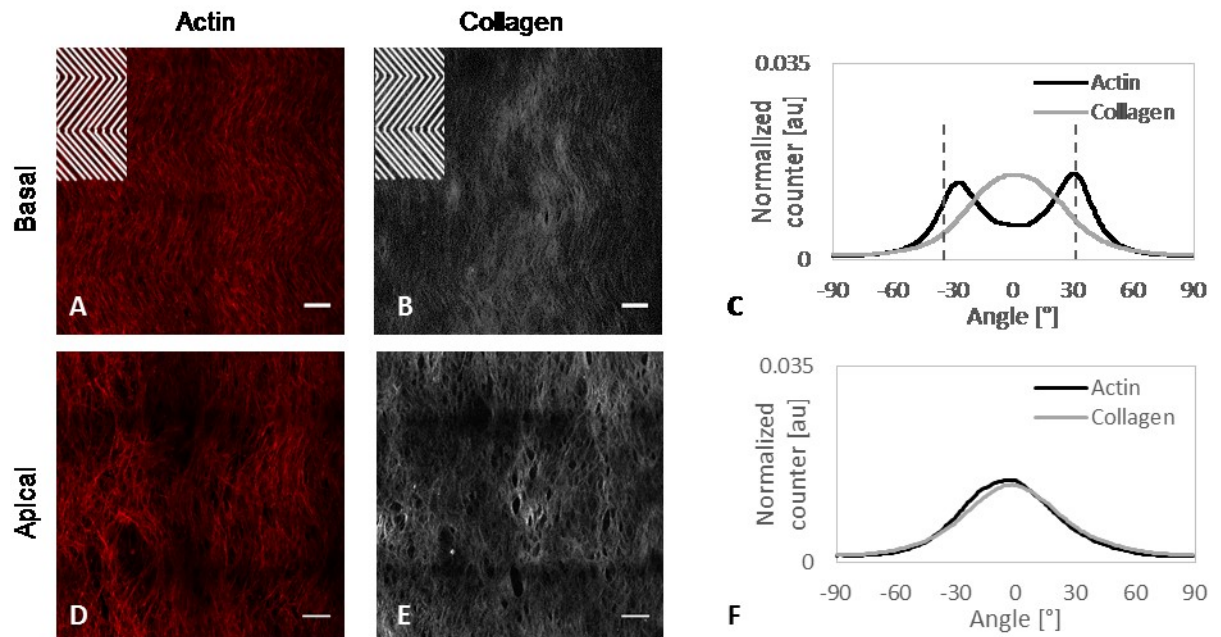


Fig. 8. Tissue sheets grown on non-linear surfaces. Confocal images of actin bundles stained with phalloidin (A, D) and collagen acquired with SHG (B, E). Top left inset in A and B represent the pattern features. Bars 100 μm . Distribution of orientations, determined with the OrientationJ plugin, of the actin (black) and collagen (grey) signals of the basal (C) and the apical (F) plane. Dashed lines in c represent the pattern directions.

As a further step to characterize the role of cell-mediated remodelling in affecting the spatial arrangement of collagen fibrils, we performed cell culture experiments on linear patterns, flat surfaces or non-linear patterns in presence of the contractility inhibitor ML7. This was added after 1 week of culture in normal conditions, thus allowing cells to lay down a provisional matrix template for the formation of a bilayered structure. Image analysis revealed that both basal and apical collagen of tissues grown on patterned substrates still displayed a preferential direction of alignment, which corresponded to that of the pattern, and were markedly similar to the orientations of actin fibres (Fig. 9A, B, D, and E). However, the distributions were broader with respect to those measured in normal culturing conditions (Fig. 9C, F and Tab. 1).

Similarly, apical collagen fibrils of tissues grown on flat surfaces exhibited a very broad distribution of orientations, which was similar in shape to that of the basal collagen (Fig. 9G, H, I, J, K, L). In the case of tissue grown on non-linear pattern, ML7 inhibitor induced a collagen configuration in the basal plane which resembled the distribution of

actin filaments (Fig. 9M, N). In fact, in the distribution of collagen, two different peaks were distinguishable (Fig. 9O), even though the distribution was markedly broader than that in normal condition of culture. Both collagen and actin of the apical plane showed a broad distribution of alignment along a single direction (Fig. 9R).

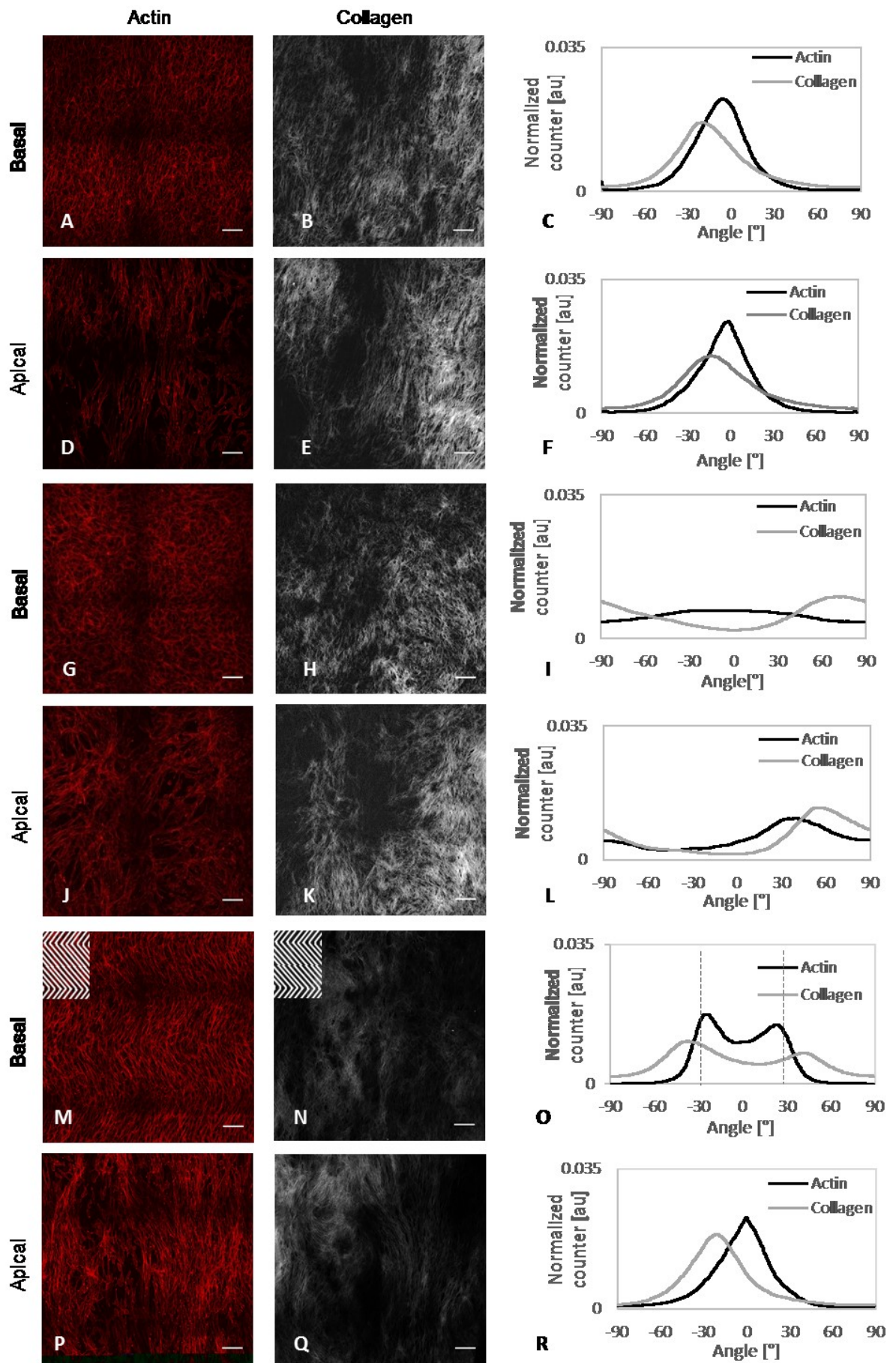


Fig. 9. Tissue sheets grown on substrates with linear patterns (A-F), flat surfaces (G-L) or non-linear pattern (M-R) in presence of the ML7 inhibitor. The inhibitor was added after 1 week of culture. Confocal images of actin bundles stained with phalloidin (A, D, G, J, M, P) and collagen acquired with SHG (B, E, H, K; N, Q). Top left inset in M and N represent the pattern features. Bars 100 μm . Distribution of orientations, determined with the OrientationJ plugin, of the actin (black) and collagen (grey) signals of the basal (C, I, O) and apical (F, L, R) plane. Dashed lines in O represent the non-linear pattern principal direction.

These data demonstrate that while topographic signal provide an initial guidance to the *de novo* synthesized matrix, the actomyosin contractility plays an important role in the maturation of tissue sheets as it dictates the spatial configuration of cells and collagen fibres within the tissue sheet.

For further demonstration of the importance of cell contractility in the spatial organization of collagen matrix, we performed experiments in the presence of Blebbistatin, an inhibitor of the ATPase function of nonmuscle myosin which blocks the motor function of filaments (31, 32). The experimental conditions in this case was the same of those used in the presence of ML7 inhibitor. The addition of Blebbistatin after one week of standard cell culture, did not allow the actin filaments to assemble, which were therefore not recognizable by phalloidin staining. Collagen fibrils were clearly visible in the whole tissue thickness, both in the linear and in the flat cases and, therefore, we limited our analysis on collagen fibrils only. First, we still observed that pattern collagen coalignment existed in the linear tissue (Fig. 10). Here, however, the distribution was much broader with respect to that observe in the samples treated with ML7, which still enables actin fibres formation and some level of contractility (Tab.1).

<i>FWHM (°)</i>	<i>Basal Collagen</i>	<i>Apical Collagen</i>
<i>Normal culture conditions</i>	25.0	24.4
<i>ML7 suppl. Media</i>	32.7	29.6
<i>Blebbistatin suppl. media</i>	35.6	31.6

Tab. 1. Full width at half maximum (FWHM) of peaks exhibited by collagen distributions of linear tissue sheets grown in normal culture conditions, in medium supplemented with ML7 or Blebbistatin.

Second, we observed that the distributions of fibres of the basal plane of flat and non-linear tissues were remarkably similar to these of the apical plane, with almost overlapped peaks and shoulders (see Fig. 10A, 10B). These results suggest that a strong inhibition of contractility, does not allow apical cells to reorient the surrounding collagens which retains a similar orientation to the collagen fibrils laid on the basal plane.

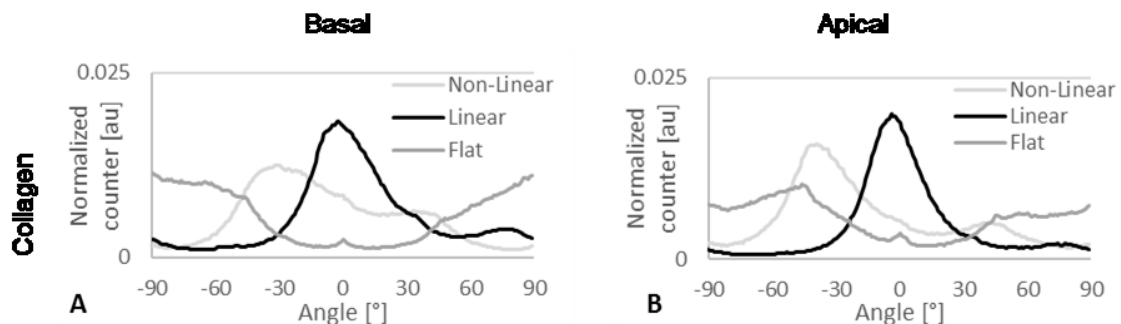


Fig. 10. Distribution of orientations, determined with the OrientationJ plugin, of the collagen signal in non-linear (light grey), linear (black) and flat (dark grey) tissues treated with Blebbistatin inhibitor of the basal (A) and the apical (B) plane.

A further confirmation of our hypothesis is the fact that superficial (apical) collagen observed with SEM is in the form of short fibrils with a small diameter (Fig. 11), whereas in normal conditions collagen bundles are often observed (for an example see Fig. 2 in Chap.3).

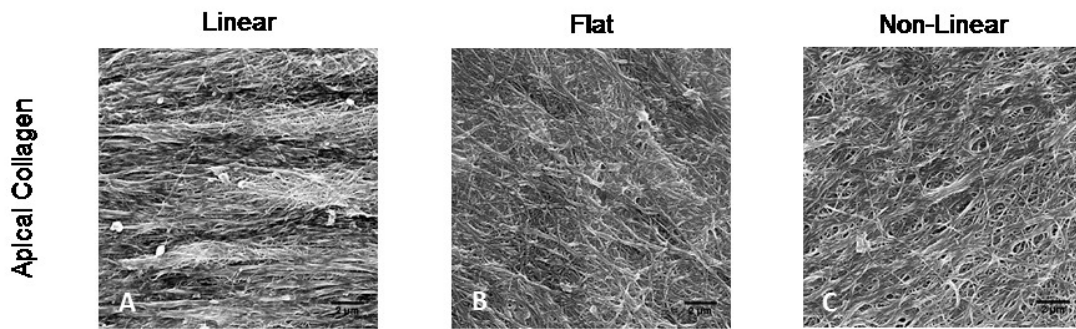


Fig. 11. Apical collagen SEM of linear (A), flat (B) and non-linear (C) tissue sheets treated with Blebbistatin, decellularized in order to purge out cellular remains and achieve a direct view of the collagenous matrices. Bars are 2 μ m.

Taken together these data suggest that the establishment of the cell-matrix architecture in the apical plane follows mechanisms that are not exclusively dictated by the microstructural features of the basal plane. Rather, our data suggest that the structure of the basal collagen is affected by contractile forces exerted by cells on the apical plane.

The fibrous ECM also provides a mechanical microenvironment in which the mutual relationships between cells and ECM have a profound impact on both cell and nuclear morphology (33, 34). As the nuclear envelope is variously interconnected with the actin cytoskeleton, we hypothesized that cell generated forces could also influence nuclear shape. To this aim, we evaluated nuclear aspect ratios in cells populating the apical plane and the basal plane.

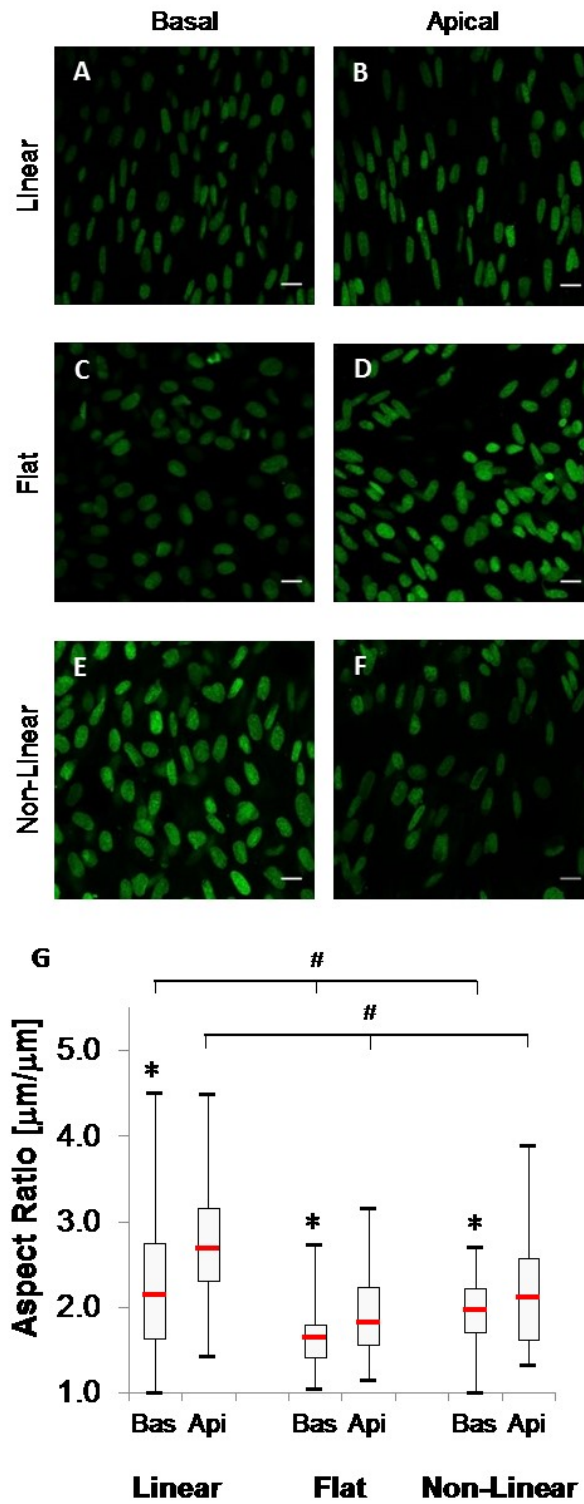


Fig. 12. Confocal images of nuclei stained with sytox green. Images are collected from basal and apical plane of tissues grown on linear substrates (A, B), flat surfaces (C, D) and non-linear pattern (E, F). Bars 20 μm . Boxplot of the nuclear aspect ratios of basal (Bas) and apical (Api) cells. * indicates significant differences with respect to the apical cell case. # indicates significant differences among linear, flat and non-linear groups.

Nuclei of cells in the apical plane are always more elongated with respect to those of the basal plane. And this occurrence was independent from the pattern features (Fig. 12A-F). Yet, cells on the linear pattern displayed the highest values of nuclear aspect ratio (Fig. 12G). This suggests that cells that find themselves in a highly anisotropic and unidirectional matrix effectively stretch along the oriented fibrous matrix. This creates a favourable condition for the actin fibres to exert a coordinated action around the nucleus, ultimately compressing it. Conversely, cells on flat surfaces displayed a polygonal shape and the contractile forces of the actin bundles do not cause excessive nuclear squeezing, which results in low nuclear aspect ratio values of the cell on the basal plane. This notwithstanding, cells on the apical plane can locally reorient collagen fibres thus creating patches of aligned collagen, in which cells elongate and display squeezed nuclei. However, this process is less effective as a remodelling phase need to precede cell elongation and nuclear lateral compression. In this context, the non-linear pattern is an intermediate case in which cells in the apical plane initially perceive a short-range order, which is eventually modified in long-term culture by straightening the wave-like collagen assembly.

The data presented so far demonstrate that the mutual interplays between cells and matrix define both the shape of cells and nuclei along with the microstructural architecture of the tissue. The latter, has a profound influence in dictating the macroscopic mechanical response. In order to assess whether the observed differences in collagen orientation affected the overall mechanical properties of the tissue sheets, we performed uniaxial traction tests on the three types of tissues (Fig. 13A). Tissue sheets grown on linear patterns were tested in the direction either parallel or perpendicular to that of the pattern. We will refer to these samples as “longitudinal” or “transversal” respectively.

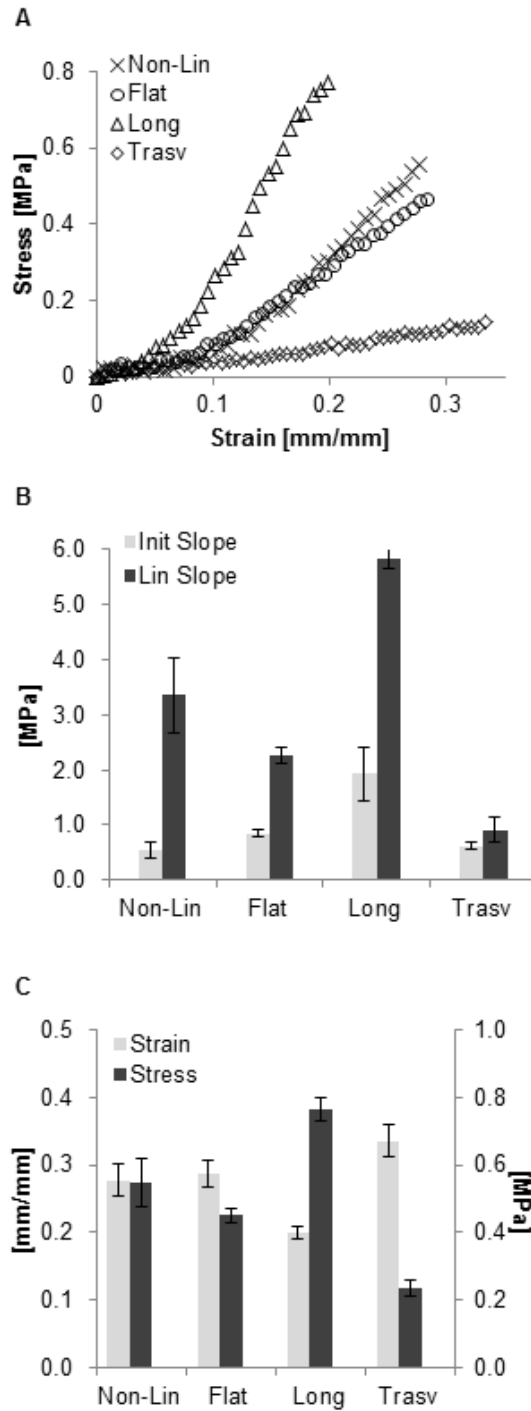


Fig. 13. A. Representative stress strain curves obtained with uniaxial test on non-linear (cross), flat (circle), longitudinal (triangle) and transversal (diamond) tissue sheets; B. histograms reporting the initial slope (grey) and the slope of the linear region (black); C. histogram of the strain at brake (grey) and ultimate tensile strength (black). Asterisks denote significant difference with respect to the longitudinal case. Groups expressing linear slope in A or tensile stress in B are all significant different from each other.

The mechanical tests revealed that tissue sheets possessed a J-shaped stress-strain curve that is characteristic of soft biological tissues. The mechanical response of the tissues we produced is analogous to that of composite laminates, in which the orientation of the fibrous reinforcement depends on the specific lamina within the composite.

Since transverse, flat and non-linear tissues had similar initial modulus (Fig. 13B) it is possible that the initial mechanical response is independent from the tissue microarchitecture and is dominated by an isotropic matrix. Such a matrix is responsible for transferring the applied load among the fibres, throughout the sample. However, matrix loading was not the main mechanism of mechanical response for samples displaying a considerable amount of fibres initially oriented along the load direction, as in the case of longitudinal tissues. In fact, in these samples fibres are readily stretched even at low deformations, which cause the initial modulus to attain higher values.

At higher deformations, the load transfer between the matrix and the fibres, causes the fibres to change their spatial configuration that ultimately results in fibre reorientation along the direction of the applied load. Fibre recruitment is scarcely effective in transverse tissues since the isotropic matrix undergoes failure before fibres can participate in withstanding the applied load. Indeed, these samples displayed the lowest values of the linear modulus and of the ultimate tensile stress. Conversely, longitudinal tissues, having almost all the fibres oriented along the direction of the applied load, possessed the highest linear modulus and tensile strength. Flat and non-linear tissues displayed intermediate values of linear modulus compared to the transverse and longitudinal ones (Fig.13B). Flat tissues have a not negligible fraction of fibres orthogonal or nearly-orthogonal to the direction of the applied load which scarcely contribute to the tissue total stress even at large deformations (Fig. 6C, F). This results in a reduced linear modulus and ultimate strength compared to the longitudinal and non-linear tissues (Fig. 13C). Non-linear tissues exhibit a considerable amount of fibres whose orientation is close to the direction of the applied load (Fig. 8C, F). However, collagen fibre distribution is broader than that observed in the case of linear tissues (Fig. 5C, F), which results in an increased toe-region, i.e. the transition zone between low stress and high stress linear regimes, in the stress-strain curve (Fig. 13).

2.4 Discussion

Tissue morphogenesis depends on matrix production as much as on its assembly and organization. These processes are strongly regulated by cells and exogenous stimuli among which mechanical forces play an important role (35). *In vitro*, the existence of a directional guidance provided by material signals affected cell shape and orientation collectively, as well as matrix production and assembly (18, 22, 28). More specifically, substrates displaying patterns of parallel and straight channels, obtained either with microcontact printing or with soft-lithography, markedly affected micro constituent assembly within the *in vitro* generated tissues. This was observed during the production of different tissue types. Williams et al. reported a microcontact printing-based technique to produce aligned smooth muscle cell sheets (36). A further development of the technique consisted in an ordered stacking of aligned cell sheets to produce thick membranes displaying comparable histology as that observed in native vascular media tissues (37). Furthermore, the same group also reported that aligned myoblast cell sheet was able to determine the spatial arrangement of the underlying sheets (5). Therefore, the spatial assembly of cells within multi-layered tissues could be modulated with the staking process.

Different cell types, however, are able to spontaneously generate multi-layered structures *in vitro* if subjected to adequate culturing conditions. The pioneering works of Bard and Elsdale demonstrated that fibroblasts cultures on plastic dishes spontaneously formed multi-layered structures (38). However, the dynamics leading to tissue sheet formation *in vitro* has never been elucidated. By conjugating cell multilayering and substrate patterning, Guillemette et al. were able to produce corneal, vascular media and dermal tissues sheets, whose internal structure resembled the one found *in vivo* (22). In particular, cells in close contact with the substrate followed the pattern features, whereas overlaying cells were oriented displaying a characteristic angle shift that depended on the specific cell type. A different trend was reported by Isenberg et al., who cultivated aortic smooth muscle cells on micro-grated substrates and obtained a thick tissue characterized by cells homogeneously oriented in a single direction (20). Conversely Pietak et al. found that the ordering effect imposed by the underlying pattern is lost when tissue surpasses 20 micron in thickness (21). Altogether, these data demonstrate that even though cells can produce multi-layered tissues, the possibility of finely controlling the spatial assembly of ECM components is not straightforward as several factors may play an important role in

the process of tissue assembly, for instance material stimuli, cells type and their interactions with the surrounding environment.

This is a central issue in the case of *in vitro* tissue regeneration, as tissue architecture and mechanics ultimately dictate its functions. For instance, Zhao et al. reported that the contribution of material nanopatterning and low tension stimulates hMSCs to produce aligned tissues rich in fibrillary collagen that proved to preserve hMSCs multipotency *in vitro* (39). Similarly, Xing et al. found that highly aligned nanofibrous matrices derived from fibroblasts cultivated on nanopatterned surfaces dramatically reduced immune response compared to randomly oriented tissues, making them interesting systems for *in vivo* applications (19). Within this context, several reports demonstrated that orderly arrays of de novo synthesized matrix components also confer the tissue with appealing properties in perspective of transplantation. For example, Kim et al. produced functional myocardial tissues on nanograted PEG hydrogels (3). In particular tissues grown on specifically patterned hydrogels exhibited improved electrophysiological features and higher expression of gap junction markers with respect to tissues grown on flat surfaces (3). In the context of regenerating connective tissues, micro- and nano-patterned substrates have been extensively used. These were predominantly aimed at stimulating orderly arrays of fibres exhibiting anisotropic properties. An early work by Curtis et al. demonstrated that tubular micro-patterned guides proved to stimulate the biosynthesis of parallel collagen bundles reminiscent of normal tendon histology even in an *in vivo* context (40). More recently, Isenberg et al. demonstrated that mechanically anisotropic tissues can be obtained by using micro-grated substrates that were effective in controlling the alignment of the de novo synthesized matrix (20).

These findings undoubtedly demonstrate the importance of the spatial assembly of the de novo synthesized matrices in affecting or regulating cells behaviour and tissue functions. However, a thorough understanding of the way material stimuli influence matrix production and assembly may enable developing strategies to exploit these stimuli to control the 3D tissue assembly *in vitro* and hence tissue functions. It has been recently demonstrated that material stimuli in the form of surface nano-patterning was effective in stimulating hMSCs to assemble and produce a fully differentiated tendon *in vitro* by guiding not only the spatial assembly of cells and ECM but also to guide stem cells through complex differentiation pathways (28).

Here, we investigated the spatial assembly, its dynamics and the mechanical response of tissue sheets grown on different types of patterns. First, we observed that the ordering

effect induced by the linear pattern was maintained through the tissue sheet thickness, thus producing a highly-aligned tissue. Second, we found that cell contractility was also involved in the establishment of the tissue sheet structure, as even modest amount of myosin inhibitor ML7 strongly altered the distribution of orientations of both actin fibres and collagen. In particular, the orientation of the basal plane correlated with the orientation of cells and collagen in the apical plane, and such a correlation persisted when inhibitors were used. These observations did not allow us to unequivocally conclude that the surface patterning while effective in ordering cells adjacent to the basal plane, do not induce a direct order away from the basal plane. Rather, the guidance of material signals dictate the initial spatial assembly of cells and matrix, whereas cells on the apical plane remodel in time the structure of the whole tissue. This was even clearer when we used non-linear patterns constituted by periodic units of short-range patterns. In short time cultures, in which bilayered structures were barely visible, the wave-like shape of the de novo synthesized collagen was evident. However, at longer culturing times the contractile forces of cells in the apical plane dramatically deformed the structure. Additionally, we observed that in presence of Blebbistatin, the final matrix architecture was strongly different from the normal culture condition case. In particular, we noticed that the collagen distributions of the basal and apical plane were very similar to each other, suggesting that cell contractility play a crucial role in the development and the organization of the apical plane. Tissues grown on non-linear surface show in normal condition of culture a principal direction of alignment in the apical plane which was different of that imposed by the pattern features, due probably to the remodelling effect exerted by cell contractility. Whereas, non-linear tissues cultured in presence of Blebbistatin possessed an apical plane in which the two principal directions of alignment imposed by the pattern were clearly discriminable.

Taken together these data suggest that the ordering effect of material signals provide cells (and the early matrix) with a specific directional guidance. Cells in the apical plane are free to contract and remodel the underlying matrix and the magnitude and direction of contractile forces depends on the initial arrangement of cells and matrix. In the case of linear patterns, cells in the apical plane are already oriented along the direction of the matrix and cell generated forces end up in enhancing collagen alignment and promoting cell stretching and nuclear squeezing. Apical cells of flat, isotropic tissues can still contract the underlying matrix, but since they lack of a collective guidance, they produce patches of compact and aligned tissues with elongated cells, but with no macroscopic, long-range

order. The role of cell contractility also explains why the ordering effect of short-range patterns is not entirely transferred through the tissue thickness. In fact, cell generated forces within the apical plane are sufficient to straighten the shallow wave-like contour of the underlying collagen matrix towards a more mechanically stable array of parallel fibres. These markedly different structures that formed on the three substrates also determined very different mechanical response of the tissue sheets when tested in uniaxial tension. Linear longitudinal tissues are constituted by a considerable fraction of fibres directed along the direction of the applied load, which endow the tissue with high stiffness and tensile strength. Conversely, tissue grown on flat surfaces exhibited a more compliant behaviour and reduced strength with a more pronounced toe-region connecting the low- to the high- strain regime. Tissues grown on non-linear pattern displayed an intermediate behaviour mostly detected by the broad distribution of orientation of collagen fibrils. Concerning collagen production, we did not observe any significant difference of the collagen content produced on linear, flat or non-linear, suggesting that the topographic signal indirectly affects the initial arrangement of collagen but not its amount (Fig. 12).

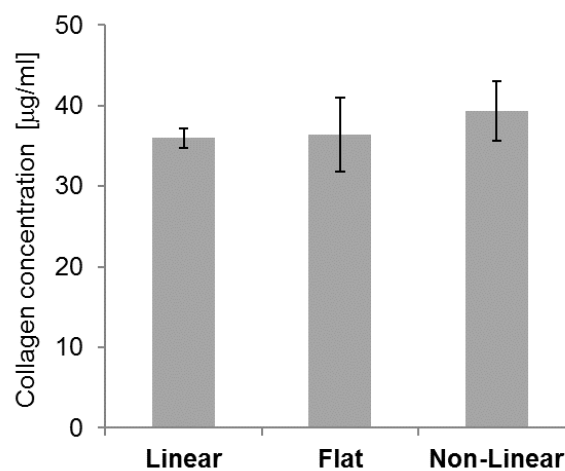


Fig. 12. Histogram of the collagen concentration measured with the Sircol assay.

Indeed, the ultimate tensile stress of non-linear tissues is higher with respect to the flat case, while strains at break are almost identical. Our data showed that if the tissue sheet architecture possessed a remarkable fraction of fibres completely or nearly aligned along a

single direction, the fibre compaction is promoted and fibre strength and hence ultimate properties are improved.

In this experimental campaign, we shed light on relevant aspects that relate the guiding effect provided by material patterning to the microarchitecture and cell organization of tissues grown *in vitro*. While the material signal in the form of linear gratings with long-range order is effective in guiding cells to synthesize and assemble a highly-aligned matrix, periodic repetitions of short-range orders, as in the form of a wave-like pattern, are not faithfully reproduced throughout the tissue thickness. In this case, cells residing away from the material are able to remodel the underlying matrix through contractile forces. We hypothesized that the material signals can provide an initial guidance to cells and tissues, yet cells modify the initial arrangement towards more mechanically stable configurations. This action creates matrices with specific spatial structures whose characteristics act locally, by affecting cell and nuclear shape and possibly mechanotransduction pathways, or globally, by affecting the gross mechanical response of the tissue. Such an aspect of dynamic interplay between apical, i.e. cells far away from the material surface, remodelling and basal cells must be taken into account when designing material platform for the *in vitro* generation of tissue with specific microstructural assemblies.

2.5 Bibliography

1. Y. Izu *et al.*, Dysfunctional tendon collagen fibrillogenesis in collagen VI null mice. *Matrix Biol.* **30**, 53–61 (2011).
2. M. Sun *et al.*, Collagen V is a dominant regulator of collagen fibrillogenesis: dysfunctional regulation of structure and function in a corneal-stroma-specific Col5a1-null mouse model. *J. Cell Sci.* **124**, 4096–4105 (2011).
3. D.-H. Kim *et al.*, Nanoscale cues regulate the structure and function of macroscopic cardiac tissue constructs. *Proc. Natl. Acad. Sci. U. S. A.* **107**, 565–570 (2010).
4. J. Wu, Y. Du, S. C. Watkins, J. L. Funderburgh, W. R. Wagner, The engineering of organized human corneal tissue through the spatial guidance of corneal stromal stem cells. *Biomaterials.* **33**, 1343–1352 (2012).
5. H. Takahashi, M. Nakayama, K. Itoga, M. Yamato, T. Okano, Micropatterned thermoresponsive polymer brush surfaces for fabricating cell sheets with well-controlled orientational structures. *Biomacromolecules.* **12**, 1414–1418 (2011).
6. A. W. Feinberg *et al.*, Functional differences in engineered myocardium from embryonic stem cell-derived versus neonatal cardiomyocytes. *Stem Cell Rep.* **1**, 387–396 (2013).
7. G. Imparato, F. Urciuolo, C. Casale, P. A. Netti, The role of microscaffold properties in controlling the collagen assembly in 3D dermis equivalent using modular tissue engineering. *Biomaterials.* **34**, 7851–7861 (2013).
8. M. Ventre, F. Causa, P. A. Netti, Determinants of cell-material crosstalk at the interface: towards engineering of cell instructive materials. *J. R. Soc. Interface.* **9**, 2017–2032 (2012).
9. D. W. Hutmacher, M. Sittinger, M. V. Risbud, Scaffold-based tissue engineering: rationale for computer-aided design and solid free-form fabrication systems. *Trends Biotechnol.* **22**, 354–362 (2004).
10. A. Marino, C. Filippeschi, V. Mattoli, B. Mazzolai, G. Ciofani, Biomimicry at the nanoscale: current research and perspectives of two-photon polymerization. *Nanoscale.* **7**, 2841–2850 (2015).
11. D. Thomas *et al.*, Scaffold and scaffold-free self-assembled systems in regenerative medicine. *Biotechnol. Bioeng.* **113**, 1155–1163 (2016).
12. E. Cukierman, R. Pankov, D. R. Stevens, K. M. Yamada, Taking cell-matrix adhesions to the third dimension. *Science.* **294**, 1708–1712 (2001).
13. Y. Haraguchi *et al.*, Fabrication of functional three-dimensional tissues by stacking cell sheets in vitro. *Nat. Protoc.* **7**, 850–858 (2012).
14. K. A. Athanasiou, R. Eswaramoorthy, P. Hadidi, J. C. Hu, Self-organization and the self-assembling process in tissue engineering. *Annu. Rev. Biomed. Eng.* **15**, 115–136 (2013).
15. Y. Shudo *et al.*, Spatially oriented, temporally sequential smooth muscle cell-endothelial progenitor cell bi-level cell sheet neovascularizes ischemic myocardium. *Circulation.* **128**, S59-68 (2013).

16. Y.-C. Lin *et al.*, Evaluation of a multi-layer adipose-derived stem cell sheet in a full-thickness wound healing model. *Acta Biomater.* **9**, 5243–5250 (2013).
17. M. Ventre, P. A. Netti, Engineering Cell Instructive Materials To Control Cell Fate and Functions through Material Cues and Surface Patterning. *ACS Appl. Mater. Interfaces.* **8**, 14896–14908 (2016).
18. J. H.-C. Wang, F. Jia, T. W. Gilbert, S. L.-Y. Woo, Cell orientation determines the alignment of cell-produced collagenous matrix. *J. Biomech.* **36**, 97–102 (2003).
19. Q. Xing, C. Vogt, K. W. Leong, F. Zhao, Highly Aligned Nanofibrous Scaffold Derived from Decellularized Human Fibroblasts. *Adv. Funct. Mater.* **24**, 3027–3035 (2014).
20. B. C. Isenberg *et al.*, Micropatterned cell sheets with defined cell and extracellular matrix orientation exhibit anisotropic mechanical properties. *J. Biomech.* **45**, 756–761 (2012).
21. A. Pietak, A. McGregor, S. Gauthier, R. Oleschuk, S. D. Waldman, Are micropatterned substrates for directed cell organization an effective method to create ordered 3D tissue constructs? *J. Tissue Eng. Regen. Med.* **2**, 450–453 (2008).
22. M. D. Guillemette *et al.*, Surface topography induces 3D self-orientation of cells and extracellular matrix resulting in improved tissue function. *Integr. Biol. Quant. Biosci. Nano Macro.* **1**, 196–204 (2009).
23. J. Schindelin *et al.*, Fiji: an open-source platform for biological-image analysis. *Nat. Methods.* **9**, 676–682 (2012).
24. R. Rezakhaniha *et al.*, Experimental investigation of collagen waviness and orientation in the arterial adventitia using confocal laser scanning microscopy. *Biomech. Model. Mechanobiol.* **11**, 461–473 (2012).
25. B. D. Ratner, Plasma deposition for biomedical applications: a brief review. *J. Biomater. Sci. Polym. Ed.* **4**, 3–11 (1992).
26. S. H. Tan, N.-T. Nguyen, Y. C. Chua, T. G. Kang, Oxygen plasma treatment for reducing hydrophobicity of a sealed polydimethylsiloxane microchannel. *Biomicrofluidics.* **4**, 32204 (2010).
27. J. Zhou, A. V. Ellis, N. H. Voelcker, Recent developments in PDMS surface modification for microfluidic devices. *ELECTROPHORESIS.* **31**, 2–16 (2010).
28. M. Iannone *et al.*, Nanoengineered surfaces for focal adhesion guidance trigger mesenchymal stem cell self-organization and tenogenesis. *Nano Lett.* **15**, 1517–1525 (2015).
29. L. D. Quarles, D. A. Yohay, L. W. Lever, R. Caton, R. J. Wenstrup, Distinct proliferative and differentiated stages of murine MC3T3-E1 cells in culture: An in vitro model of osteoblast development. *J. Bone Miner. Res.* **7**, 683–692 (2009).
30. E. T. den Braber, J. E. de Ruijter, L. A. Ginsel, A. F. von Recum, J. A. Jansen, Orientation of ECM protein deposition, fibroblast cytoskeleton, and attachment complex components on silicone microgrooved surfaces. *J. Biomed. Mater. Res.* **40**, 291–300 (1998).
31. J. S. Allingham, R. Smith, I. Rayment, The structural basis of blebbistatin inhibition and specificity for myosin II. *Nat. Struct. Mol. Biol.* **12**, 378–379 (2005).

32. M. Kovács, J. Tóth, C. Hetényi, A. Málnási-Csizmadia, J. R. Sellers, Mechanism of blebbistatin inhibition of myosin II. *J. Biol. Chem.* **279**, 35557–35563 (2004).
33. Z. Yin *et al.*, The effect of decellularized matrices on human tendon stem/progenitor cell differentiation and tendon repair. *Acta Biomater.* **9**, 9317–9329 (2013).
34. M. Krause, K. Wolf, Cancer cell migration in 3D tissue: negotiating space by proteolysis and nuclear deformability. *Cell Adhes. Migr.* **9**, 357–366 (2015).
35. T. Mammoto, D. E. Ingber, Mechanical control of tissue and organ development. *Dev. Camb. Engl.* **137**, 1407–1420 (2010).
36. C. Williams *et al.*, Aligned Cell Sheets Grown on Thermo-Responsive Substrates with Microcontact Printed Protein Patterns. *Adv. Mater.* **21**, 2161–2164 (2009).
37. C. Williams, A. W. Xie, M. Yamato, T. Okano, J. Y. Wong, Stacking of aligned cell sheets for layer-by-layer control of complex tissue structure. *Biomaterials.* **32**, 5625–5632 (2011).
38. T. Elsdale, J. Bard, Cellular interactions in mass cultures of human diploid fibroblasts. *Nature.* **236**, 152–155 (1972).
39. F. Zhao *et al.*, Low Oxygen Tension and Synthetic Nanogratings Improve the Uniformity and Stemness of Human Mesenchymal Stem Cell Layer. *Mol. Ther.* **18**, 1010–1018 (2010).
40. A. S. G. Curtis *et al.*, An in vivo microfabricated scaffold for tendon repair. *Eur. Cell. Mater.* **9**, 50–57; discussion 57 (2005).

Chapter 3

3.1 Introduction

Extracellular matrix (ECM) is a highly organized and complex assembly of macromolecules, also acting as signalling factors. A main task of ECM consists in enabling adhesions and interactions of cells with the surrounding matrix and to providing the tissue with mechanical structural integrity. ECM displays cues for cell migration, proliferation, differentiation and survival, essential characteristics to development, homeostasis and tissue repair. ECMs are predominantly constituted by fibrillar proteins, including collagens, fibronectin, laminin, glycosaminoglycans, proteoglycans and other matricellular proteins. ECM components are responsible of the overall structural and mechanical properties of tissue, such as strength, compliance, elasticity and viscoelasticity. Additionally, these components are involved in the binding, sequestration and stabilization of signalling molecules incorporated within the matrix (1). The ECM is constantly deformed, degraded, synthesized, remodelled, as the environment changes and in response to tissue and organ demands (2), so that it is possible to affirm that ECM is in a dynamic equilibrium state.

Tissue engineering and regenerative medicine aims at producing biomaterials that can adequately recapitulate the multifactorial aspects of ECM functions. This notwithstanding, matrices formed from synthetic or biological materials (fibrin, hyaluronan or collagen), are not able to reproduce the molecular organization of native tissues. For this reason, the use of native ECM itself as a biomaterial has been pursued.

In the past decade, whole tissues or organs decellularization was suggested as an interesting technique to produce biological scaffolds composed of ECM. Decellularized ECM from donor tissue has been utilized in the repair of bladder (3), heart valve (4), skin (5) and small intestinal submucosa (6). Currently, allogenic or xenogenic tissues derived matrices, has been widely used as natural biomaterials (7, 8). The retention of tissue architecture provided by decellularization of tissues and organs, enabled the introduction of this system also for tissue engineering applications (9–11).

However, matrices derived from natural tissues have a limited capability of being manipulated both mechanically and architecturally, and possess uncontrolled variability depending on the age, health and gender of individual sources. Matrices derived from mammalian cells in culture provide an alternative to native tissue-derived ECMs. Cell derived matrices (CDM) contain a plethora of macromolecules that can mimic natural tissue microenvironments. In contrast to tissue ECM, properties of CDM can be modulated by selecting: the type(s) of cells used to produce the ECM; the culture system; the application of external stimuli. Another opportunity to act on CDM characteristics lies in the ability to genetically modify the source cells to augment or silence the expression of target molecules.

CDMs were used to confer bioactivity to synthetic scaffolds through the deposition of matrix molecules on the scaffold surface. The principal disadvantage in the use of CDMs with respect to the whole tissue decellularization is their typical weak mechanical properties. However, this issue can be overruled by mechanical preconditioning, which shown significantly improvement in the mechanical properties of CDM, particularly for cardiovascular applications (12, 13).

Therefore, decellularized matrices derived from *in vitro* cell constructs (or decellularized cell derived matrices, dCDMs) offer a valid alternative to decellularized whole tissues for tissue engineering applications. Furthermore, dCDMs can be created *in vitro* using patient-specific cells such as mesenchymal stem cells (MSCs) (14), fibroblasts, osteoblasts (15) or chondrocytes (16).

Concerning their performances *in vitro*, several studies aimed at assessing cell recognition and reaction to specific dCDM features. Of particular interest in tissue engineering applications, the response of undifferentiated cells to dCDM has gained large attention in the recent past. For example, Prewitz et al. (17) compared matrices generated by mouse embryonic fibroblasts (MEFs), human umbilical vein endothelial cells (HUVECs) and human neonatal dermal fibroblasts to matrices generated by human MSCs

grown in osteogenic factors (osteodCDM) or ascorbic acid (aadCDM). MSC-dCDM was thicker than the other matrices, and showed an elastic modulus in the same range of that exhibited by the native bone marrow, whereas other dCDMs showed higher values of the elastic modulus. Additionally, aadCDM showed a significantly higher content of collagen and growth factors with respect to the osteodCDM. Compared to cell culture dishes (CCDs), the MSC-dCDM brought in several advantages, such as higher proliferation rates; greater osteogenic and adipogenic differentiation efficiencies; increased secretion of growth factors in cultured MSCs. The enhanced expansion of the MSC populations were attributed to the characteristic of the aadCDM that resembled the native bone marrow niche (17).

The multipotency of MSCs lies in their ability to differentiate into several musculoskeletal cell types. However, this kind of stem cells is not abundant in native tissue, so that, *ex vivo* expansion becomes crucial to obtain clinically relevant cell numbers. *In vitro* expansion of MSC, in long culturing conditions, typically diminishes their differentiation potential and leads to cellular senescence. In order to avoid such a problem, several efforts attempted to produce a microenvironment similar, as much as possible, to the bone marrow niche. Bone marrow cell (BMC) derived matrix contained a composition similar to bone marrow, including the presence of typical macromolecules such as collagen I and III (18). Lai et al. showed that MSCs expanded on BMC-derived matrix exhibited a higher degree of proliferation rate, multipotency and reduced intracellular levels of reactive oxygen species, in comparison with MSCs expanded on CCDs. MSCs expanded on dCDMs retained their potential for osteogenesis, while cells cultured on CCDs had reduced osteogenic potential after 7 passages (18). Similar results were demonstrated for foetal MSC-derived matrix (19, 20).

Even though several results are promising, a substantial variability in the reported effects of CDM *in vitro* and *in vivo* applications still exists. This probably because of the many differences in the intrinsic variability of primary stem cells, as well as in methods and applications examined thus far.

Recently, immortalized cells were proposed to be used as potential source of CDMs. These cells provide various technical advantages, such as improved stability, easier manipulation conditions along with their ability to provide a large number of homogeneous cells. Artificial depletion or enhancement of specific molecular key elements production within a CDM may be also enabled by genetic engineering of cell lines (21). A second important consideration that affects CDM production is the cell culturing conditions.

Culture methods for CDM generation offer flexibility and versatility to the desired applications. For example, adherent cells grown in monolayers deposit a thin layer of matrix molecules, whereas, cells cultured as multicellular aggregates produces three-dimensional matrices, without the need for a carrier scaffold. However, the most common and easy methods for generating CDM are to culture cells as monolayers (2D).

Additional considerations may also include mechanical pre-conditioning to improve the mechanical properties of the resulting material (12, 13), or altering the environmental conditions (e.g. hypoxic conditioning (22)) to better model *in vivo* microenvironments (0.5–14% O₂, depending on tissue vascularization (23), compared to 21% O₂ in classic culture conditions). Once a sufficient amount of ECM has been deposited, the cellular component can be disrupted and removed from the ECM through a decellularization method, involving the use of chemical, physical, and biological treatments and their combinations (24).

Unlike cellular material, ECM components are predominantly conserved among species, thus the primary goal of decellularization is the removal of cellular antigens and other immunogenic components, such as DNA, to minimize the risk of adverse immunological responses (7). This objective must be balanced against preserving the molecular composition, bioactivity and structural integrity of the matrix itself, thus careful consideration and subsequent evaluation must be taken when selecting/developing a decellularization method.

Given these premises, we aimed at investigating these two aspects: first, we analysed whether dCDM of a stable cell line could be used as support for MSC culture and expansion; second, we investigated how the combination of signals, like biochemical, mechanical and structural, displayed by different MC3T3 dCDMs can influence stem cells fate.

3.2 Materials and methods

3.2.1 Preparation of micropatterned substrates

Linear patterned substrates were obtained by replica moulding of polydimethylsiloxane (PDMS, Sylgard 184, Dow Corning) on a polycarbonate master consisting of 2 cm² nanograted (700 nm ridges with 1.4 mm pitch and 250 nm depth). Flat PDMS substrates were used as control and were produced by using a polystyrene dish as master. PDMS was prepared by mixing elastomer base and curing agent at 10:1 weight ratio. The solution was degassed, poured onto the master and then cured at 60°C for 2 h. PDMS substrates were treated with oxygen plasma in order to improve cell adhesion. Briefly, the treatment was performed with a Plasma Femto (Diener) equipped with 13.56 MHz 100 W power generator for the plasma excitation. Plasma exposure was 1 min and then substrates were sterilized by UV exposure for 30 min. Samples were then incubated with serum-supplemented culture medium overnight prior to cell culturing experiments.

3.2.2 CDMs production

The production of a 3D-organized matrix was carried out by cultivating MC3T3-E1 preosteoblasts (ATCC) for 2 weeks on linear or flat surfaces. Cells were cultured in alpha-MEM with deoxyribonucleosides, ribonucleosides and 2 mM L-glutamine, supplemented with 10% foetal bovine serum, penicillin (100 units ml⁻¹), streptomycin (100 mg ml⁻¹) (Gibco). MC3T3 were incubated at 37 °C in a humidified atmosphere of 95% air and 5% CO₂. The culture medium was changed every two days. After 3 days of culture, MC3T3-E1 cells were detached with trypsin/EDTA (0.25% w/v trypsin/0.02 mM EDTA) (Gibco) and seeded on linear and flat substrates

Collagen rich tissue sheets derived from MC3T3-E1 cells were produced by seeding cells at the density of 2x10⁴ cells·cm⁻² (sub-confluent) on the linear pattern or flat substrates, and cultivating the cells for 2 weeks in presence of 25 µg/mL of ascorbic acid.

3.2.3 Decellularization

In order to obtain a decellularized cell derived matrix (dCDM) a decellularization protocol similar to that reported by Wolf et al. (25) was performed. Briefly, once a thick tissue sheet (2 cm²) was produced on linear or flat surfaces, a PMMA mask with two holes (d = 3 mm) was put on it to avoid the tissue detachment during the decellularization. The

PMMA mask was glued over the samples Twinsil glue (Picodent). A 2ml TrypLE express 1X (Gibco) solution was added to each sample for 20 min, to allow cell detachment avoiding ECM degradation. Samples were then rinsed twice with dH₂O for 20 min on a tilting plate at 30 rpm. In order to purge out from the CDM every cellular remnant, samples were covered with a 0.69% Trizma base (Sigma), 0.26% EDTA (Sigma) and 1% Triton X-100(Sigma) solution. After 1 h, samples were rinsed thoroughly with dH₂O and then left on a tilting plate at 30 rpm overnight. The next day the obtained dCDMs were incubated with fresh medium (DMEM) for 12 h.

For the experiments concerning the mechanical pre-conditioning, a treatment with genipin (Sigma) was performed to increase the stiffness of the matrix (26). Briefly, after the decellularization protocol, samples were incubated in a 2.5% filtered solution of genepin diluted in DMSO (Sigma) and PBS (1:1) overnight. The next day samples were rinsed thoroughly with dH₂O twice for 30 min and then were incubated with DMEM for 12 h.

3.2.4 dCDM ultrastructural characterization (SEM)

dCDMs were dehydrated through an ascending series of water/ethanol solutions (10% steps, 10 min each) ending in 100% ethanol. Ethanol soaked samples were dried in a critical point dryer (EM CPD300, Leica). Afterwards, samples were coated with a 10 nm gold layer with a 208hr sputter coater (Cressington). Scanning electron microscopy (SEM) imaging was performed by means of an Ultra Plus Scanning Electron Microscope (Zeiss, Germany) with a 10 kV tension.

3.2.5 Mechanics characterization of dCDMs

Young's moduli of decellularized cell derived matrices (dCDM) were measured by means of an atomic force microscope (JPK Nanowizard) using a silicon nitride cantilever (Bruker MLCT-O10) with a spherical polystyrene probe (6 μ m diameter). The deflection sensitivity of the cantilever was measured using glass as a stiff surface. The cantilever spring constant was estimated using the thermal fluctuation method. The manufacturer's nominal value for the cantilever spring constant (k) was 0.05 N/m, and the experimental values obtained were generally 0.05–0.06 N/m. Glass substrates with dCDM were planed under the AFM tip and the force curves were captured in different locations along the matrices. Force curves for either linear or flat samples were taken at room temperature in PBS. The AFM procedure was done by scanning a region of interest (24x24 μ m) using

contact mode, with an extension speed of 0.5 $\mu\text{m/s}$. Data are acquired until a vertical deflection of 90nm was achieved. All curves were fit to the Hertz– Sneddon model for a paraboloid indenter with the JPK Data Processing software:

$$F_{paraboloid} = \frac{4}{3} \left(\frac{E}{1 - \nu^2} \right) R^{1/2} \delta^{3/2}$$

in which $F_{paraboloid}$ is the force exerted by the indenter, E is the Young's modulus of the matrix, R is the curvature radius of the indenter, and d is the distance between the indenter and the sample. The matrices were assumed to be nearly incompressible with a Poisson's ratio of 0.5. The Young's modulus was found for each force curve using the fitting algorithm provided by the JPK software. A maximum indentation of approximately 500nm was chosen for fitting. The contact point of the cantilever with the sample was chosen to be the point at which the derivative of the force–distance curve became nonzero. Thus, data were fit from the contact point to the maximum indentation value. Average Young's modulus was computed by averaging all force curves for a given condition (linear and flat samples).

3.2.6 Stem cells culture

D1-ORL UVA murine mesenchymal stem cells (passage 3) (ATCC) were cultured in DMEM with 2 mM L-glutamine, supplemented with 10% foetal bovine serum, penicillin (100 units ml^{-1}), streptomycin (100 mg ml^{-1}) (Gibco) respectively. Stem cells were incubated at 37°C in a humidified atmosphere of 95% air and 5% CO_2 . The culture medium was changed every two days. After 3 days of culture, D1-ORL UVA cells were detached with trypsin/EDTA (0.25% w/v trypsin/0.02 mM EDTA) (Gibco) and seeded on dCDMs and on cell culture dishes (CCD) at a 1.5×10^4 cell cm^{-2} density (sub-confluency).

The experiments on the differentiation of D1-ORL UVA cells were performed by using differentiating media, i.e. MesenCult™ Osteogenic Stimulatory medium and MesenCult™ Adipogenic Stimulatory medium (StemCell) directly on cells grown on dCDMs and CCDs. Media were replaced 3 times per week. For the evaluation of the loss of the differentiation potential of cells, D1-ORL UVA MSCs were cultured on dCDMs and CCDs in maintenance medium (DMEM) for 2 weeks. Then, cells were collected from each surface, by a trypsin and collagenase treatment. Briefly, a trypsin/EDTA (0.25% w/v trypsin/0.02 mM EDTA) (GIBCO) was used for cell detachment. Samples were then

treated with collagenase (2.5mg/ml, Roche) for 20min at 37°C. Then, supernatants were removed and the remaining cells were re-suspended in DMEM before the reseeded. Cells collected were seeded on CCDs at a 2×10^4 cell cm^{-2} density (sub-confluency) and cultured in differentiating media for additional 2 weeks.

3.2.7 Cell staining

Cells were fixed with 4% paraformaldehyde for 20 min and then permeabilized with 0.1% Triton X-100 (Sigma) in phosphate-buffered saline (PBS). For the differentiation tests Alizarin Red and Oil Red O staining was performed in order to verify osteogenic and adipogenic commitment respectively. Alizarin red solution was added to the samples for 45 min, then the solution was rinsed twice with dH₂O. To verify adipogenesis, samples were fixed in 60% iso-propanol for 5min and then put into a solution of Oil Red O and water (2:3) for additional 5 min. Images were collected with an upright optical microscope XC51(Olympus). For immunostaining experiments, samples were blocked in PBS/bovine serum albumin 1% solution (Sigma) for 30 min, to avoid non-specific binding. Markers staining was performed by incubating samples with an anti-Sca-1 and anti-CD29 (Abcam) primary antibodies in PBS (1:100) over night at 4 °C. The secondary antibody (pseudo-colored green) was Goat Anti-Rat IgG H&L (Alexa Fluor 488 1:1000) and Goat Anti-Rabbit IgG H&L (Alexa Fluor 488 1:1000) for 1hour at room temperature. For nuclear staining, samples were incubated with a 1:10000 solution of Dapi (Sigma) in PBS for 10 min at 37 °C. Samples were thoroughly rinsed in PBS and mounted on glass slides. Fluorescent images of Sca1 and CD29 were collected with a Leica TCS SP 5 (Leica Microsystems). Samples were excited with 488 nm laser lines, and the emissions were collected in the 500–530 nm range. Dapi was visualized through multiphoton microscopy, exciting the samples with a femtosecond laser (Coherent) at 700 nm and the emission was collected in the 415-425 nm interval.

3.2.8 Image analysis

Cellular density in the sample was evaluated by means of image analysis. Images of cell nuclei on dCDMs and CCDs were collected and analysed by ImageJ software. Density fold increase was calculated as the ratio of the number of nuclei in a specific region of interest (ROI) after 24h and the cell number after 2 weeks in a ROI of the same size. In order to avoid the overlapping of different nuclei, the plug-in classic watershed (IJPB-

plugins) was applied preliminary. Briefly, this plug-in allows recognizing round particles and automatically segmenting the overlapped ones.

In order to evaluate the D1-ORL UVA expression of Sca-1 and CD29 markers, images of different samples were collected with a HCX IRAPO L 25x 0.95 water immersion objective lens. No changes of the acquisition settings i.e.: gain, zoom, pinhole size, laser power etc. were made during image collection. 15 images per sample type, containing approximately the same numbers of cells were collected. Immunostaining performed on the thick tissue sheets suffers from clustering of the fluorescent secondary antibody, which creates bright spots in the image. Since CD29 and Sca-1 are membrane markers that do not form focal plaques, the bright spots were erased from the digital images with a user-independent method. More specifically, digital images were automatically subjected to a “moments” threshold with Fiji and pixels above the threshold were set as NaN values, which exclude them from the subsequent analysis. Mean fluorescence intensity and standard deviation were collected by using the command “measure” in Fiji.

3.2.9 Statistics

Significant differences among groups, i.e. cell densities among CCDs and dCDMs or Sca-1 and CD29 intensities and standard deviations, were assessed with a one-way ANOVA test followed by a Tukey’s post-hoc test written in Matlab (The Mathworks). *p* values less than 0.05 were considered significant.

3.3 Results

In order to generate bio-support, synthesized by cells *in vitro*, which could be used as stem cell scaffold, we used MC3T3 preosteoblasts, which are known to produce abundant ECM in a consistent manner. Additionally, we were interested in evaluating whether biophysical features of the supporting matrices affected stem cell behaviour in terms of stemness retention or differentiation potential. To this aim, we produced two different matrices by exploiting the ordering power exhibited by nanopatterned surfaces. Linear substrates, as shown in Chap.2, induced the production of an approximately 50 μ m thick tissue sheet with mature and parallel collagen fibrils in 2 weeks of culture. Conversely, flat substrates induced a random configuration of collagen fibrils. Once a well-formed structure was obtained, we performed a decellularization procedure in order to obtain a dCDM with a specific architecture dictated by the pattern features. Our decellularization protocol purges the structure from any cellular material, preserving the cell self-assembled ECM architecture, as shown in Fig. 1. Here, we were not able to detect remnants of filamentous actin or nucleic acids. Collagen was clearly visible in SHG mode and the fibrillar structure was similar to that observed in normal matrices (see Chap. 2).

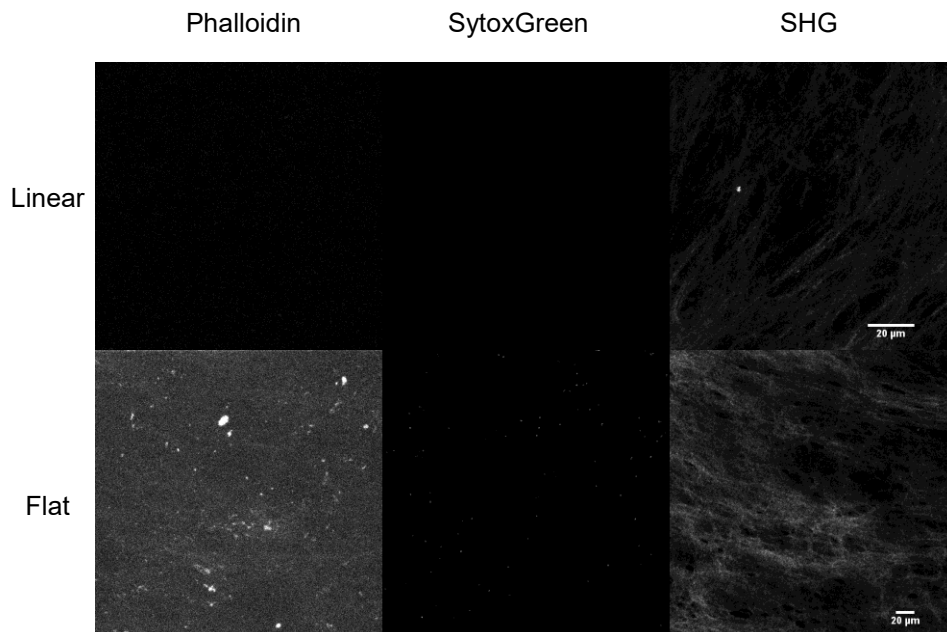


Fig. 1. Z-projection of MC3T3 multi-layered dCDM grown on linear or flat substrates. Bars are 20 μ m.

The dCDMs thus obtained showed different structures, in terms of collagen bundling and spatial arrangement. SEM micrographs clarify this aspect. The unidirectional traction forces exerted by cells in a parallel configuration induced a remodelling effect that caused a marked compaction of collagen fibrils (Fig.2). This effect produced a more bundled structure in comparison with the flat case, in which fibrils are randomly distributed. Such a configuration and a non-polarized traction force exerted by cells, did not allow extensive compaction of collagen fibrils.

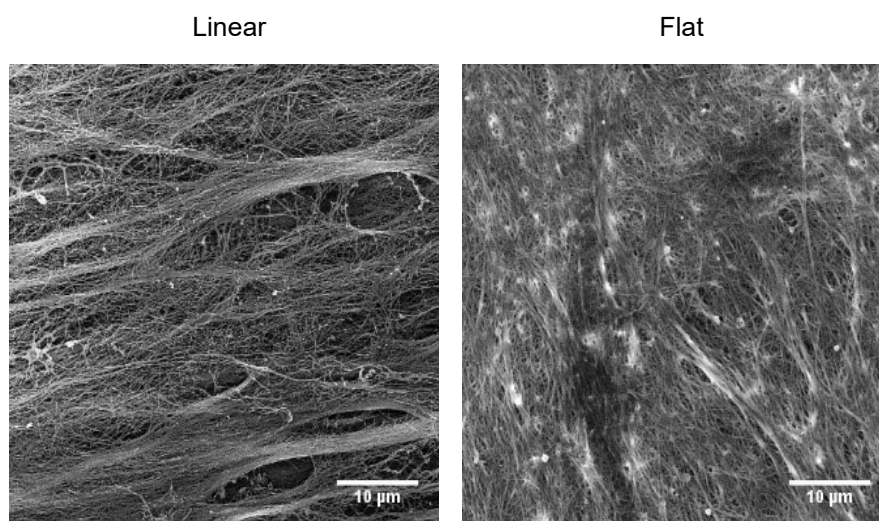


Fig. 2. SEM of MC3T3 multi-layered dCDM grown on different patterns for 2 wk. Bars are 10 μ m

We then asked if such a difference in collagen arrangement affected the mechanical characteristics of the obtained structure. To this aim, we performed AFM mechanical tests. Young's moduli were in the 10-100Pa range. Although linear dCDM displayed higher values of Young's modulus with respect to flat dCDM such a difference was not significant (Fig.3).

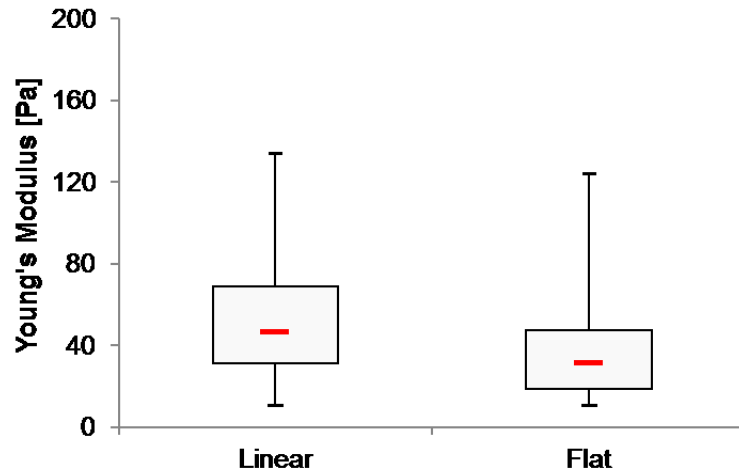


Fig. 3. Young's moduli of dCDM measured on linear and flat decellularized tissue sheets.

Next, we verified if dCDMs were suitable for cell cultures by performing a low-density cell seeding on the matrix directly. In particular, we used D1 ORL-UVA cells, murine mesenchymal stem cells, as they represent a consistent cellular model to study commitment under effect of exogenous stimuli (27). Our structures induced the adhesion and the elongation of cells, as shown in Fig. 4.

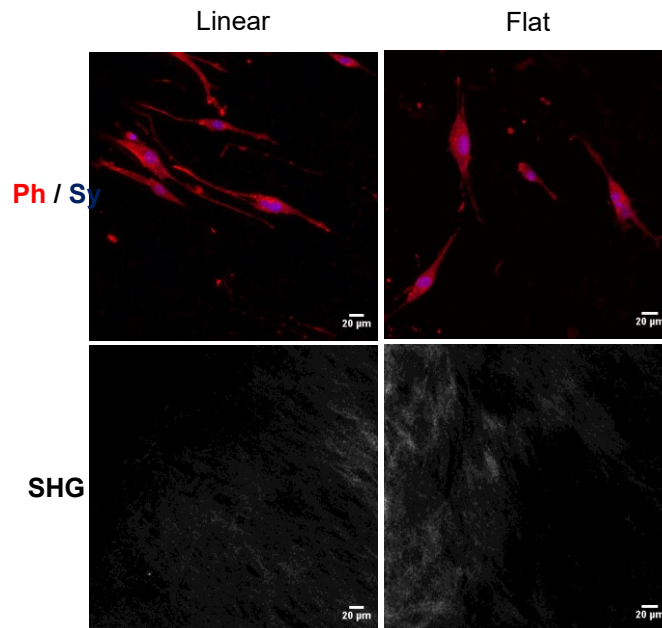


Fig.4. D1 ORL-UVA seeded at low density on MC3T3 dCDM after 72 h of culture. Bars are 20μm

Cells seeded on linear dCDM were elongated along a common direction, i.e. direction of collagen alignment induced by the pattern, whereas cells in contact with flat dCDM were elongated along different directions. Additionally, SEM images showed that the D1 ORL UVA cells strongly interacted with the surrounding matrix by producing protrusions firmly adhering and pulling the fibrillar matter (Fig. 5).

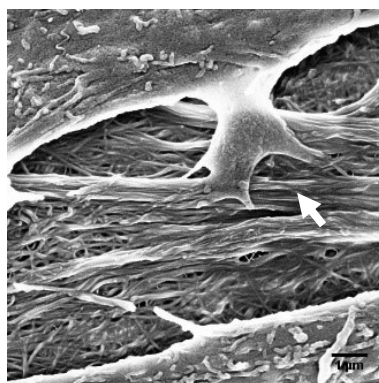


Fig. 5. SEM of D1 ORL-UVA seeded at high density on a linear 2 wk MC3T3 dCDM after 72 h of culture. White arrow indicates cell protrusion interacting with collagen fibrils. Bar is 1 μm.

Once assessed that dCDMs allowed cell adhesion we asked whether the morphological and mechanical features of the bio-support could affect stem cells behaviour. First, we performed a proliferation test. Briefly, we performed a high density D1 ORL UVA seeding both on dCDMs and on cell culture dish (CCD), whether evaluated the number of cells per cm² after 24h, which was considered to be the time 0, and 2 weeks of culture. We observed that dCDMs displayed an approximately 25-fold increase in cell density with respect to time 0, which was also significantly higher than the fold increase on CCD substrates (Fig. 6).

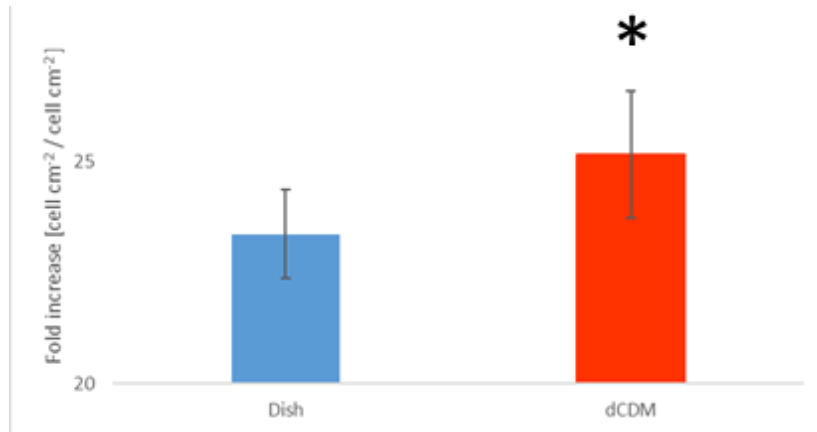


Fig. 6. Histogram of D1 ORL-UVA density fold increase in 2 wk culture. Cells were seeded at high density either on dCDMs or on cell culture dish. Asterisk indicates significant difference from Dish sample.

Second, we asked if dCDMs, besides favouring cell proliferation, affected mesenchymal stem cells response to differentiation media and hence influencing their commitment. In order to understand this aspect, we carried out experiments on cell fate after 2 weeks of culture in differentiating media, i.e. osteogenic and adipogenic medium. Surprisingly cells seeded on dCDMs and supplemented with osteogenic medium did not show a commitment in the osteogenic lineage. In fact, Alizarin Red staining reported no calcium accumulation over the new cell sheet. Conversely cells stained with Oil Red O exhibited the presence of small and non-uniform distributed lipidic vacuoles more marked on flat dCDM rather than on linear one (Fig. 7A). When subjected to adipogenic medium D1-ORL UVA cells cultured on dCDMs showed very large lipidic vacuoles uniformly distributed over the whole cell sheet (Fig. 7B).

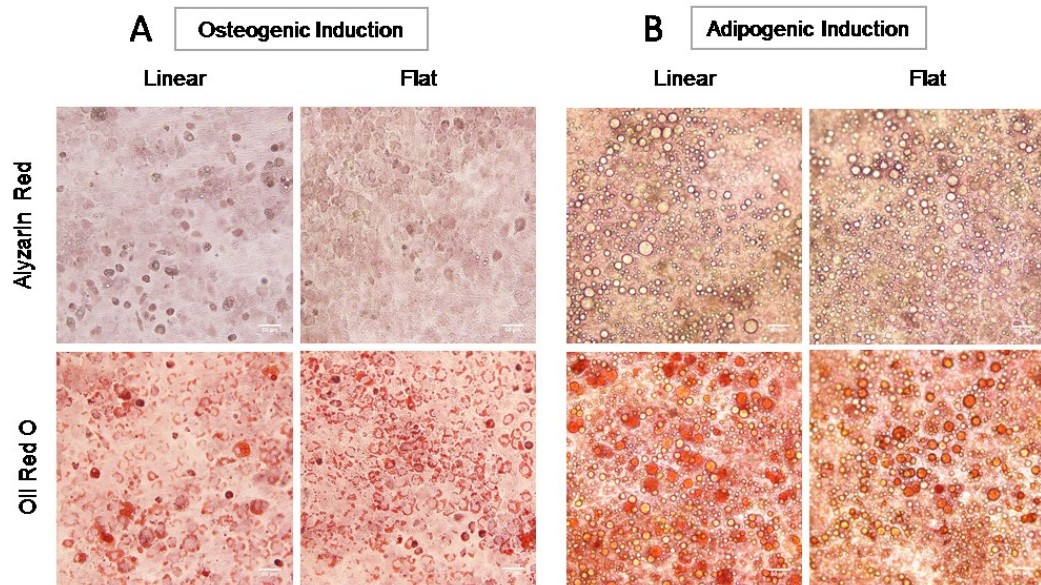


Fig.7. D1 ORL-UVA seeded at high density on a 2 wk MC3T3 dCDM after 2 wk of culture in osteogenic medium (A) and in adipogenic medium (B). Bars are 50 μ m

Such an unexpected result might arise from either a decreased capability of differentiation of D1 ORL-UVA due to senescence, or by a different response to induction media caused by the fibrillar matrix and its chemical-physical characteristics. We asked if, changing the mechanics of these support was sufficient to influence the differentiation behaviour in response to the induction media, without changing the biochemistry of the surface. We then performed the same experiments on supports treated with 2,5% solution of genipin, used as mechanical pre-conditioner to increase the Young modulus of the surface. AFM analysis showed that genipin caused the dCDM stiffness to increase significantly with respect to the non-treated samples (cfr. Fig 8 and Fig. 3; 400-700 Pa in genipin treated samples vs. 30-50 Pa in non-treated samples).

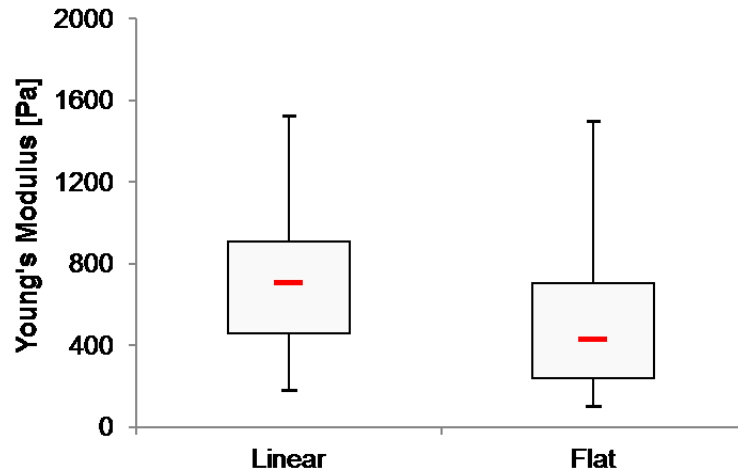


Fig.8. Young's moduli of 2.5 % Genipin treated dCDM, measured on linear and flat decellularized tissue sheets.

D1 ORL-UVA in contact with such a support, caused a different response to the induction media. In fact, as shown in Fig. 9, after 2 weeks of culture in either osteogenic or adipogenic medium, Alyzarin Red staining highlighted a strong osteogenic differentiation. Moreover, the Oil -Red O staining (Fig. 9) showed a decreased tendency to differentiate into the adipogenic lineage with respect to the case of dCDMs not mechanically pre-conditioned.

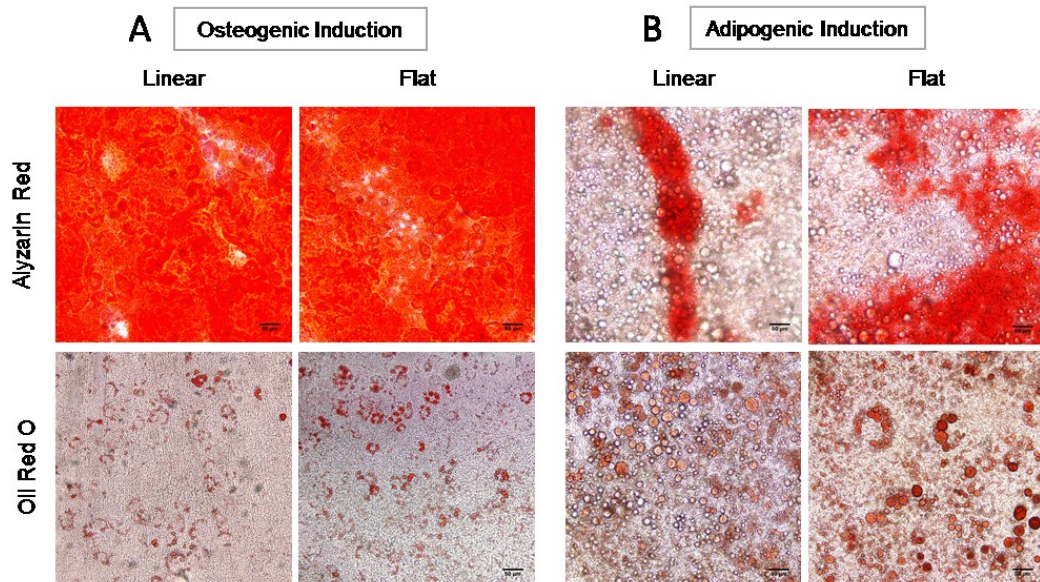


Fig.9. D1 ORL-UVA seeded at high density on a 2 weeks MC3T3 dCDM treated with a 2.5% genipin solution, after 2 weeks of culture in osteogenic medium (A) and in adipogenic medium (B). Bars are 50µm

In order to clarify the effect of the dCDM on stem cell behaviour, we verified whether if a spontaneous tendency of cells to differentiate in either adipogenic or osteogenic lineage. Thus, we performed cell cultures on dCDMs in normal condition, i.e. cultured in maintenance medium (DMEM). Cells cultivated on CCDs were used as control. Cells seeded on dCDMs, did not show a specific commitment. From the staining, cells cultivated on linear dCDM displayed a higher degree of homogeneity with respect to cells on flat dCDM, in which traces of lipidic vacuoles were visible. Cells cultivated on CCD, instead, displayed wide spread lipidic vacuoles and few mineralization nuclei (Fig.10).

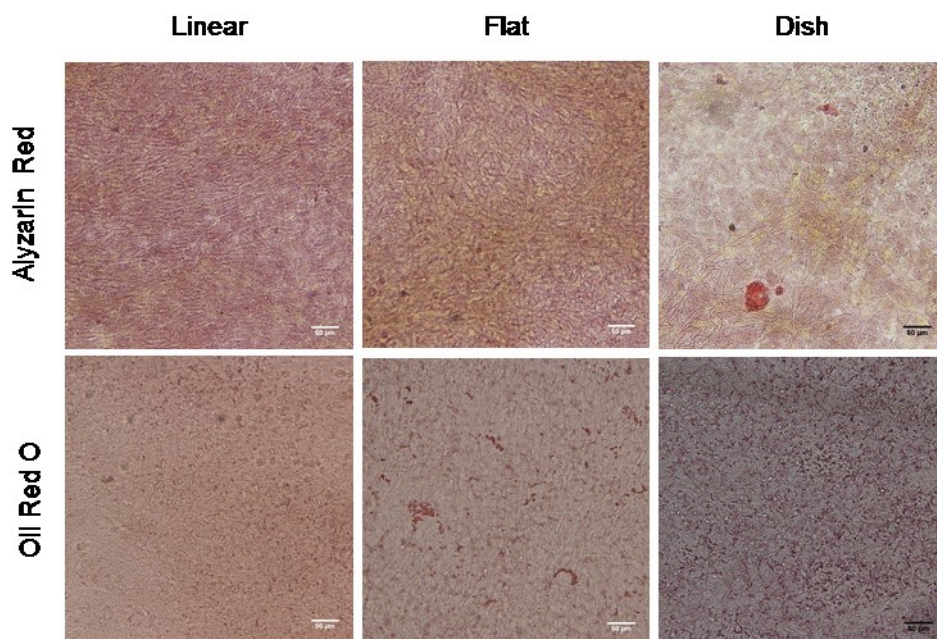


Fig.10. D1 ORL-UVA seeded at high density either on a 2 wk MC3T3 dCDM or on CCD for 2 wk in basal of culture medium (DMEM). Bars are 50µm

To verify whether stemness was maintained, immunostaining against selected markers was performed. At a first sight, it was difficult to notice any marked difference among dCDMs and CCD samples (Fig. 11). In all cases cells expressed the stemness markers Sca-1 and CD29, which were distributed throughout the sample. Thus, we performed a quantitative analysis on the immunofluorescence digital images.

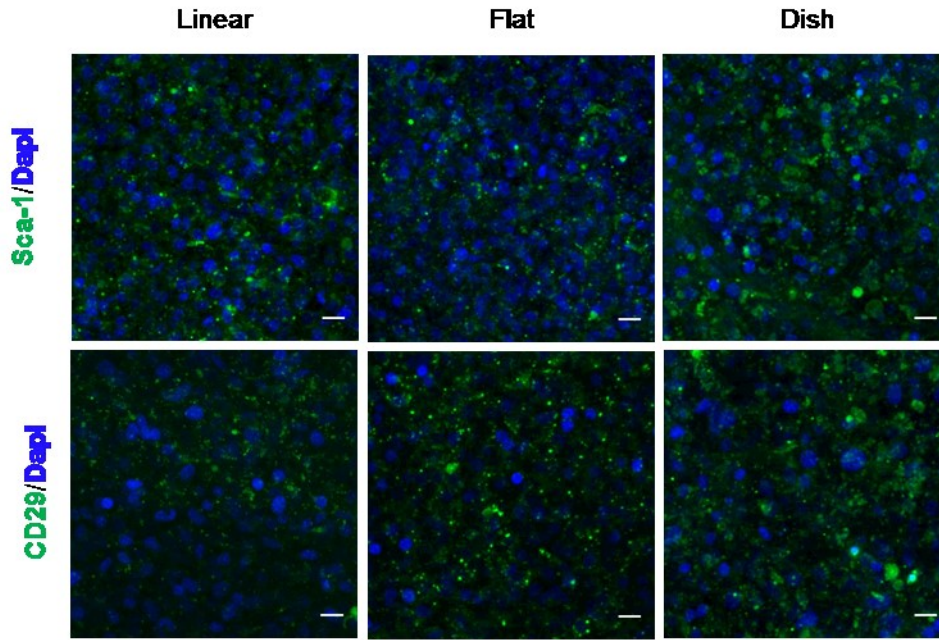


Fig. 11. Confocal images of D1 ORL-UVA on different substrates after 2 weeks of culture immunostained for Sca-1 (Top) and CD29 (Bottom). Bars are 20 μ m.

Quantitative analyses of the intensity and the homogeneity of the markers signals, revealed differences among the samples. Sca-1 marker was significantly more expressed on dCDMs samples than on CCD one (Fig. 12A). The analysis on signal homogeneity, evaluated with the standard deviation of the signal intensity, revealed that Sca-1 was significantly more homogeneously distributed on linear dCDM than on both flat dCDM and CCD samples (Fig.12B). Instead, CD29 was more expressed on dCDMs, with no significant differences between linear and flat samples, than on CCD samples (Fig.12C). No significant differences among samples in terms of CD29 signal homogeneity was observed (Fig. 12D).

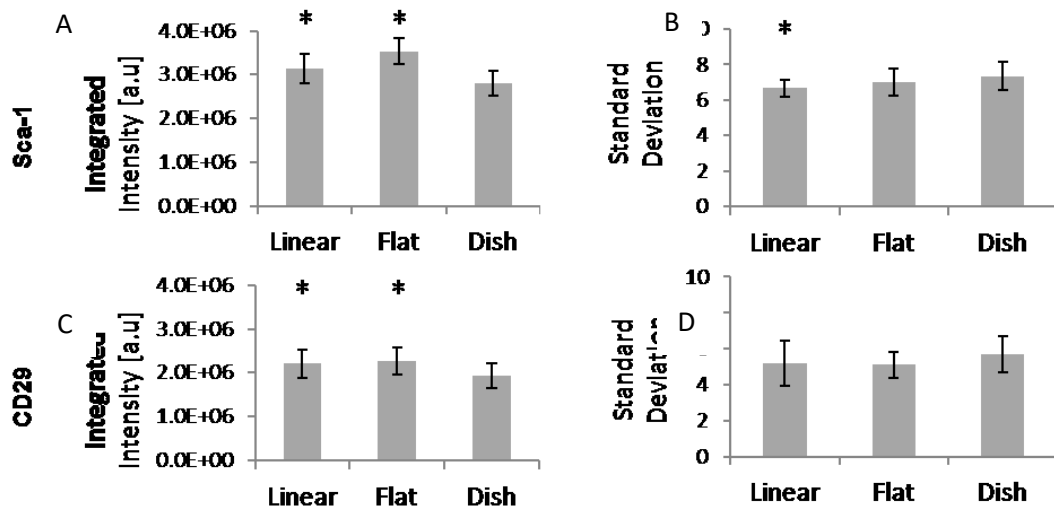


Fig.12 Sca-1 and CD29 quantitative image analysis of D1 ORL-UVA after 2 weeks' culture on different substrates. Both signal intensity (A, C) and standard deviation of the signal (B, D) are evaluated. (*) indicates a significantly difference from dish sample values

To verify if such a difference had effect on cell fate and, more specifically, if cells retained the ability to correctly undergo to adipogenesis or osteogenesis, an additional experiment was performed. We recollected cells after 2 weeks of culture in maintenance medium on the bio-supports and seeded them at the same initial density on dishes. After additional 2 weeks of culture in differentiating media on CCDs we performed either alizarin red or oil red o staining on samples and compared the results with cells cultivated on CCD in the same condition directly. Our results showed that cells cultivated on dCDMs preserved their stemness. In fact, cells derived from dCDMs were able to differentiate both in osteogenic and adipogenic lineage, in a more uniform and intense way in comparison with dish samples (Fig. 13).

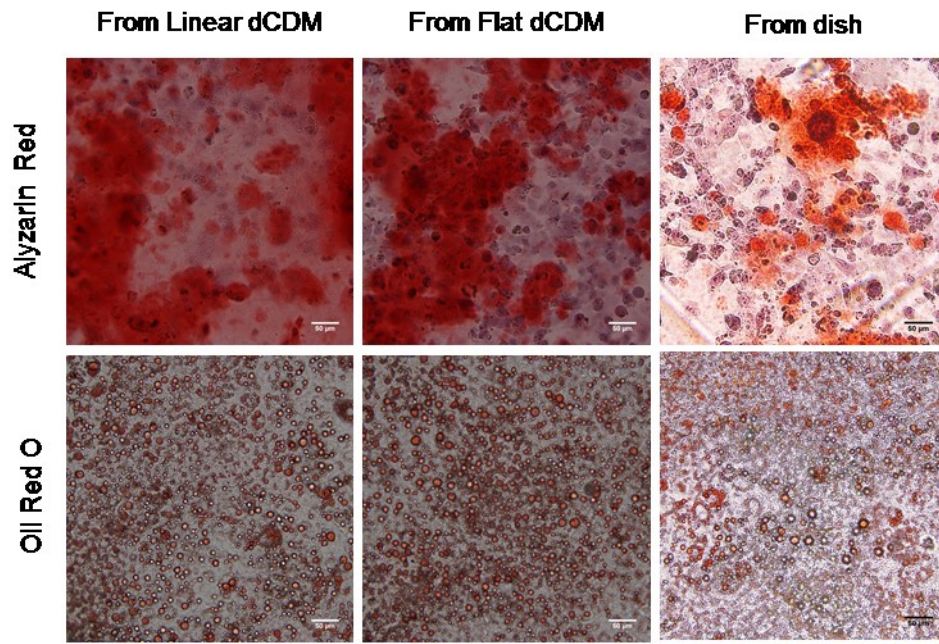


Fig. 13. D1 ORL-UVA from dCDM after 2 weeks in basal medium, seeded at high density on dish, after 2 weeks of culture in osteogenic medium (TOP) and in adipogenic medium (BOTTOM). Bars are 50 μm .

3.4 Discussion

The loss of native phenotype is a common issue in expanding mesenchymal stem cells, this is characterized by loss of function, senescence and spontaneous differentiation (18, 28, 29). A possible approach useful to mitigate culture-induced phenotypic changes, besides the use of soluble factors, is the recapitulation of the tissue-specific microenvironment. In the last decade, the production of an optimized microenvironment for phenotype retention attracted substantial attention from the scientific community. dCDMs offer a valid alternative to this aim. In order to avoid problems relative to the production of bio-support starting from native tissues, a more reliable approach for tissue engineering has been recently suggested. As a partial solution to this problem, the production of ECM *in vitro* derived from different cell types might guarantee the necessary consistency and pliancy for tissue engineering applications. Cells sourced from different tissues could be used to produce matrices mimicking the relative composition of the natural tissues. For example, fibroblast, are well known for their ability to produce a collagen-rich extracellular matrix that resemble the typical composition of connectives. This characteristic has been exploited in several biomedical applications (30, 31). MSCs are also a common source for the dCDM production due to their ability to deposit ECM that mimics various tissues (e.g. bone, cartilage, adipose) depending on culture conditions, and their prevalent use in tissue engineering applications (32).

Currently the best candidates to produce an environment which could be used as an *in vitro* stem cell niche are multipotent primary cells (MSCs, BMCs, ESCs) (19, 20, 28, 32–34). This is because primary cells harvested directly from tissues closely recapitulate their native *in vivo* phenotype, thus are able to generate a matrix which accurately resembles the native microenvironment. However, obtaining a satisfactory number of primary cells for specific applications is often cumbersome. Accordingly, primary cells are expanded *in vitro* as finite cell lines. Though, passaging of cells selects for the most rapidly dividing subpopulations and the *in vitro* environment can alter cell behaviour, resulting in a phenotypic drift from the native cell state (34, 35), so that a certain degree of reproducibility cannot be guaranteed.

Despite these drawbacks, dCDMs provide a comprehensive environment in which mechanical, biochemical and structural signals act in concert influencing cell fate and

functions. This notwithstanding the mutual contribution of these signals to the cell response is still unclear.

In this experimental campaign, we exploited the experience on the control of the morphological characteristics of *in vitro* tissues exerted by material signals (Chap. 2), to produce two different structural assemblies of tissues. We used these tissues, after a decellularization procedure, as bio-supports to control stem cells activity. In particular, we wanted to verify if the matrix produced by an immortalized cell line (E1-MC3T3) was able to maintain the characteristics of stem cells and if a long-range order impressed on the bio-support had some effect on cell functions and fate. We focused our attention on how signals, such as mechanics and topography, may influence stem cell behaviour. In an *in vitro* context, the chemical characteristics, in addition to the physical ones, of the environment strongly affect stem cell fate and behaviour (36–38). Despite it is known that biochemical signals are of fundamental importance in driving stem cell fate, the intrinsic difficulty to modulate such a signal in an environment produced endogenously by cells, drove us to verify how modulating solely the physical characteristics of the environment could affect stem cell fate.

Moreover, we demonstrated that the ability to prevent the loss of differentiation and proliferative potential of mesenchymal stem cells could be achieved by matrices derived from an immortalized cell line. In fact, proliferative potential of MSCs cultured on such a bio-support, was enhanced with respect to CCDs cultures. Furthermore, dCDMs preserved the differentiation potential over long time culture. The ability of MC3T3 cells to produce an abundant ECM rich in collagen under ascorbic acid supplementation offer a valid alternative to the production of ECMs derived from cells difficult to treat as MSCs or BMCs. Hence, MC3T3 cells are able to produce a microenvironment that potentially mimics the bone marrow niche architecture and composition. We verified that the mechanical characteristics of the MC3T3 dCDMs are in the same range of the bone marrow niche. In fact, our data shown that dCDMs mean Young's modulus is around tens of Pa, similarly to the values found in literature (17). We did not observe significant differences between supports with a characteristic long-range order and randomly oriented structures. Accordingly, linear and flat dCDMs showed comparable degrees of stemness maintenance of MSC cultured on them, with increased homogeneity of MSC population found in linear dCDMs with respect to the flat ones.

How MSCs integrate signals from the surrounding matrix and transduce them into genetic events is still unclear. Yet, it is well recognized that biophysical signals (such as

mechanical and topographical) are potent regulators of stem cell fate. For instance, the landmark study of Engler et al. demonstrated that the mechanical properties of the culturing substrates were able to dictate MSC lineage specification (39). Concerning the issue of phenotype retention Gilbert et al. demonstrated the muscular stem cells exhibited improved self-renewal capabilities if cultivated on matrices mimicking the stiffness of muscles (40). Therefore, it is likely that since our dCDMs have stiffness comparable to fat/marrow tissue, MSC are prone to retain the phenotype they exhibit in their native tissues. Additionally, when subjected to differentiation media, adipogenesis is enormously improved whereas osteogenesis is inhibited. This again could be explained in terms of the mechanical signalling arising from the soft CDM. Interestingly, adipogenesis is induced even in presence of osteogenic media, an occurrence that could be probably explained by the presence of dexamethasone in both media. In fact, Ghali et al. demonstrated that dexamethasone is responsible for adipogenic/osteogenic co-differentiation in a dose dependent manner (41). This peculiar behaviour could arise also by the overlapping of biochemical and mechanical signals. Rowlands et al. showed that human MSCs seeded on hydrogels coated with different proteins, undergo to osteogenic differentiation only if the right combination of protein and substrate stiffness is presented. In particular, they demonstrated that only hydrogels with a characteristic Young modulus (80kPa) coated with bone specific protein (Collagen I) induced osteogenic differentiation, whereas substrates coated with proteins, such as laminin or fibronectin, do not result in osteogenic marker expression despite the high substrate stiffness (42). Accordingly to this results, we observed that D1 ORL-UVA cells were able to differentiate into osteogenic lineage on stiffer dCDMs. In fact, enhancing the mechanical properties of the bio-support with a genipin treatment, we observed positive staining for the matrix mineralization in presence of either osteogenic or adipogenic media. Additionally, Zhao et al. demonstrated that hMSCs adipogenic differentiation prefers to occur on hydrogels with mechanical properties similar to those of the *in vivo* microenvironment, with respect to softer substrates (43). This suggests that a balance among chemical and physical signals should be achieved to control stem cell fate.

We found that, without changing the biochemistry of the supports, between the two physical signals that we are able to modulate, i.e. mechanical and structural, matrix stiffness played a dominant role. In fact, MSC maintain the very same characteristics when cultured on the two matrix types. Conversely, when collected from the matrix and cultivated on the CCD, cells displayed a very different behaviour with respect to those

directly cultivated on the rigid CCDs. Even though we did not perform a thorough molecular characterization of the MSC cultivated on the matrices, we speculate that the fibrillar nature of the matrix, although compliant, is able to transduce a mechanical signal up the nuclear envelope, which possibly can alter cell fate. In fact, cells cultivated on the matrices, both linear and flat, exhibit a more oblong nucleus with respect to cells cultivated on flat dishes (Fig. 13).

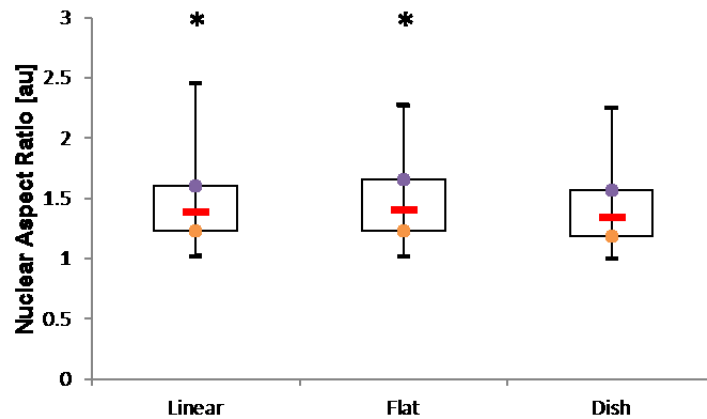


Fig. 13. Nuclear aspect ratio of D1-ORL UVA grown on different substrates after 2 weeks of culture. Asterisk indicate significant difference from the dish sample.

Li et al. demonstrated that nuclear squeezing is inversely correlated with HADC activity (44). This caused an increase in histone acetylation with a more decondensed chromatin. It is possible that increased nuclear squeezing induced cells on dCDMs to adopt a more “open” chromatin structure that favours the expression of stemness markers such as Sca-1 and CD29. If this is the case, we should expect enhanced stemness retention on aligned dCDMs rather than on flat tissues as aligned fibrils should promote cell elongation and nuclear squeezing. However, as demonstrated in the previous chapter, cells are able to remodel the surrounding structure through contractile forces. This contractility generates small islet in which cluster of cells are highly elongated and coaligned with collagen. Therefore, the short-range order of the collagenous matrix is sufficient to allow cell and nuclear elongation and this might explain why we could not observe any difference in nuclear A/R and stem cell behaviour on the two matrices. It is possible that, by modulating the mechanical properties of the dCDMs with specific enzymes or compounds could

provide cells with a different mechanical feedback that differently influence their behaviour.

Elucidating the predominant role of the mechanical features on regulate stem cell fate, will strongly affect the approach of the production of bio-supports for tissue engineering applications. Along these lines, it is crucial to understand the mutual role of the signals displayed by matrices, in order to promote a tight control on stem cell fate. Here we addressed the issue of stem cell expansion and stemness retention. However, other applications can be envisioned. For instance, dCDM can be engineered to create platform to boost cell reprogramming, as it is emerging that the biophysical environment strongly affects this process (45, 46). Using cells of human origin, may allow the production of matrices that can be integrated in or around conventional scaffolds, acting as stem cell reservoirs, which can improve the healing potential of the scaffold itself. Whether for *in vitro* or *in vivo* applications, the use of CDMs represent a convenient and effective route to provide cells with complex arrays of biochemical, mechanical and biophysical signals, similar to those observed in the native environment. To this aim, material surface need to be specifically engineered to promote and guide matrix biosynthesis and its assembly according to specific features.

3.5 Bibliography

1. L. E. Fitzpatrick, T. C. McDevitt, Cell-derived matrices for tissue engineering and regenerative medicine applications. *Biomater Sci.* **3**, 12–24 (2015).
2. D. M. Bissell, S. C. Stamatoglou, M. V. Nermut, R. C. Hughes, Interactions of rat hepatocytes with type IV collagen, fibronectin and laminin matrices. Distinct matrix-controlled modes of attachment and spreading. *Eur. J. Cell Biol.* **40**, 72–78 (1986).
3. R. S. Sutherland, L. S. Baskin, S. W. Hayward, G. R. Cunha, Regeneration of bladder urothelium, smooth muscle, blood vessels and nerves into an acellular tissue matrix. *J. Urol.* **156**, 571–577 (1996).
4. P. M. Dohmen, A. Lembcke, S. Holinski, A. Pruss, W. Konertz, Ten Years of Clinical Results With a Tissue-Engineered Pulmonary Valve. *Ann. Thorac. Surg.* **92**, 1308–1314 (2011).
5. S. A. Livesey, D. N. Herndon, M. A. Hollyoak, Y. H. Atkinson, A. Nag, Transplanted acellular allograft dermal matrix. Potential as a template for the reconstruction of viable dermis. *Transplantation.* **60**, 1–9 (1995).
6. S. F. Badylak, D. Taylor, K. Uygun, Whole-Organ Tissue Engineering: Decellularization and Recellularization of Three-Dimensional Matrix Scaffolds. *Annu. Rev. Biomed. Eng.* **13**, 27–53 (2011).
7. S. Badylak, D. Freytes, T. Gilbert, Extracellular matrix as a biological scaffold material: Structure and function. *Acta Biomater.* **5**, 1–13 (2009).
8. K. E. M. Benders *et al.*, Extracellular matrix scaffolds for cartilage and bone regeneration. *Trends Biotechnol.* **31**, 169–176 (2013).
9. H. C. Ott *et al.*, Perfusion-decellularized matrix: using nature’s platform to engineer a bioartificial heart. *Nat. Med.* **14**, 213–221 (2008).
10. B. E. Uygun *et al.*, Organ reengineering through development of a transplantable recellularized liver graft using decellularized liver matrix. *Nat. Med.* **16**, 814–820 (2010).
11. T. H. Petersen *et al.*, Tissue-Engineered Lungs for in Vivo Implantation. *Science.* **329**, 538–541 (2010).
12. Z. H. Syedain, L. A. Meier, J. W. Bjork, A. Lee, R. T. Tranquillo, Implantable arterial grafts from human fibroblasts and fibrin using a multi-graft pulsed flow-stretch bioreactor with noninvasive strength monitoring. *Biomaterials.* **32**, 714–722 (2011).
13. C. Quint *et al.*, Decellularized tissue-engineered blood vessel as an arterial conduit. *Proc. Natl. Acad. Sci.* **108**, 9214–9219 (2011).
14. N. Datta, H. L. Holtorf, V. I. Sikavitsas, J. A. Jansen, A. G. Mikos, Effect of bone extracellular matrix synthesized in vitro on the osteoblastic differentiation of marrow stromal cells. *Biomaterials.* **26**, 971–977 (2005).
15. G. Tour, M. Wendel, I. Tcacencu, Human fibroblast-derived extracellular matrix constructs for bone tissue engineering applications. *J. Biomed. Mater. Res. A.* **101**, 2826–2837 (2013).
16. T. T. Lau, L. Q. P. Lee, B. N. Vo, K. Su, D.-A. Wang, Inducing ossification in an engineered 3D scaffold-free living cartilage template. *Biomaterials.* **33**, 8406–8417 (2012).
17. M. C. Prewitz *et al.*, Tightly anchored tissue-mimetic matrices as instructive stem cell microenvironments. *Nat. Methods.* **10**, 788–794 (2013).

18. Y. Lai *et al.*, Reconstitution of marrow-derived extracellular matrix ex vivo: a robust culture system for expanding large-scale highly functional human mesenchymal stem cells. *Stem Cells Dev.* **19**, 1095–1107 (2010).
19. F. He, X. Chen, M. Pei, Reconstruction of an *In Vitro* Tissue-Specific Microenvironment to Rejuvenate Synovium-Derived Stem Cells for Cartilage Tissue Engineering. *Tissue Eng. Part A.* **15**, 3809–3821 (2009).
20. C. P. Ng *et al.*, Enhanced ex vivo expansion of adult mesenchymal stem cells by fetal mesenchymal stem cell ECM. *Biomaterials.* **35**, 4046–4057 (2014).
21. S.-H. Li *et al.*, Elastin overexpression by cell-based gene therapy preserves matrix and prevents cardiac dilation. *J. Cell. Mol. Med.* **16**, 2429–2439 (2012).
22. M. Pei *et al.*, Modulation of In Vitro Microenvironment Facilitates Synovium-Derived Stem Cell-Based Nucleus Pulposus Tissue Regeneration: *Spine.* **37**, 1538–1547 (2012).
23. Z. Ivanovic, Hypoxia or in situ normoxia: The stem cell paradigm. *J. Cell. Physiol.* **219**, 271–275 (2009).
24. T. Gilbert, T. Sellaro, S. Badylak, Decellularization of tissues and organs. *Biomaterials* (2006), doi:10.1016/j.biomaterials.2006.02.014.
25. M. T. Wolf *et al.*, A hydrogel derived from decellularized dermal extracellular matrix. *Biomaterials.* **33**, 7028–7038 (2012).
26. R. Subbiah *et al.*, Tunable Crosslinked Cell-Derived Extracellular Matrix Guides Cell Fate. *Macromol. Biosci.* **16**, 1723–1734 (2016).
27. N. Huebsch *et al.*, Harnessing traction-mediated manipulation of the cell/matrix interface to control stem-cell fate. *Nat. Mater.* **9**, 518–526 (2010).
28. M. H. Cha *et al.*, Induction of re-differentiation of passaged rat chondrocytes using a naturally obtained extracellular matrix microenvironment. *Tissue Eng. Part A.* **19**, 978–988 (2013).
29. M. Sun *et al.*, Collagen V is a dominant regulator of collagen fibrillogenesis: dysfunctional regulation of structure and function in a corneal-stroma-specific Col5a1-null mouse model. *J. Cell Sci.* **124**, 4096–4105 (2011).
30. B. Weber *et al.*, Off-the-shelf human decellularized tissue-engineered heart valves in a non-human primate model. *Biomaterials.* **34**, 7269–7280 (2013).
31. Z. H. Syedain, A. R. Bradee, S. Kren, D. A. Taylor, R. T. Tranquillo, Decellularized Tissue-Engineered Heart Valve Leaflets with Recellularization Potential. *Tissue Eng. Part A.* **19**, 759–769 (2013).
32. H. Lu *et al.*, Cultured cell-derived extracellular matrix scaffolds for tissue engineering. *Biomaterials.* **32**, 9658–9666 (2011).
33. W. Wystrychowski *et al.*, First human use of an allogeneic tissue-engineered vascular graft for hemodialysis access. *J. Vasc. Surg.* **60**, 1353–1357 (2014).
34. M. Pei, F. He, Extracellular matrix deposited by synovium-derived stem cells delays replicative senescent chondrocyte dedifferentiation and enhances redifferentiation. *J. Cell. Physiol.* **227**, 2163–2174 (2012).
35. T. Hoshiba, T. Yamada, H. Lu, N. Kawazoe, G. Chen, Maintenance of cartilaginous gene expression on extracellular matrix derived from serially passaged chondrocytes during in vitro chondrocyte expansion. *J. Biomed. Mater. Res. A.* **100A**, 694–702 (2012).
36. J. Y. Wong, J. B. Leach, X. Q. Brown, Balance of chemistry, topography, and mechanics at the cell–biomaterial interface: Issues and challenges for assessing the role of substrate mechanics on cell response. *Surf. Sci.* **570**, 119–133 (2004).

37. J. Lee, A. A. Abdeen, D. Zhang, K. A. Kilian, Directing stem cell fate on hydrogel substrates by controlling cell geometry, matrix mechanics and adhesion ligand composition. *Biomaterials*. **34**, 8140–8148 (2013).
38. D. S. W. Benoit, M. P. Schwartz, A. R. Durney, K. S. Anseth, Small functional groups for controlled differentiation of hydrogel-encapsulated human mesenchymal stem cells. *Nat. Mater.* **7**, 816–823 (2008).
39. A. J. Engler, S. Sen, H. L. Sweeney, D. E. Discher, Matrix Elasticity Directs Stem Cell Lineage Specification. *Cell*. **126**, 677–689 (2006).
40. P. M. Gilbert *et al.*, Substrate Elasticity Regulates Skeletal Muscle Stem Cell Self-Renewal in Culture. *Science*. **329**, 1078–1081 (2010).
41. O. Ghali *et al.*, Dexamethasone in osteogenic medium strongly induces adipocyte differentiation of mouse bone marrow stromal cells and increases osteoblast differentiation. *BMC Cell Biol.* **16**, 9 (2015).
42. A. S. Rowlands, P. A. George, J. J. Cooper-White, Directing osteogenic and myogenic differentiation of MSCs: interplay of stiffness and adhesive ligand presentation. *AJP Cell Physiol.* **295**, C1037–C1044 (2008).
43. W. Zhao, X. Li, X. Liu, N. Zhang, X. Wen, Effects of substrate stiffness on adipogenic and osteogenic differentiation of human mesenchymal stem cells. *Mater. Sci. Eng. C.* **40**, 316–323 (2014).
44. Y. Li *et al.*, Biophysical Regulation of Histone Acetylation in Mesenchymal Stem Cells. *Biophys. J.* **100**, 1902–1909 (2011).
45. T. L. Downing *et al.*, Biophysical regulation of epigenetic state and cell reprogramming. *Nat. Mater.* **12**, 1154–1162 (2013).
46. M. Caiazzo *et al.*, Defined three-dimensional microenvironments boost induction of pluripotency. *Nat. Mater.* **15**, 344–352 (2016).

Chapter 4

4.1 Introduction

Micro and nano- patterning material surfaces or, more specifically, patterning the cell adhesive properties of materials, provides an extraordinary opportunity to control cell behaviour *in vitro*. In fact, patterns in the form of micro contact printing stripes or topographic pattern, proved to dramatically affect cell migration, elongation and orientation (1–3). A sapient harnessing of patterning might pave the way towards designing instructive platforms that exert a fine control on cells and, possibly, provide an effective guidance for tissuegenesis. However, the instructive power of patterned material surface has been mostly studied and characterized on isolated cells. While instrumental to gain a better insight into cell-material interactions, this condition is far from being comparable to those observed within a tissue regeneration context. In this case, extensive cell-cell and cell-matrix interactions occur, which can alter the perception of the material signals or even overrule them.

In the last thirty years, different approaches in tissue engineering and regenerative medicine have been developed, among which scaffold-less technologies are of particular interest due to their capabilities of taking advantage of cells' natural ability to synthesize tissue and respond to signals. Scaffold-less approaches include the employment of any platform that does not require cell seeding or adherence on a three-dimensional and exogenous material (4, 5). According to this approach, ECM rich tissues spontaneously form once the processing conditions are optimized. This promotes cell-cell interactions that can increase ECM production (6–8), thus favouring a substantial degree of cell-matrix interaction, which might be beneficial for the development of a mature and functional tissue *in vitro*.

This stated, the way material features affect the genesis and spatial assembly *in vitro* has been scarcely investigated. In Chapter 2, we demonstrated that, in a scaffold-less context, material nanopatterning mostly affected the arrangement of basal cells whereas the arrangement of the *de novo* synthesized ECM and apical cells was also affected by other factors, such as cell contractility and local cell clustering. Material patterning dictates the initial assembly of cells and ECM but the cell-mediated remodelling ultimately drives tissue structure towards mechanically stable configurations.

In agreement with the tensional homeostasis theory, a confluent layer of cells and matrix represents a continuum, in which cells build-up stresses that are transmitted through cell-cell and cell-matrix contacts and are balanced by substrate and ECM resistance, until equilibrium is reached (9). Any modification in matrix stiffness, material properties or cell assembly induces the system to move towards a new equilibrium point. A discontinuity in the culturing substrate represents a locus of instability as cell-cell and cell-matrix contacts are suddenly interrupted. This can cause a force unbalance and extensive remodelling, which might affect cell behaviour in terms of proliferation and migration (10). This effect becomes more evident when bio-supports for tissue genesis are geometrically constrained (11). Several literature reports demonstrate that physical cues, as mechanics and geometry, are crucial factors to regulate morphogenesis (12, 13). Confining cells on surfaces with micropatterning, exerted a dramatic effect cell proliferation, tissue shape and mechanics (11). Within the context of ECM rich tissues, it has been reported that fibroblasts cultured in collagen gels exerts high contractile forces throughout the extracellular environment, which determines the final tissue shape (14). Because the assembly of tissue structure is defined by the mutual interplay between cell adhesion, force generation and mechanics, it is presumptive that boundaries within the culturing environment alter the mechanical identity of the tissue and therefore its dynamic assembly (15). Even though geometry, mechanics and tension transmission are emerging as parameters to the biological control, the mechanisms through which cells interpret these elements to form *de novo* tissues are still far from being clear.

Here, we asked whether a chance to control the spatial assembly of the apical plane existed, thus allowing to generate CDM with specific 3D assemblies of collagen in a deterministic manner. We hypothesize that the presence of sharp edges in the cell culturing systems alters the force balance between cell contraction and matrix resistance thus initiating a cell and matrix reconfiguration. More specifically, sharp edges act as a meso-scale biophysical constraint (0.1 – 1.0 mm) that exerts its action on multi-cell arrangements (16). This, ultimately defines the structure of the apical plane, which as previously reported, affects the basal assembly of collagen. The understanding of such a *phenomenon* could lead to advances for the *in vitro* tissue regeneration for biomedical applications. biomedical applications.

4.2 Materials and methods

4.2.1 Preparation of nanopatterned substrates and tissue devices

Both patterned and flat substrates for cell cultures were fabricated as described in Chapter 2. Briefly, polydimethylsiloxane (PDMS, Sylgard 184, Dow Corning), prepared by mixing elastomer base and curing agent at 10:1 weight ratio, was poured on a polycarbonate master consisting of 1.5 cm² nanograted (700 nm ridges with 1.4 μm pitch and 250 nm depth). Flat PDMS substrates were used as control and were produced by using a polystyrene dish as mold.

Experiments concerning the study of the spatial propagation of the edge effect were performed on specifically designed platforms referred as tissue devices (TDs). Such devices were produced by a rapid prototyping procedure, followed by pouring PDMS either on nanograted polycarbonate or on polymethylmethacrylate (PMMA, Goodfellow) slab. The polymer master molds were designed by AutoCAD and carved with micromilling machine (Minithech CNC Mini-Mill). Three different kind of geometry were chosen: circular (diameter = 1mm), square (side = 1mm) or rectangular (1 x 10mm).

The PDMS solution was degassed, poured onto the master and then cured at 60°C for 2 h. Cured PDMS substrates were treated with oxygen plasma in order to improve cell adhesion. The treatment was performed with a Plasma Femto (Diener) equipped with 13.56 MHz 100 W power generator for the plasma excitation. Plasma exposure was 1 min and then substrates were sterilized by UV exposure for 30 min. Samples were then incubated with serum-supplemented culture medium overnight prior to cell culturing experiments.

4.2.2 Cell culture

MC3T3-E1 preosteoblasts (ATCC) were cultured in alpha MEM with deoxyribonucleosides, ribonucleosides and 2 mM L-glutamine, supplemented with 10% fetal bovine serum, penicillin (100 units ml⁻¹), streptomycin (100 mg ml⁻¹) (Gibco). The cells were incubated at 37°C in a humidified atmosphere of 95% air and 5% CO₂. The culture medium was changed every two days. After 3 days of culture, cells were detached with trypsin/EDTA (0.25% w/v trypsin/0.02 mM EDTA) (Gibco) and seeded on linear, and flat substrates.

Tissue sheets were produced by seeding cells at the density of 2·10⁴ cells·cm⁻² (sub-confluent) on the patterned or flat substrates, and cultivating the cells for 2 weeks in presence of 25 μg/mL of ascorbic acid. Tissue samples for the study on the propagation of the edge effect were produced by seeding cells at the same density of above on TDs and cultivated for 1 week in presence of 25 μg/mL of ascorbic acid.

4.2.3 Tissue staining and image acquisition

After culturing, cells were fixed with 4% paraformaldehyde for 20 min and then permeabilized with 0.1% Triton X-100 (Sigma) in phosphate-buffered saline (PBS). Samples were blocked in PBS/bovine serum albumin 1% solution (Sigma) for 30 min, to avoid non-specific binding. Actin staining was performed by incubating samples with TRITC-phalloidin (Sigma) in PBS for 30 min at room temperature. Then, for nuclear staining, samples were incubated with a 1:10000 solution of SYTOX Green (Invitrogen, 10 mg/mL in dimethyl sulfoxide) in PBS for 5 min at room temperature. Samples were thoroughly rinsed in PBS and mounted on glass slides.

Fluorescent images of actin bundles and nuclear DNAs were collected with a Leica TCS SP 5 (Leica Microsystems). Samples were excited with 543 nm (actin) and 488 nm (nuclei) laser lines, and the emissions were collected in the 560–650 nm and 500–530 nm ranges, respectively. Collagen fibres were visualized through second harmonic generation (SHG) microscopy, i.e. samples were excited with a femtosecond laser (Coherent) at 840 nm and the emission was collected in the 415-425 nm interval.

4.2.4 Edge effect characterization

In order to gain a better insight into the ordering effect exerted by the edges of the sample on tissue architecture, z-stacks of tile-scans in the edge zones were collected. Tile-scans were obtained by a digital stitching of 4 images organized in a 2x2 grid. Image analysis of the stacked confocal micrographs was performed by running OrientationJ plug-in in Fiji software (17). The plug-in measures the distribution of actin filaments or collagen fibres direction. To assess whether variations in the distribution of orientations occurred through the tissue thickness in presence of a sample edge, the algorithm was applied to the basal and apical plane. In more details, tile-scans of the basal or apical plane were divided into 4 non-overlapping regions (region of interest) and the algorithm was applied to each region. We specified the following parameters for the algorithm: Gaussian window dimension $\sigma=1.5$ pixel; Min. coherency = 20%; Min. energy=2%. Min. coherency and energy represent the anisotropy and the orientation degree respectively. Briefly, coherency is in a 0 – 100% range, in which the highest value indicates highly oriented structures and the lowest one the isotropic areas. Energy is a value correlated to the intensity of each pixel of the entire image, higher values correspond to pixels in an oriented structure (18).

The characteristic length with which the edge affected the tissue architecture, was evaluated with the command “measure” in Fiji. Briefly, in the digital images of the apical planes in the edge

zones the “measure” command was run on lines starting from the edge and ending on the last cell aligned with it.

In order to characterize tissue dynamics, i.e. to evaluate the space-temporal variations of the displacement and velocity of tissue elements, a particle image velocimetry (PIV) analysis was performed. This allowed to analyse the velocity vector of two sequential images by loading the image sequences of the time-lapse videomicroscopy it was then possible to obtain the distribution of the components of velocity vectors on different TDs. Briefly, time-lapse videomicroscopy of whole TDs were collected by recording videos using an Olympus IX81 inverted microscope at 10x magnification, equipped with a digital camera (Hamamatsu, ORCA-Flash2.8). Three images of each device were captured every 30min from day 3 to day 5 of culture and from day 5 to day 7. A PIV analysis was performed on the videos using the plug-in of Matlab (The Mathworks) PIV_LAB by William Thielicke (19).

In order to characterize the velocity of the retraction front we analysed the time-lapse video microscopy with the Kymograph tool of Fiji. Briefly, the Kymograph displays the time variation of grey-scale intensity profiles of a ROI in a single chart. More specifically a ROI defined by a m pixel long segment is positioned within a n frame long time lapse video. The plugin gives back a $n \times m$ chart in which the i -th row represent the intensity profile of the ROI at time “ i ”, whereas the j -th column is the time variation of intensity at the position “ j ” within the ROI. By fitting the Kymograph space-time curves with a polynomial, it was possible to evaluate the mean velocity of a representative element. This tool was used for evaluating the velocity of element located within the first $150\mu\text{m}$ (from the edge) as well as those in the $150 - 300\mu\text{m}$ range (from the edge of TDs).

Tissue thickness was directly measured between the basal and the apical actin planes, visualized by the plug-in “3D projection” in Fiji run on z-stacked digital images of tissues.

Significant differences among groups, i.e. characteristic length of the edge effect, mean velocity of tissue front retraction, were assessed with a one-way ANOVA test followed by a Tukey’s post-hoc test written in Matlab (The Mathworks). p values less than 0.05 were considered significant.

4.2.5 TDs characterization (SEM)

PDMS TDs were coated with a 10nm gold layer with a 208hr sputter coater (Cressington). Scanning electron microscopy (SEM) imaging was performed by means of an Ultra Plus Scanning Electron Microscope (Zeiss, Germany) with a 10kV tension.

4.3 Results

We have previously determined that the presence of topographic signals was able to strongly influence the architecture and mechanical response of tissues characterized by an abundant collagen matrix. We then asked if it was possible to gain a better control over the three-dimensional arrangement of tissues produced by a scaffold-less approach. We have frequently observed that the presence of a discontinuity in the culturing substrate, in the form of sharp edges, dramatically affected cell and tissue arrangement. In particular, cells near edges were usually found to coalign with edge direction and acquired a very elongated shape. Furthermore, cells formed assemblies that were thicker to those observed far from the edges, resembling rolled-over sheets. This observation prompted us to hypothesize that sharp edges act as meso-scale signals that locally alter cell and tissue assembly. We then asked whether such a signal propagated throughout the tissue sheet thus altering its structure. To this aim, we produced tissues by cultivating MC3T3 cells in presence of ascorbic acid either on patterned or flat surfaces. We carried out the same kind of analyses performed in Chapter 2 on basal and apical plane of tissues, this time near the edges of the substrate of culture, which represent a strong discontinuity to the culture condition in the central zone of the sample.

We found that, in presence of patterned surface, cells spontaneously formed a multi-layered structure in which a basal and an apical plane were distinguishable and coaligned with each other, in terms of cell morphology as well as of collagen fibrils (see Fig. 5 in Chap. 2). In presence of an edge parallel to the pattern direction, we observed that, cells and collagen, both in the basal and in the apical plane, were aligned with the pattern direction, as shown in the distributions of orientation of actin and collagen (Fig. 1).

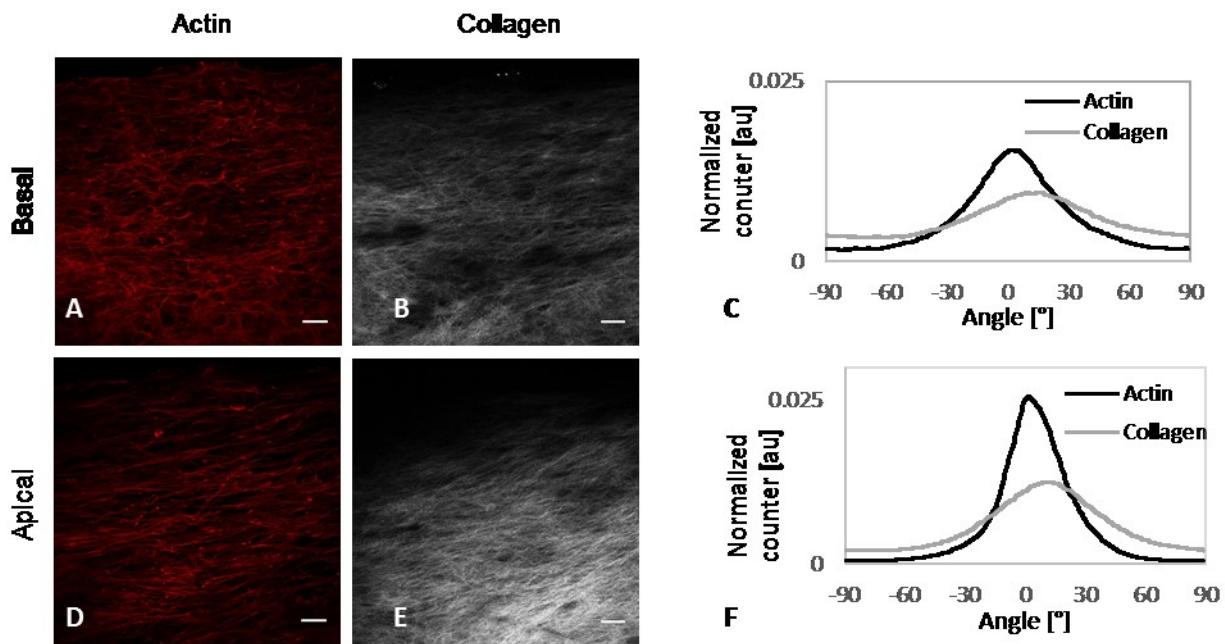


Fig. 1. Structural features in proximity of the sample edge of tissue sheets grown on linear surfaces. ROIs were chosen in order to analyse the edge effect in presence of parallel pattern and edge. Confocal images of actin bundles stained with phalloidin (A, D) and collagen acquired with SHG (B, E). Bars 50 μm . Distribution of orientations, determined with the OrientationJ plugin, of the actin (black) and collagen (grey) signals of the basal (C) and the apical (F) plane. 0° represents the pattern direction.

A very different trend was seen in presence of an edge orthogonal to the pattern direction. In this case, basal cells in close proximity with the edge were coaligned with it (Fig. 2A, B), whereas cells located towards the centre still preserved their usual alignment along the pattern direction. This was also confirmed by the analysis of the distributions of orientations. Basal actin plane showed a distribution with two peaks, 90° apart: one in the direction of the pattern and a broad one approximately located along the edge direction. Collagen distribution of the basal plane exhibited a similar trend, in this case, however, the distribution of orientations close to the edge was narrower with respect to those observed in the actin distribution (Fig. 2C). The apical plane displayed a different arrangement of its constituents. Both actin and collagen were strongly coaligned with the edge direction, and no peaks were observed close to the pattern direction (Fig. 2D, E).

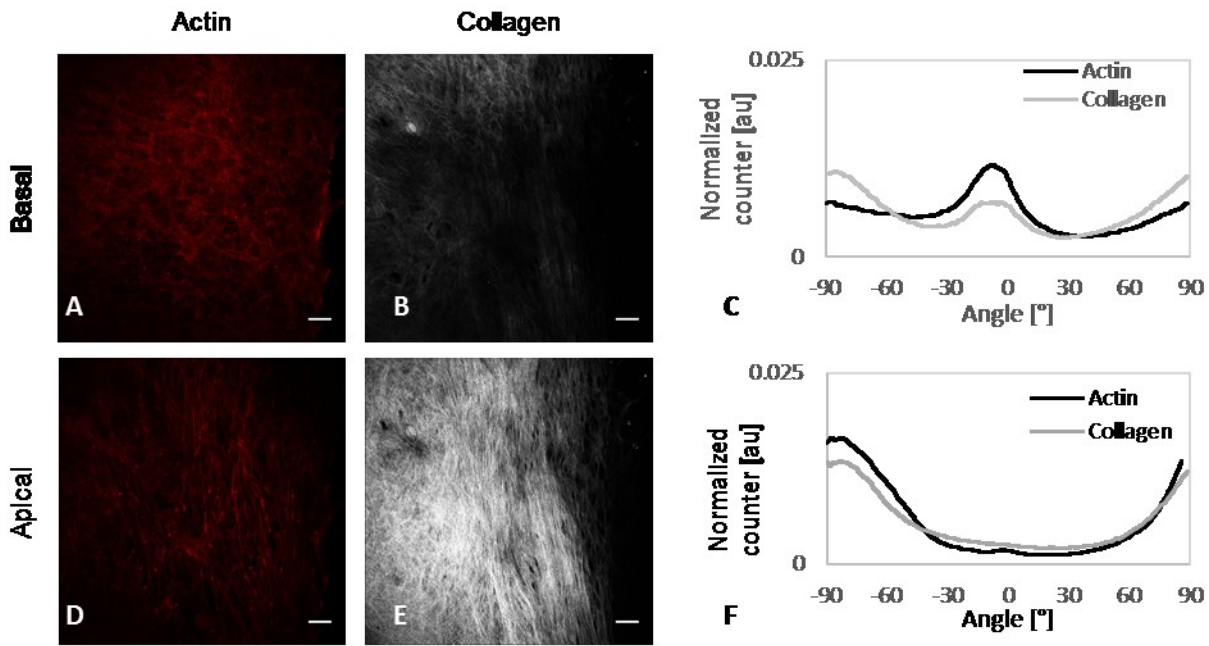


Fig. 2. Structural features in proximity of the sample edge of tissue sheets grown on linear surfaces. ROIs were chosen in order to analyse the effect of the edge perpendicular to the pattern direction. Confocal images of actin bundles stained with phalloidin (A, D) and collagen acquired with SHG (B, E). Bars 50 μm . Distribution of orientations, determined with the OrientationJ plugin, of the actin (black) and collagen (grey) signals of the basal (C) and the apical (F) plane. 0° represent the pattern direction.

Hence, we observed that a discontinuity in the geometry of the sample strongly affected the assembly of the apical plane of multi-layered tissues overruling the effect imposed by the topographic signal. Thus, we were able to discriminate two different order of magnitude of signals: geometric constrains (strong) and topographic (weaker). To further confirm that sharp edges act as a signal *per se*, thus affecting tissue micro-architecture, we performed the same analysis on tissues grown on flat surfaces. We observed that the fibrillar elements of the basal plane possessed a predominantly random distribution, even if a very broad peak in the direction of the edge was observed (Fig. 3A, B, C). In particular, basal collagen distribution showed a shallow peak coaligned with the one of the apical collagen (Fig. 3F) confirming the basal/apical interactions described in Chapter 2.

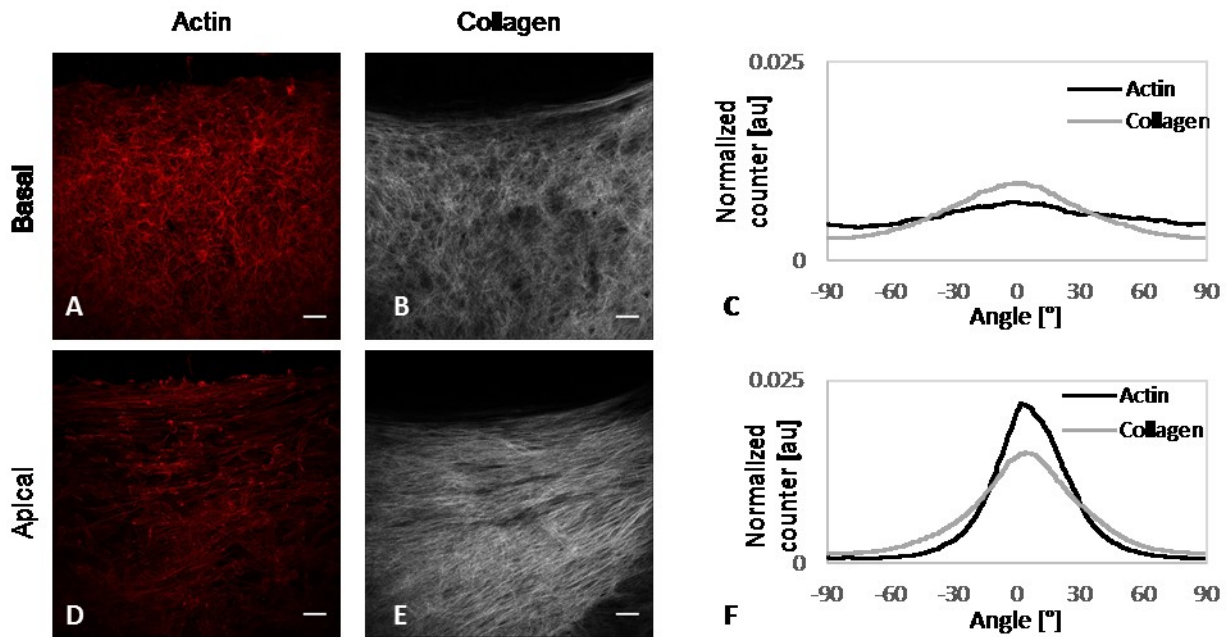


Fig. 3. Structural features in proximity of the sample edge of tissue sheets grown on flat surfaces. Confocal images of actin bundles stained with phalloidin (A, D) and collagen acquired with SHG (B, E). Bars 50 μm . Distribution of orientations, determined with the OrientationJ plugin, of the actin (black) and collagen (grey) signals of the basal (C) and the apical (F) plane.

This suggests that geometric signals were able to influence the assembly of the apical plane, affecting the organization of the basal plane by means of the transmission of the signal through cells contractility.

Owing to the potency of such a meso-scale signal, we asked how far it propagated from the sharp edge towards the centre of the sample. We observed that the effect imposed by the boundary conditions was transmitted in the apical plane with a characteristic length that was similar on the both patterned and flat surfaces (Fig. 4). We then asked if such an effect was static or evolved in time. In order to verify this aspect, we cultivated tissues on either pattern or flat surfaces for 3 weeks, and we evaluated the characteristic length of the edge effect. Although in this case no differences were observed among patterned and flat tissues, we observed that the transmission of the alignment imposed by the edges was significantly increased in time, as showed in Fig. 4.

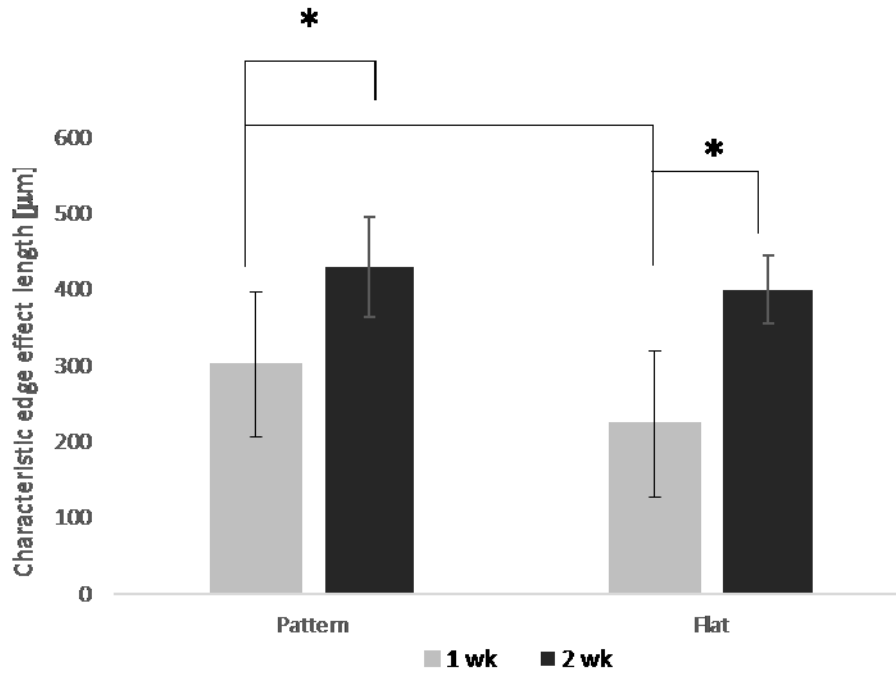


Fig. 4. Histogram of the mean value of the characteristic length with which the edge effect arises. Edges influenced the tissue apical plane conformation, this effect increase in time as shown by the two different series. (*) Indicates significantly difference among samples.

Stated that boundary conditions strongly affected the three-dimensional organization of multi-layered tissues, we wanted to exploit this effect to have a control over tissue architecture throughout its thickness. Thus, we produced substrates with defined geometries and dimensions, in order to guarantee that the ordering effect of edges was effectively transmitted through the tissue. This was possible by producing centrosymmetric isles of PDMS, i.e. tissue device (TD), having characteristic length twice as that of the edge effect ($\approx 500\mu\text{m} \times 2$). Such a design ensured that the edge effect completely covered the substrates. The geometries chosen were circles (CTD) and squares (STD) (Fig.5). We characterized tissues grown on either patterned or flat TDs, namely pTD and fTD respectively.

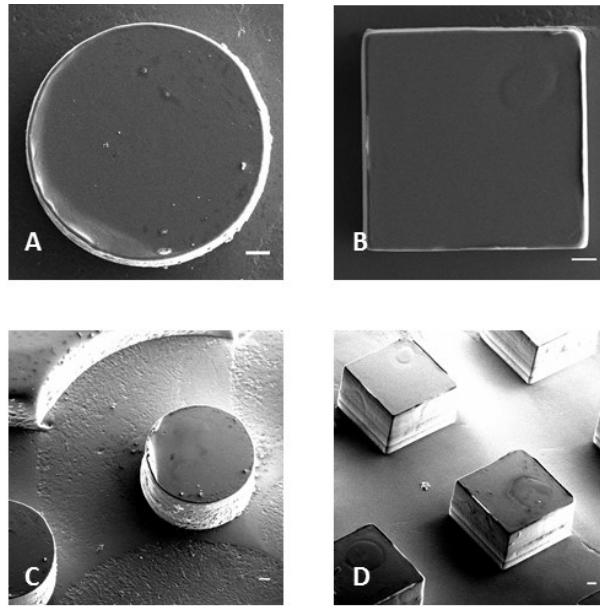


Fig. 5. SEM images of circle or square tissue devices, namely CTD and STD respectively. A, B are images of top view, whereas C, D are acquired with a high tilting angle. Bars are 100 μ m.

In order to understand the dynamics of the development of tissues on TDs we performed time-lapse video microscopy of the first week of culture. We observed that cells formed a confluent tissue within two days (data not shown). Thus, we analysed the movements of the whole tissue during the following 5 days of culture by means of PIV. The analysis was performed on bright-field images, therefore, we were not able to discriminate either basal or apical planes. On patterned substrates, the distribution of velocities in the directions parallel to the pattern direction was broader with respect to that measured in perpendicular direction (Fig. 6A, B). Since PIV referred to the whole tissue dynamics, we cannot conclude that the differences in velocity distributions solely arose from the presence of the pattern, because edge movement could play a role. To verify this aspect, we run the PIV tool on time lapse videos of tissues grown on flat surfaces, namely fCTD and fSTD. In both cases, we found isotropic distributions of velocity (Fig. 6C, D). However, tissues on fSTD exhibited narrower distributions with respect to those recorded on fCTD. This observation promotes the hypothesis that edge curvature plays a dominant role in tissue dynamics. In particular, visual observation of the time lapse videos revealed that the tissue in close proximity of the edge of CTD displayed a fast and centripetal flow (see colormaps in Fig. 6A, C). A fast, centripetal flow was also observed on patterned STD (pSTD) and more specifically on the case of edge and pattern in an orthogonal assembly (Fig. 6B). When pattern and edges were in a parallel configuration or when tissue was grown on fSTD its dynamics was almost stationary (see colormap in Fig. 6D). These observations explain the scatterplots in Fig. 6 in which high flow velocities were measured either in presence of curved edges or in the case of orthogonal pattern and edges setting.

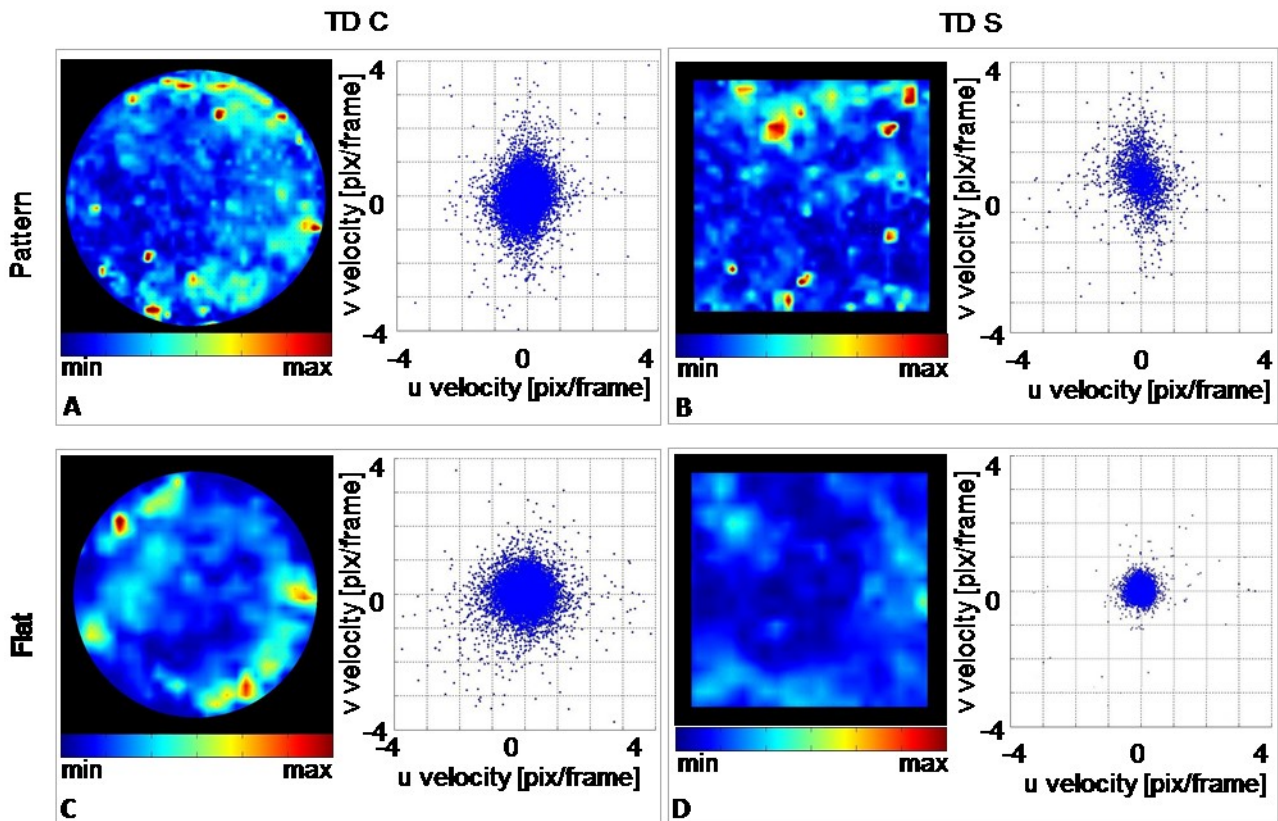


Fig. 6. Colormaps of the velocity magnitude and scatterplots of the velocity vectors $V(u, v)$ components. Velocity vectors are evaluated by means of PIV analysis carried out on time-lapse video microscopy of the tissue sheets morphogenesis during 1 week of culture. Tissues were grown on either CTD (A, C) and STD (B, D) with patterned (A, B) or flat (C, D) surfaces. In A and B vertical axis coincides with the pattern direction.

Given these premises, we further hypothesized that such a behaviour could affect the genesis of the tissue apical plane. Therefore, we performed confocal microscopy on tissues grown on TDs after 1 week of culture. Digital images we acquired confirmed our insight. In fact, tissues grown on pCTD exhibited a homogeneous apical plane with cells aligned with the direction imposed by the edges, i.e. circumferentially (Fig. 7E), laid on an aligned basal plane (Fig. 7A). The architecture of the collagen matrix was influenced by the device, in fact a clear alignment with the pattern direction was not readily recognizable in the basal plane (Fig. 7B), whereas in the apical plane collagen was co-aligned with the edge (Fig. 7F).

We observed a similar behaviour in fCTD. In this case, tissues displayed a basal plane with randomly distributed microconstituents (Fig. 7C, D), and showed a mature apical plane, with cells aligned with the edges (Fig. 7G). Furthermore, cells were arranged circumferentially and were strongly elongated, inducing a strong nuclear squeezing in the direction of alignment. Collagen was

present even if a clear alignment with edges was not detected (Fig. 7D, H). Probably, 1 week of culture was not sufficient to allow randomly distributed cells to completely exert their remodelling power, whereas, if an initial alignment existed, cells were facilitated in performing the matrix compaction.

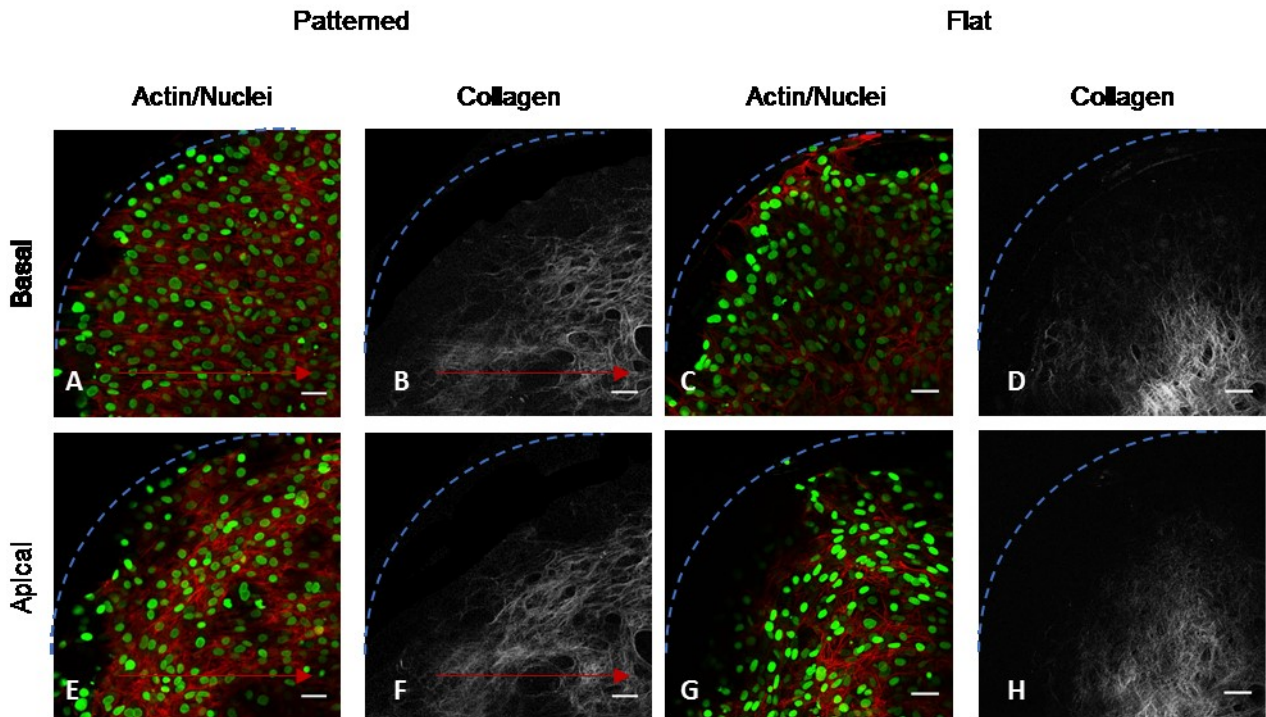


Fig. 7. Details of tissue sheets grown on CTD with patterned (A, B, E, F) or flat (C, D, G, H) surfaces. Confocal images of actin bundles stained with phalloidin merged with nuclei stained with sytox green (A, C, E, G) and collagen acquired with SHG (B, D, F, H). Bars 50 μm . Red arrows and blue dashed lines represents the pattern direction and the TD edges respectively. For clearer illustrative purposes, only one quadrant of the CTD is reported.

The structure of tissues grown on STD showed a very similar trend of those grown on CTD. In particular, pSTD induced a configuration of the microconstituents that resembled the pattern direction in the basal plane (Fig. 8A, B). Apical plane was aligned according to edge direction, and was well developed with densely packed cells and collagen when the edge was orthogonal to the pattern, as opposed to sparsely arranged cells and tissues observed in proximity of edges parallel to the pattern (Fig. 8E). The structure of apical collagen displayed a strong reminiscence of the basal assembly, even though a beginning of alignment in the direction of edges was appreciated. In fSTD, tissues displayed a randomly distributed basal plane (Fig. 8C, D) and a mature apical plane with actin bundles aligned with the direction of the bisector of the two close edges (Fig. 8G). Here,

collagen assembly exhibited a more ordered configuration with respect to the fCTD, in fact it was clearly aligned with the edges generating a square like configuration (Fig. 8H).

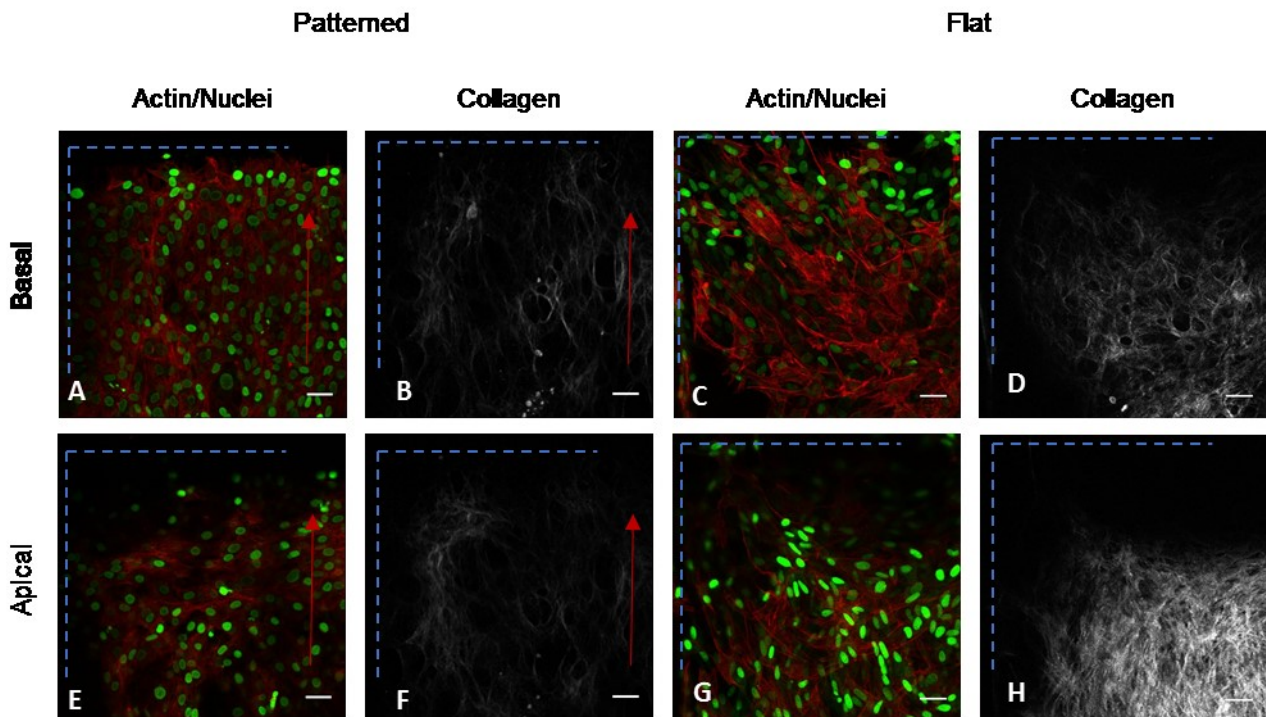


Fig. 8. Details of tissue sheets grown on STD with patterned (A, B, E, F) or flat (C, D, G, H) surfaces. Confocal images of actin bundles stained with phalloidin merged with nuclei stained with sytox green (A, C, E, G) and collagen acquired with SHG (B, D, F, H). Bars 50 μm . Red arrows and blue dashed lines represents the pattern direction and the TD edges respectively. For clearer illustrative purposes, only one quadrant of the STD is reported.

To understand how different geometries could affect the dynamics of the structuring apical plane, we studied in deeper details the centripetal flow of the tissues near edges. To this aim we performed kymograph analysis in the early time of assembly of the apical plane, i.e. 3-5 days of culture. Through this analysis, it was possible to evaluate the velocity of the retraction of the tissue front in presence of the edges. The centripetal flow of features in the images (which might be cells clusters or tissue elements) was represented in the position-time plane as curves with a negative slope. By interpolating these curves, we estimated the velocity flow of the centripetal tissue movement. This analysis showed that patterned TD exhibited two different rates of edge retraction, in fact the velocity was very low nearby the edges parallel to the pattern direction, whereas when

the edges were orthogonal to the pattern direction^a the slopes of the fitting curves were very steep indicating high velocities (Fig. 9A-D). Flat TDs showed an intermediate situation (Fig. 9E, F). At a first sight, no significantly differences were observed among CTD and STD.

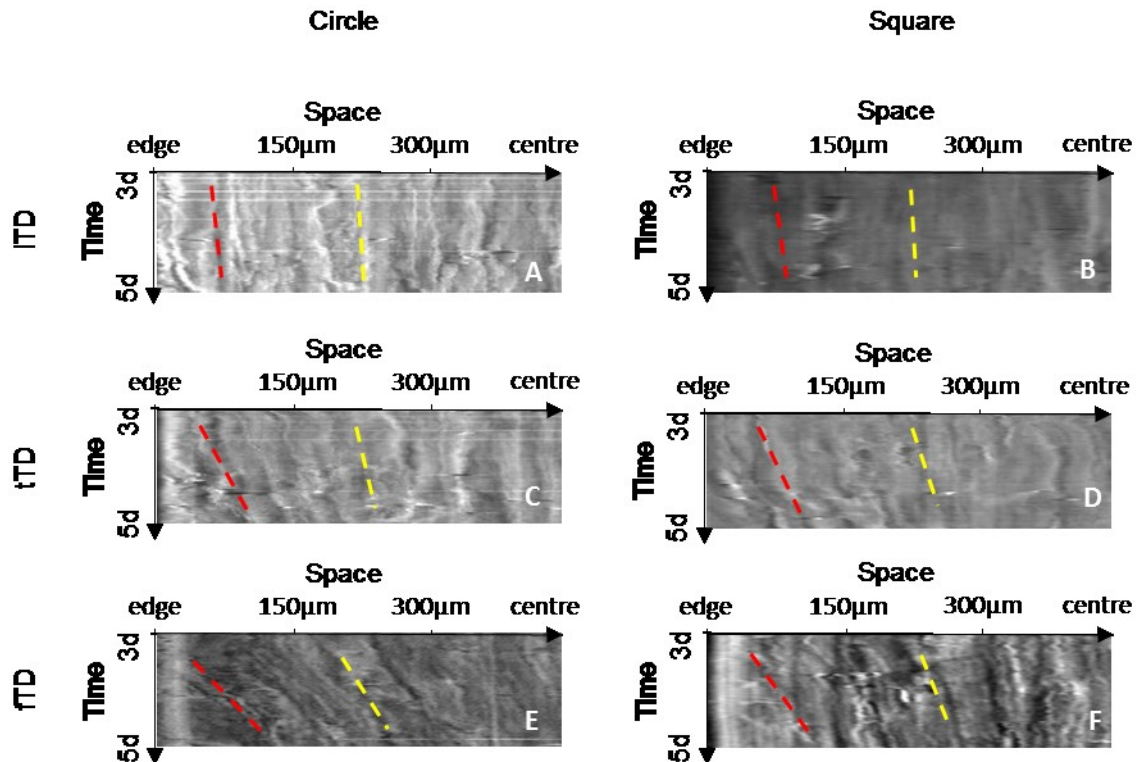


Fig. 9. Kymographs of tissue grown on tissue devices circle (A, C, E) or square (B, D, F). These graphs represent the time variation of grey-scale intensity profile of a line. Time interval analysed is during 3-5 days of culture, whereas space interval represents half device, starting from the edge since the device centre. The tissue retraction was analysed in presence of edges longitudinal to the pattern direction (ITD) (A, B), orthogonal to the pattern direction (tTD) (C, D), or in presence of edges on tissue device with flat surfaces (fTD) (E, F). Red and yellow dashed lines represent the linear fit line of a space-time curve of a tissue element during retraction in the 0 - 150µm and 150 - 300 µm ranges far from the edge, respectively.

In order to gain a better insight on the different dynamics among the samples, we carried out a quantitative analysis on the mean velocity of the tissue front retraction. Generally, we found that the

^a While the expression, edge parallel to the pattern direction might be intuitive for square samples, it might be less obvious in the case of circular TDs, in which no straight edges exist. We will refer in this case to parallel or perpendicular edge and pattern direction when the latter is parallel or perpendicular to the tangent line to the circle respectively.

retraction speed of the tissue front achieved low values when measured in proximity of edges parallel to the pattern direction, i.e. lSTD and lCTD (Fig.10). Conversely, fast retractions were observed when measurements were performed near the edges orthogonal to the pattern direction, i.e. tSTD and tCTD (Fig. 10). This suggests that sample edges and pattern in a parallel configuration provide the tissue with improved stability, ultimately slowing down the centripetal flow. In the absence of a topographic signal, we observed that the retraction speed of the tissue near the edge was higher with respect to that measured on patterned samples, when pattern and edges were parallel, but of comparable magnitude to that measured close to edges orthogonal to the pattern direction and this occurred irrespective of the sample geometry, i.e. fSTD and fCTD (Fig. 10). When the same measurements were performed towards the centre of the tissue, we generally found lower retraction speeds, probably owing to a local densification of the tissue.

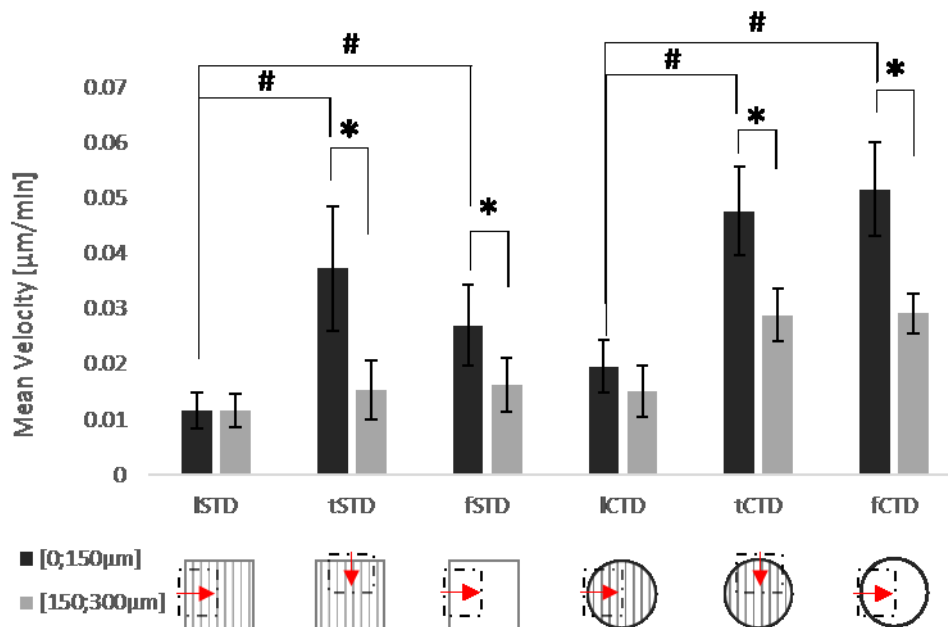


Fig.10. Mean retraction speed of the tissue near the edge, evaluated with kymographs analysis between day 3 and 5 of culture on either square or circle TDs, namely STDs or CTDs respectively. “l” or “t” prefixes represent zones of samples where edges are longitudinal or transversal to the pattern direction, respectively. Black columns refer to values evaluated in the spatial range 0 - 150µm far from the edge, grey columns refer to values evaluated in spatial range 150 - 300 µm far from the edge. (*) indicates significantly differences between samples evaluated with t-test, (#) indicates significantly differences among samples evaluated with ANOVA test. Dashed ROIs in cartoons represents the zones analysed in the different samples. Red arrows indicate the retraction flow analysed.

We then asked if during the maturation of the tissue the velocity of the front retraction varied, thus we performed the same analysis on TDs between 5-7 days of culture. The trend was similar to that seen in the previous case: sample edge and pattern in a parallel configuration stabilize tissue from retraction and the tissue dynamics towards the centre of the sample is slower. Differently from the 3-5 days of culture, at longer culturing times we found lower retraction speeds on fCTD samples.

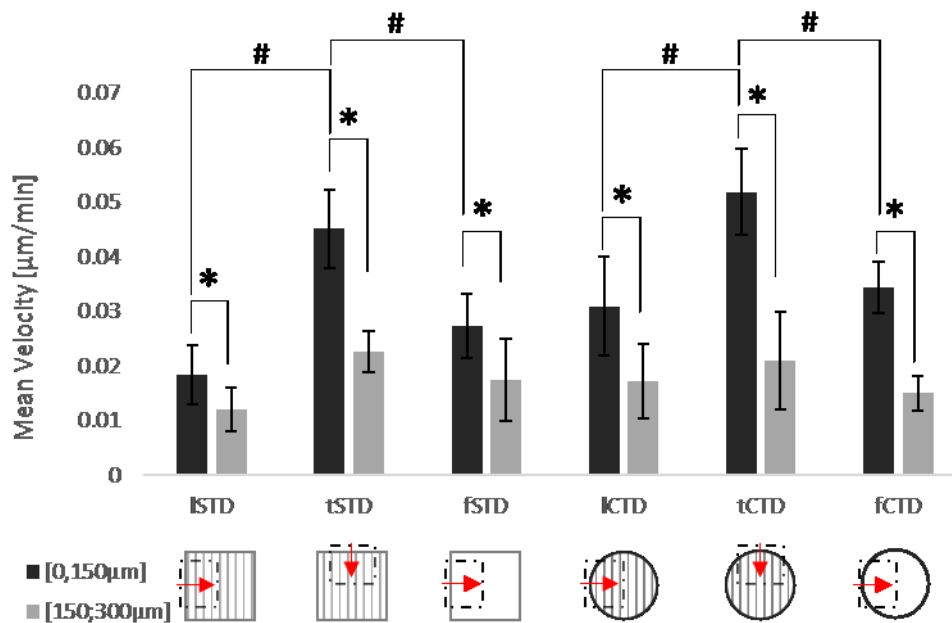


Fig. 11. Mean retraction speed of the tissue near the edge, evaluated with kymographs analysis between day 5 and 7 of culture on either square or circle TDs, namely STDs or CTDs respectively. “l” or “t” prefixes represent zones of samples where edges are longitudinal or transversal to the pattern direction, respectively. Black columns refer to values evaluated in the spatial range 0 - 150µm far from the edge, grey columns refer to values evaluated in spatial range 150 - 300 µm far from the edge. (*) indicates significantly differences between samples evaluated with t-test, (#) indicates significantly differences among samples evaluated with ANOVA test. Dashed ROIs in cartoons represents the zones analysed in the different samples. Red arrows indicate the retraction flow analysed.

Taken together our observations suggest that pattern and shape of the sample edges exert a coordinated action that affect the formation and assembly of the apical plane starting by the sample edges, which then propagates throughout the tissue owing to a centripetal motion. Therefore, by combining pattern direction, edge shape and culturing substrate size, it is in principle possible to define the spatial assembly of tissue microconstituents. We then asked whether we could exploit the mechanism and dynamics observed thus far to generate homogeneous and larger tissues which can be potentially used in tissue engineering applications or as tissue models in vitro.

To this aim, we fabricated high aspect ratio TDs in which one dimension was comparable to the edge effect (1 mm) and the other much larger (10 mm). More specifically, we fabricated rectangular TDs with patterned surfaces longitudinal to the device long axis (lRTD) or transversal to that direction (tRTD) and flat surfaces (fRTD).



Fig. 12. SEM images of rectangle tissue devices RTDs. Bars are 250 μ m.

Tissue grown on IRTDs exhibited a strong actin-collagen-pattern coalignment, both in the basal and in the apical planes, which was concordant to the edge direction. While basal plane was densely and homogeneously populated (Fig. 13B, C), apical plane displayed a patchy structure in which cells were usually found in clusters (Fig. 13D, E).

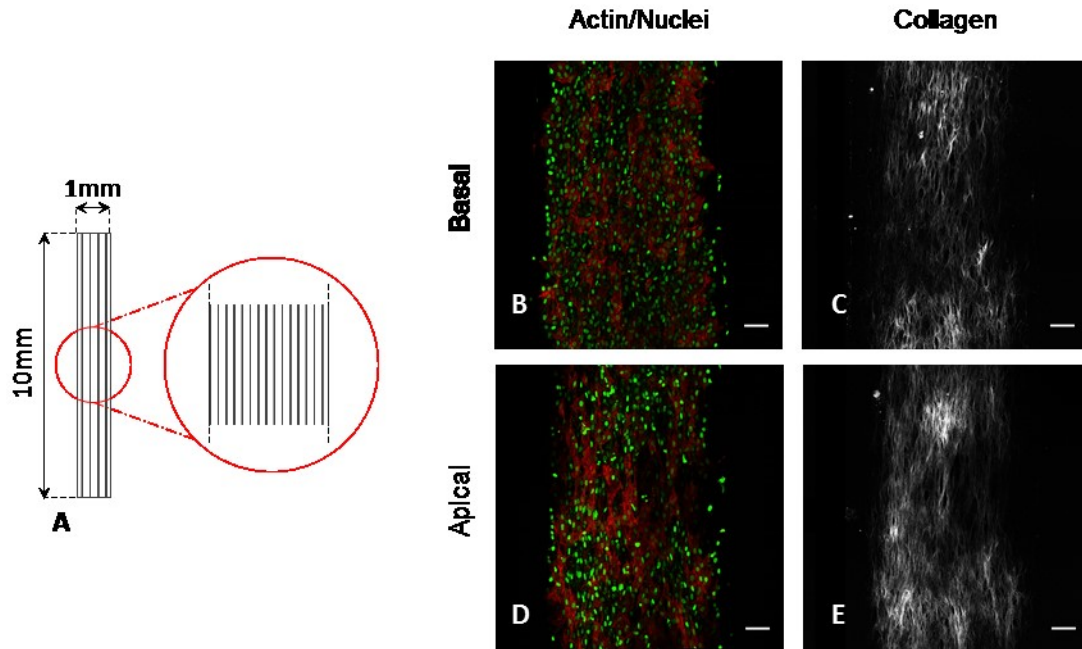


Fig. 13. Tilescons of the central zone of tissues grown on patterned IRTD. Schematic of the device and pattern arrangement. Confocal images were acquired in the central region highlighted by the red circle (A). Images of actin bundles stained with phalloidin merged with nuclei stained with sytox green (B, D) and collagen acquired with SHG (C, E). Bars 100 μm .

Conversely, tissues grown on tRTDs were homogeneously populated in both planes. Cells on the basal plane still retained the same orientation with the pattern direction (Fig. 14B). Whereas, collagen fibres displayed a random arrangement (Fig. 14C). Apical cells and collagen fibres were strongly aligned along the samples edges (Fig. 14D, E).

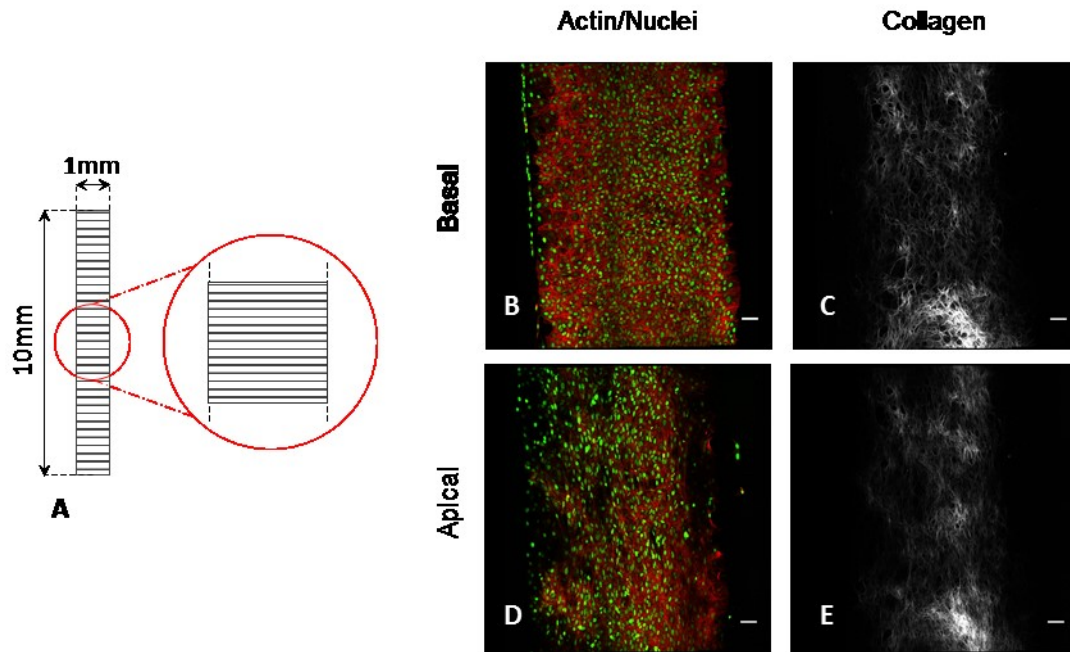


Fig. 14. Tilescons of the central zone of tissues grown on patterned tRTD. Schematic of the device and pattern arrangement. Confocal images were acquired in the central region highlighted by the red circle (A). Images of actin bundles stained with phalloidin merged with nuclei stained with sytox green (B, D) and collagen acquired with SHG (C, E). Bars 100 μm.

Similar results were obtained in the case of fRTDs in which both basal cells and fibrillar collagen were randomly oriented (Fig. 15B, C), whereas apical cells and collagen were strongly coaligned with sample edges (Fig. 15D, E).

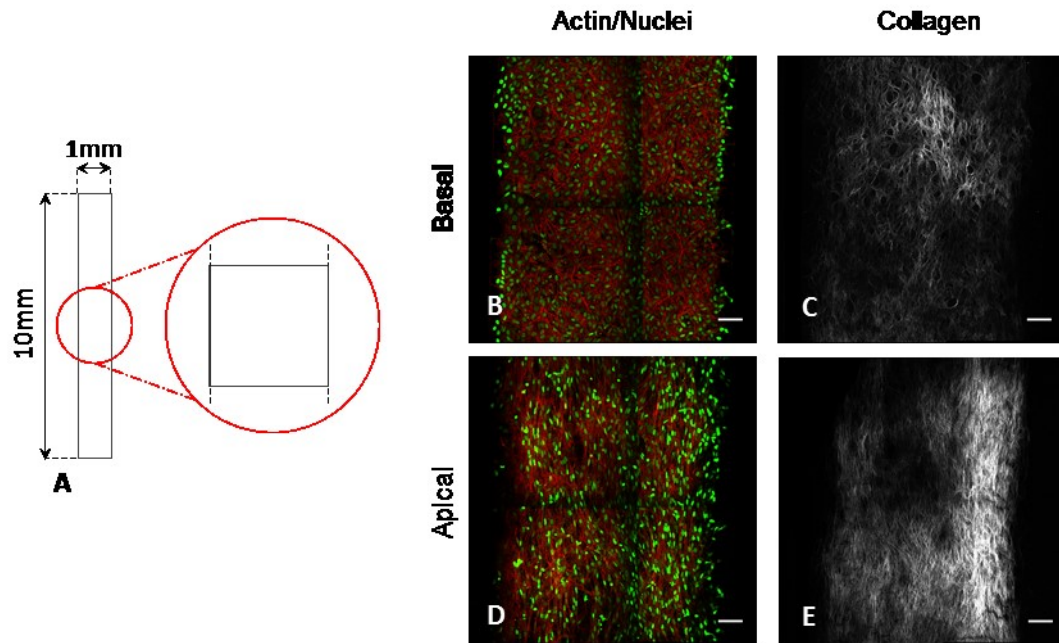


Fig. 15. Tilescons of the central zone of tissues grown on patterned fRTD. Schematic of the device (A). Confocal images were acquired in the central region highlighted by the red circle. Images of actin bundles stained with phalloidin merged with nuclei stained with sytox green (B, D) and collagen acquired with SHG (C, E). Bars 100 μm .

This stated, it might seem that the presence of a surface with nano-topographic features was irrelevant when dealing with larger tissues. It might even seem detrimental in the lRTD case, as it leads to non-homogeneous tissues (Fig. 13D). However, we found that surface nanopatterning strongly affected tissue thickness, as depicted in Fig. 16.

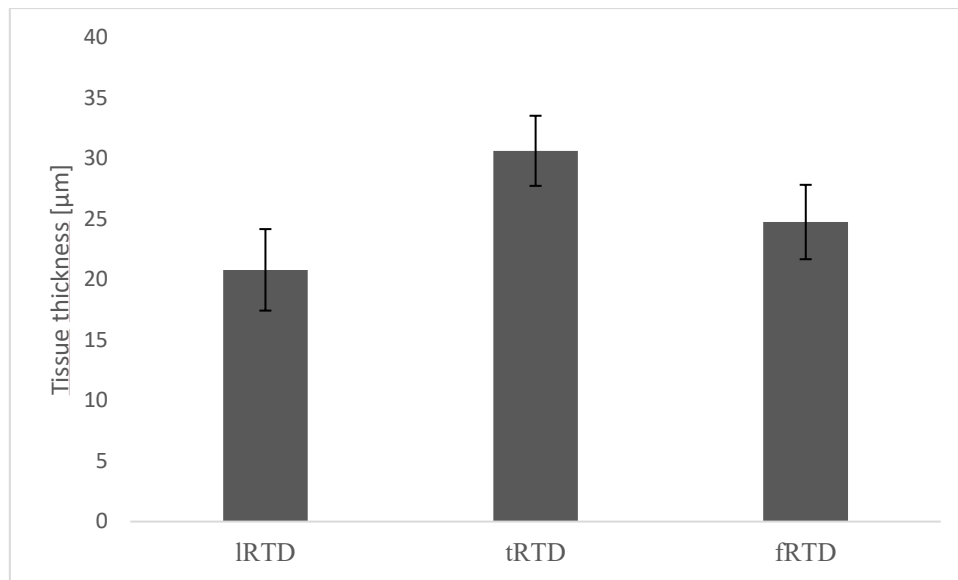


Fig. 16. Mean thickness of tissues grown on RTDs with different surfaces' features. Values are significantly different with each other.

Therefore, patterns that are orthogonal with respect to sample edges not only accelerated tissue front retraction (Fig. 10, 11), but also contribute to the formation of thicker and homogeneous tissues.

4.4 Discussion

Morphogenesis has always attracted the interest of scholars and scientists. The steps that lead the complex transformations from clusters of undifferentiated cells to functional tissues and organs have been thoroughly observed and described, however the intricate mechanisms regulating morphogenesis are far from being clear. How nature orchestrates a multitude of signals both in time and space remains an absolute mystery. This notwithstanding, the initial attempt to clarify such a complex cascade of *phenamona* might pave the way towards the development of novel strategies to replicate a functional tissue *in vitro*. Along this line, reductionists approaches based on the cultivation of cells, undifferentiated or differentiated, in simplified environments *in vitro*, started to shed light on the role of cell-cell interaction on the self-organization of supracellular structures. In the seminal work of Nicol and Garrod (20) subsequently re-interpreted by Steinberg (21), the differential adhesion hypothesis (DAH) was proposed. According to this hypothesis, aggregates with specific spatial assembly of different cell types, spontaneously form *in vitro*, in a *phenomenon* driven by intercellular adhesions and surface tension.

However, the morphogenesis of complex tissues *in vitro* cannot be determined solely by cell-cell adhesion and surface tension, since matrix biosynthesis and compacting also takes place along with the build-up of cell generated stresses which may participate in sculpting the final geometry of the tissue. A recent publication by Czajka et al. (22) highlighted the importance of cytoskeletal generated forces and more specifically of cortical actin in the morphogenesis of cell aggregates *in vitro*. Therefore, in order to guide tissue morphogenesis *in vitro*, it is necessary to take into account the magnitude of cell generated forces as well as the way these forces are directed and transmitted through the tissue.

The concept of tension build-up in tissues is a crucial aspect that regulates its dynamical behaviour. *In vivo*, tension homeostasis has been long recognized as a fundamental paradigm in biology, according to which cells and tissues organize in order to maintain mechanical tension at a preferred set-point value. *In vitro*, the stress experienced by tissue might involve fluctuations. The results reported by Canovic et al. (23) suggest that traction-free boundaries, which are present in cell monolayers *in vitro*, create a favourable condition for intercellular stress build-up that is caused by force transmission from cells near to the boundary (force unbalanced portion) to adjacent cells towards the centre. If forces along the boundary are not balanced, as it might happen during a wound healing experiment, stress fluctuations occur, which determine a dynamic stress state of the monolayer.

In the experimental set-up we described in this chapter, an additional level of complexity represented by matrix production is present. In this *scenario*, cells are able to transmit forces to neighbouring cells through cell-cell adhesions or to ECM components through cell-matrix adhesions. Furthermore, the presence of an endogenous matrix provides cells with additional binding sites thus creating space which cells can migrate in and subsequently remodel.

We observed that cells are able to form a monolayer on TDs and faithfully follow the pattern direction. In proximity of the sample edge, cells formed a by-layered structure, in which cells on the basal plane were mostly aligned along the nanopattern direction, whereas apical cells predominantly followed the edge contour. Cells in the apical plane are in a configuration that could be explained by the alignment mechanism proposed by Bischof and Schwarz (15) in which cell at a free boundary senses maximal stiffness parallel to the edge and align it-self along this. The effect of edge-induced order does not get depleted in the immediate proximity of the sharp edge, but propagates towards the centre of the sample.

Similar results, even though obtained on substrates different from the ones we used, have been already reported in the literature. For instance, Duclos et al. (24) found that confluent fibroblasts layers cultivated on adhesive patches exhibit $\approx 500\mu\text{m}$ wide aligned domains. Gilchrist et al. used μCP adhesive islands containing both meso-scale boundaries and micro-scale adhesive patterns and reported that boundary effect dominates over micropatterning, inducing MSC to strongly align along the boundary (16). They suggested that the boundaries “funnel” cell movement and orientation in a preferred direction, i.e. boundary direction. This also had dramatic effects on matrix orientation. Several works investigated the effects of ECM biosynthesis and assembly in concave/convex porous structures, a context that has obvious implications in tissue engineering. For instance, Rumpler et al. (25) observed that the rate of tissue generation is related to the curvature of the surface. Additionally, the type of curvature, i.e. concaves or convex, is also found to be important. Similarly, Bidan et al. (26) reported that on either flat or convex surfaces, contractility induce a downward motion of the cell; whereas, on concave surfaces, contractility results in a cell stretching towards the centre of the curvature. Since cells are free to occupy the space inward the curvature, such behaviour certainly influence the final outcome of the biosynthetic process. Taken together these data highlight the importance of cell orientation and cell generated forces during in vitro tissue genesis. When using exogenous collagen as supporting matrix, Bischof et al. (27) show that gels populated of fibroblasts, pinned to flat surfaces acquire a macroscopic shape dictated by contractile forces exerted by cells. They found that the active contraction of the contour of the filamentous network in which cells are embedded, reduces its rest-length, so that structurally reinforcing the boundary strongly influences tissue shape. Our investigations go beyond these

points and analyse the dynamics of 3D tissue assembly with the final aim of exploiting meso-scale confinement and nanopatterning to control tissue structure.

Visual inspection of the time-lapse videos showed that the oriented peripheral region of the tissue underwent centripetal flow. This flow could arise from apical cell contractility in which case cells transfer forces to neighbouring cells in an end-to-end fashion and/or contraction of the tissue core, that recruits the peripheral region. Of the two mechanisms involved, we believe that apical cell contraction exerts a dominant role as circular TDs usually displayed higher retraction velocities with respect to those calculated on square TDs. In fact, if we consider cells as contractile dipoles connected end-to-end and arranged along a circle, contraction would produce a non-zero resultant force directed towards the centre. If such a curvature is absent (as virtually occurs in STDs) centripetal motion is much slower (Fig. 6, 17).

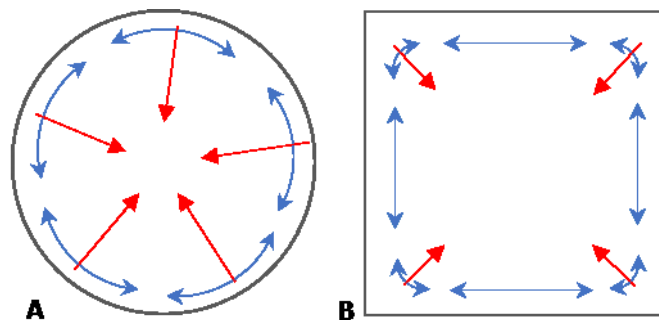


Fig. 17. Schematic representation of the centripetal flow of the apical plane on CTD (A) and STD (B). Blue arrows represent the direction of the contractile forces exerted by the apical cells. Red arrows are the presumptive resultant forces driving the tissue edge retraction.

The presence of a surface pattern also affected the dynamics of tissues. In particular, patterns orthogonal to the edge direction induced a fast centripetal flow, whereas pattern and edge in a parallel configuration formed a more stable setting (Fig. 10, 11). We believe that owing to matrix production and cell density increase, cells migrate from the basal plane to the apical one in a mechanism similar to that discussed in Chapter 2. On the apical plane, cells perceive the strong signal provided by the boundary, which causes them to reorient. Upon contraction, the tissue front retraction is facilitated if the underlying cell and collagen layers are oriented along the direction of tissue retraction, which occurs on edge and pattern in orthogonal settings, whereas the tissue movement is hindered when the underlying matter is assembled orthogonal to the front movement. Few hints that support this view might be found in Fig. 7C and 8C, in which basal cells are directed

according to the motion of the apical plane that might be results of the drag forces exerted by the apical plane. This also explains why tissues grown on devices with a pattern orthogonal to the edge direction were thicker, since in this setting the apical dynamics is fast thus allowing to compact and structure the tissue faster than what measured in case of flat or parallel patterns (Fig. 16). Interestingly, when a tissue front is displaced inwards, a new front quickly formed, recapitulating the same fate as the previous one. This is consistent with the observation that tissue dynamics is considerably slowed down in the centre owing to densifications.

Taken together our results suggest that the presence of regions in which forces acting on the tissue are unbalanced, promotes stratification and remodelling of the microstructure. Here, the regions of force unbalance were represented by the sharp edges of the culturing substrates. In different setting they were created by adhesion boundaries (16). Boundaries may also form within the tissue. In fact, Garfinkel et al. (28) showed that vascular mesenchymal cells evolve from uniform monolayers to patterned tissues *in vitro*. Tissue patterns are composed of densely populated ridges separated by scarcely cell-populated regions. More recently, Iannone et al. (29) demonstrated that tissue patterning is dramatically affected by surface nanotopography. In more details, MSCs on nanogrooved surfaces forme zipper-like structures orthogonal to the nanogrooved direction upon local disruption of the tissue continuity. The authors also emphasized the role of cell contractility in this tissuegenetic event.

Even though all these evidences have been collected *in vitro*, it is tempting to speculate that similar mechanism might occur also *in vivo*. Morphogenesis is sprinkled of examples in which boundaries exert a spatial confinement over cell clusters, eventually regulating cell orientation and migration (30). In this context, the presence of boundaries induces a force unbalance, which triggers essential morphogenetic processes like cell extrusion and intercalation (31). Probably, this anticipates matrix secretion, which stabilizes the whole structure (32).

Material surfaces can therefore be designed to exploit both nanopatterning acting on individual cell adhesion plaques and meso-scale edges thus affecting the orientation of cell clusters. This would allow to exert a fine control on tissues architecture. Beside this important aspect, geometric control on tissue assembly also implies the definition of peculiar stress states in which cells might activate mechanotransduction pathways. This might directly impact lineage specification and, hence, tissue functions.

We envisioned that, arrays of ECM rich tissues with ordered microconstituents, can be conveniently and consistently produced on specifically assembled microdevices. Tissues thus generated might find application not only in tissue engineering and regenerative medicine, but also in *in vitro* models for drug discovery and testing.

4.5 Bibliography

1. M. Ventre, P. A. Netti, Engineering Cell Instructive Materials To Control Cell Fate and Functions through Material Cues and Surface Patterning. *ACS Appl. Mater. Interfaces*. **8**, 14896–14908 (2016).
2. J. H.-C. Wang, F. Jia, T. W. Gilbert, S. L.-Y. Woo, Cell orientation determines the alignment of cell-produced collagenous matrix. *J. Biomech.* **36**, 97–102 (2003).
3. Q. Xing, C. Vogt, K. W. Leong, F. Zhao, Highly Aligned Nanofibrous Scaffold Derived from Decellularized Human Fibroblasts. *Adv. Funct. Mater.* **24**, 3027–3035 (2014).
4. K. S. Furukawa *et al.*, Rapid and large-scale formation of chondrocyte aggregates by rotational culture. *Cell Transplant.* **12**, 475–479 (2003).
5. Z. Zhang, J. M. McCaffery, R. G. S. Spencer, C. A. Francomano, Hyaline cartilage engineered by chondrocytes in pellet culture: histological, immunohistochemical and ultrastructural analysis in comparison with cartilage explants. *J. Anat.* **205**, 229–237 (2004).
6. S. H. Elder *et al.*, Chondrocyte response to cyclic hydrostatic pressure in alginate versus pellet culture. *J. Orthop. Res. Off. Publ. Orthop. Res. Soc.* **24**, 740–747 (2006).
7. J. C. Meredith *et al.*, Combinatorial characterization of cell interactions with polymer surfaces. *J. Biomed. Mater. Res. A.* **66**, 483–490 (2003).
8. D. M. Yoon, J. P. Fisher, Chondrocyte signaling and artificial matrices for articular cartilage engineering. *Adv. Exp. Med. Biol.* **585**, 67–86 (2006).
9. R. A. Brown, R. Prajapati, D. A. McGrouther, I. V. Yannas, M. Eastwood, Tensional homeostasis in dermal fibroblasts: Mechanical responses to mechanical loading in three-dimensional substrates. *J. Cell. Physiol.* **175**, 323–332 (1998).
10. S. J. Streichan, C. R. Hoerner, T. Schneidt, D. Holzer, L. Hufnagel, Spatial constraints control cell proliferation in tissues. *Proc. Natl. Acad. Sci.* **111**, 5586–5591 (2014).
11. C. M. Nelson *et al.*, Emergent patterns of growth controlled by multicellular form and mechanics. *Proc. Natl. Acad. Sci. U. S. A.* **102**, 11594–11599 (2005).
12. S. Huang, D. E. Ingber, The structural and mechanical complexity of cell-growth control. *Nat. Cell Biol.* **1**, E131-138 (1999).
13. T. Lecuit, P.-F. Lenne, Cell surface mechanics and the control of cell shape, tissue patterns and morphogenesis. *Nat. Rev. Mol. Cell Biol.* **8**, 633–644 (2007).
14. D. Stopak, A. K. Harris, Connective tissue morphogenesis by fibroblast traction. I. Tissue culture observations. *Dev. Biol.* **90**, 383–398 (1982).
15. I. B. Bischofs, U. S. Schwarz, Cell organization in soft media due to active mechanosensing. *Proc. Natl. Acad. Sci.* **100**, 9274–9279 (2003).
16. C. L. Gilchrist, D. S. Ruch, D. Little, F. Guilak, Micro-scale and meso-scale architectural cues cooperate and compete to direct aligned tissue formation. *Biomaterials.* **35**, 10015–10024 (2014).
17. J. Schindelin *et al.*, Fiji: an open-source platform for biological-image analysis. *Nat. Methods.* **9**, 676–682 (2012).

18. R. Rezakhaniha *et al.*, Experimental investigation of collagen waviness and orientation in the arterial adventitia using confocal laser scanning microscopy. *Biomech. Model. Mechanobiol.* **11**, 461–473 (2012).
19. W. Thielicke, E. J. Stamhuis, PIVlab – Towards User-friendly, Affordable and Accurate Digital Particle Image Velocimetry in MATLAB. *J. Open Res. Softw.* **2** (2014), doi:10.5334/jors.bl.
20. A. Nicol, D. R. Garrod, The sorting out of embryonic cells in monolayer, the differential adhesion hypothesis and the non-specificity of cell adhesion. *J. Cell Sci.* **38**, 249–266 (1979).
21. M. S. Steinberg, Differential adhesion in morphogenesis: a modern view. *Curr. Opin. Genet. Dev.* **17**, 281–286 (2007).
22. C. A. Czajka, A. N. Mehesz, T. C. Trusk, M. J. Yost, C. J. Drake, Scaffold-Free Tissue Engineering: Organization of the Tissue Cytoskeleton and Its Effects on Tissue Shape. *Ann. Biomed. Eng.* **42**, 1049–1061 (2014).
23. E. P. Canović, A. J. Zollinger, S. N. Tam, M. L. Smith, D. Stamenović, Tensional homeostasis in endothelial cells is a multicellular phenomenon. *Am. J. Physiol. - Cell Physiol.* **311**, C528–C535 (2016).
24. G. Duclos, S. Garcia, H. G. Yevick, P. Silberzan, Perfect nematic order in confined monolayers of spindle-shaped cells. *Soft Matter.* **10**, 2346–2353 (2014).
25. M. Rumpler, A. Woesz, J. W. . Dunlop, J. T. van Dongen, P. Fratzl, The effect of geometry on three-dimensional tissue growth. *J. R. Soc. Interface.* **5**, 1173–1180 (2008).
26. C. M. Bidan *et al.*, How Linear Tension Converts to Curvature: Geometric Control of Bone Tissue Growth. *PLoS ONE.* **7**, e36336 (2012).
27. I. B. Bischofs, F. Klein, D. Lehnert, M. Bastmeyer, U. S. Schwarz, Filamentous Network Mechanics and Active Contractility Determine Cell and Tissue Shape. *Biophys. J.* **95**, 3488–3496 (2008).
28. A. Garfinkel, Y. Tintut, D. Petrusek, K. Bostrom, L. L. Demer, Pattern formation by vascular mesenchymal cells. *Proc. Natl. Acad. Sci.* **101**, 9247–9250 (2004).
29. M. Iannone *et al.*, Nanoengineered surfaces for focal adhesion guidance trigger mesenchymal stem cell self-organization and tenogenesis. *Nano Lett.* **15**, 1517–1525 (2015).
30. J. B. L. Bard, *Morphogenesis: the cellular and molecular processes of developmental anatomy* (Cambridge University Press, Cambridge [England] ; New York, 1990), *Developmental and cell biology series*.
31. B. Ladoux, W. J. Nelson, J. Yan, R. M. Mège, The mechanotransduction machinery at work at adherens junctions. *Integr Biol.* **7**, 1109–1119 (2015).
32. E. G. Canty *et al.*, Coalignment of plasma membrane channels and protrusions (fibripositors) specifies the parallelism of tendon. *J. Cell Biol.* **165**, 553–563 (2004).

Chapter 5

5.1 Conclusions

Understanding cell-material interactions has been a subject of profound investigations in the last decade. Within a tissue engineering context, it acquires a special value: deciphering the intricate relationships between cell and biochemical/biophysical signals would provide novel designing *criteria* to engineer functional scaffolds for an effective tissue regeneration. The production of even complex tissues *in vitro* has been recently proved. However, the cascade of *phenomena* triggered by material signals eventually regulating *in vitro* tissueogenesis is still far from being elucidated. A thorough understanding of what happens when a single cell interacts with a material surface with specific characteristics, such as its topography, mechanics and biochemistry, was obtained through a *plethora* of research. However, when the complexity of the system increases, as in the case of tissues, defining the role of the material signals in affecting the mutual interactions among tissue micro-constituents is not straightforward. In such a situation, it is possible to define a tripartite module, composed by cell, ECM and material signals, in which even a slight variation in one element may induce dramatic changes in the others.

In this thesis, from the one side we shed light on the potential role of material-biophysical signals on the self-organization of growing tissues *in vitro*; from the other, we exploited arrays of those signals to exert a control on tissue structure and mechanics. This was possible by embossing on the surface signals which are stable and easy to reproduce. We verified that the topography provides an initial guidance to cells, which regulates supra-cellular organization and eventually tissue architecture. Then cell remodelling kicks in, altering the morphology of the tissue towards mechanically stable configurations. Matrices with peculiar architectures can then be produced by altering surface patterning and culturing conditions. Tissues characteristics affect cell and nuclear

shape and possibly mechanotransduction pathways locally. Additionally, the gross mechanical response of the whole tissue is also affected. Hence, the dynamic interplay occurring in a 3D environment and matrix subjected to external constrains, must be considered in the design of material platform for the control of *in vitro* tissueogenesis.

The management of the ECM spatial arrangement in concert with its chemical-physical characteristics represents a powerful tool to control stem cell fate. In fact, such an ECM could be used as a direct bio-support for culturing stem cell populations, with the specific characteristic of the native tissues microenvironment. Along this line, material surfaces could be engineered to promote and guide matrix biosynthesis and its assembly according to specific features for *in vitro* or *in vivo* applications. For instance, we employed endogenous ECMs, namely decellularized cell derived matrices, to address the issue of stem cell expansion and stemness retention.

We verified also that other kinds of signals, in addition to topography, can be employed to obtain multi-layered tissues in which the structure is controlled over tissue thickness. In particular, we found that geometrical constrains have a direct effect on the remodelling of the environment through cell contractility. In the presence of a spatial discontinuity, constituted by the sharp edges of the culturing substrate, cells far from the surface tend to elongate along the direction imposed by the edge, explicating a high contractile fallout, i.e. edge effect, that remodel the ECM in that direction. The knowledge of such a *phenomenon*, might pave the way to produce complex and organized tissues for both *in vitro* and *in vivo* tissue engineering applications.

In this work of thesis, we laid the foundation stone for the tight control on complex tissues architecture. Yet, fundamental issues still need to be addressed, such as the potential use of morphogenesis on tissue assembly, as well as the introduction of dynamic stress states on tissue maturation. However, to the best of our knowledge, this is the first time in which the role of material signals, in the form of nanoscale patterns and mesoscale constrains, have been reported to exert an important and possibly regulatory role in *in vitro* tissueogenesis.